Lehrstuhl für Organische Chemie und Biochemie der
Technischen Universität München

Spectroscopic Studies on Flavoproteins

Monika Joshi

Vollständiger Abdruck der von der Fakultät für Chemie der Technischen Universität München zur Erlangung des akademischen Grades eines

Doktors der Naturwissenschaften

genehmigten Dissertation.

Vorsitzender: Univ.-Prof. Dr. Johannes Buchner

Prüfer der Dissertation:

1. Univ.-Prof. Dr. Dr. Adelbert Bacher
2. Univ.-Prof. Dr. Sevil Weinkauf

Die Dissertation wurde am 26.04.2007 bei der Technischen Universität München eingereicht und durch die Fakultät für Chemie am 22.05.2007 angenommen.

Acknowledgement

I would like to express my deep and sincere gratitude to Professor Dr. Dr. Adelbert Bacher, for providing me an opportunity to perform my Ph.D. study in Germany. His wide knowledge and logical way of thinking have been of great value for me. His understanding, encouraging and personal guidance have provided a good basis for the present thesis.

I am deeply grateful to my supervisor, PD Dr. Wolfgang Eisenreich, for introduction to the experimental NMR spectroscopy and its constant discussion, his detailed and constructive comments, helpfulness and for his important support throughout this work.

I wish to express my warm and sincere thanks to Professor Dr. Markus Fischer, University of Hamburg, who introduced me to the field of molecular biology. His ideas and concepts provided a remarkable influence on my entire research. I owe my sincere gratitude to Professor Dr. Gerald Richter of Cardiff University, my former supervisor for his support and the constant helpfulness.

I warmly thank PD Dr. Stefan Weber and Dr. Erik Schleicher of Free University of Berlin for outstanding co-operation within the ranges of EPR and ENDOR spectroscopy. Their valuable advice and extensive discussions around my work have been very helpful for this study. My sincere thanks are due to Dr. Boris Illarionov and PD Dr. Felix Rohdich for their kind support and guidance and special thanks to PD Dr. Nediljko Budisa of Max Planck Institute of biochemistry, Martinsried for tryptophan auxotrophic *E. coli* strain.

I am grateful to Mr. Fritz Wendling for his professional assistance with computer and HPLC problems and Mr. Richard Feicht for his help and advice in protein purification.

I have great regard and I wish to extend my warmest thanks to all my colleague; Miss Susan Lauw, Mrs. Heidi Hofner, Miss Ryu-Ryun Kim, Dr. Victoria Illarionova, Dr. Werner Römisch, Mrs. Astrid König, Mrs. Elena Ostrojenkova, Dr. Tanja Radykewicz, Mr. Christoph Grassberger, Miss Martina Winkler, Mr. Matthias Lee, Mrs. Christine Swartz, Dr. Johannes Kaiser, Dr. Ferdinand Zepeck, Dr. Tobias Gräwert, Dr. Stefan Hecht, Dr. Ralf Laupitz, Miss Brigit Keil, Miss Katrin Gärtner, Miss Silke Marsch, Miss Eva Sicklinger, Miss Eva Eylert, Miss Sabine Saller, Mr. Stefan Kraut, Mr. Thomas Wojtulewicz, Dr. Lilla Margl, Dr. Ilka Haase, Miss Young-Eun Woo, Miss So-Young Kim, Mr. Oliver Ladebeck, Dr. Chan Yong Lee.

My special gratitude is due to my entire families for their loving support, without their encouragement and understanding it would have been impossible for me to finish this work.

Table of Contents

Abbreviations

8-HDF	8-Hydroxy-5-Deazaflavin
Å	Angstrom
ADP	Adenosine-5'-diphosphate
AMP	Adenosine-5'-monophosphate
APS	Ammonium peroxide sulphate
ATP	Adenosine-5'-triphosphate
bp	Base pair
CD	Circular Dichroism
CIDNP	Chemically Induced Dynamic Nuclear Polarisation
CPD	Cyclobutane pyrimidine dimers
Da	Dalton
DNA	Deoxyribonucleic acid
dNTP	Deoxynucleotide triphosphate
DTT	Dithiothreitol
EDTA	Ethylenediaminetetraacetic acid
ENDOR	Electron Nuclear Double Resonance
EPR	Electron Paramagnetic Resonance
FAD	Flavin adenine dinucleotide
fldA	Flavodoxin
FMN	Flavin mononucleotide
FPLC	Fast Protein Liqiud Chromatography
FTIR	Fourier Transform Infrared Spectroscopy
GTP	Guanosine triphosphate
h	hour
HEPES	4-[2-Hydroxyethyl]-1-piperazineethanesulfonic acid
HPLC	High Performance Liquid Chromatography
Hz	Hertz
INADEQUATE	Incredible Natural Abundance Double Quantum Transfer Experiment
IPTG	Isopropyl-β-thiogalactopyranoside
ISC	Inter System Crossing
J	Coupling constant

LB-Medium	Luria-Bertani Medium
LOV	Light Oxygen Voltage
min	Minute
MTHF	Methylenetetrahydrofolate
NADP	Nicotinamide adenine dinucleotide phosphate
NMR	Nuclear Magnetic Resonance
OD	Optical density
PAGE	Polyacrylamide Gel Electrophoresis
PAS	PER/ARNT/SIM
PCR	Polymerase Chain Reaction
PEP	Phosphoenol pyruvate
PMSF	Phenylmethanesulphonylfluoride
ppm	Parts per million
RNA	Ribonucleic acid
RPM	Round per minute
RT	Room temperature
SDS	Sodiumdodecyl sulphate
SDS-PAGE	Sodiumdodecylsulphate polyacrylamide electrophoresis
T	Tesla
Taq	*Thermus aquaticus*
TCA	Trichloro acetic acid
TEMED	Tetramethylethylendiamine
Tris	Tris-(hydroxymethyl)-aminomethane
U	Uniform
UV	Ultra violet
vis	Visible
TARF	Tetraacetylriboflavin
TLC	Thin layer chromatography

1 INTRODUCTION

Flavoprotein: Flavoproteins are ubiquitous proteins that use flavins as prosthetic groups. Since their discovery, and chemical characterization in the 1930s, flavins have been recognized as being capable of both one and two electron transfer processes, and as playing a pivotal role in coupling the two-electron oxidation of most organic substrates to the one-electron transfer of the respiratory chain. Besides their central role in redox biochemistry, flavins are also involved in a variety of nonredox processes, such as blue light pereception in plants (Briggs and Huala, 1999), photorepair of photodamaged DNA (Sancar, 1994), and in circadian time-keeping (Cashmore et al., 1999). The common flavin cofactors are flavin mononucleotide (FMN) and flavin adenine dinucleotide (FAD), which are biosynthesized from riboflavin. Riboflavin is phosphorylated to FMN by the action of riboflavin kinase (Spencer et al., 1976; Karthikeyan, 2003). FAD is then generated by the transfer of an AMP moiety from another ATP molecule to FMN by the action of FAD synthetase (Manstein and Pai, 1986). The redox active isoalloxazine moiety of the flavin cofactor may undergo one- or two-electron transitions (Massey, 2000). The oxidised form is reduced to a radical or semiquinone by one electron reduction. A second one-electron reduction converts the radical to fully reduced forms $FADH_2$ or $FMNH_2$.

In most flavoproteins, the flavin is tightly, but noncovalently bound. However, in a subset of flavoproteins, the flavin is covalently attached to the polypeptide chain (Mewies et al., 1998).

In order to gain insight into how the protein environment influences the reactivity of the flavin, it is desirable to remove the native prosthetic group from the protein in a nondestructive way. The flavin prosthetic group can be replaced with an artificial (Ghisla and Massey, 1986; Smith et al., 1977) or isotopically enriched analog (Moonen et al., 1984). Replacement with a flavin analog should result in the (functionally active) reconstituted holoprotein. FMN and FAD analogs can be synthesized conveniently from riboflavin, either chemically (Spencer et al., 1976) or enzymatically (Manstein and Pai, 1986) and can be isotopically enriched (Müller, 1992).

Isotopically enriched flavins are suitable to get a detailed view into the molecular and submolecular structure of the protein-bound flavin molecule. Flavocoenzymes labeled with stable isotopes are important reagents for the study of flavoproteins using isotope sensitive methods such as NMR, ENDOR, infrared and Raman spectroscopy. ^{13}C and ^{15}N have a natural abundance of 1.1% and 0.4%, respectively and therefore, the flavoprotein has to be

reconstituted with ^{13}C- and ^{15}N-enriched flavocoenzymes. ^{13}C and ^{15}N NMR chemical shifts can reveal π electron density, conformational changes, and dynamic behaviour of the flavin moiety, as well as the presence of specific hydrogen at the carbon and nitrogen atoms investigated.

Labeled riboflavin can be prepared by enzyme-assisted biotransformation *in vitro* and by biotransformation *in vivo* (Römisch et al., 2002; Illarionov et al., 2004). Both approaches are necessarily based on the biosynthetic pathway of the riboflavin (vitamin B_2).

The biosynthetic pathway can be harnessed for *in vitro* biotransformation using ^{13}C-labeled glucose as a starting material. The technology for the preparation of riboflavin carrying 2 to 8 ^{13}C atoms in the xylene ring is summarized in figure 1.1. A variety of ^{13}C-substituted glucose isotopomers are commercially available. It is therefore possible to generate a variety of riboflavin isotopomers with ^{13}C substitution of the xylene ring from appropriate glucose substrates. Briefly, appropriately labeled glucose (**1**, Fig. 1.1) is converted to ribulose 5-phosphate (**4**, Fig. 1.1) in three enzymatic steps requiring 1 equivalent of ATP and 2 equivalents of $NADP^+$. ATP can be regenerated *in situ* by pyruvate kinase using phosphoenolpyruvate (PEP) as phosphate donor, and $NADP^+$ can be regenerated *in situ* by glutamate dehydrogenase using 2- ketoglutarate as oxidant. The enzyme-catalyzed conversion of ribulose 5-phosphate to 3,4- dihydroxy-2-butanone 4-phosphate involves the release of the C(4) of ribulose phosphate as formate and is thermodynamically irreversible (Volk and Bacher, 1990). 3,4-Dihydroxy-2-butanone 4-phosphate (**5**, Fig. 1.1) is formed enzymatically from ribulose 5-phosphate (**4**, Fig. 1.1) by the catalytic activity of 3,4-dihydroxy-2-butanone 4-phosphate synthase (Kis and Bacher, 1995). 5-Amino-6-ribitylamino-2,4(1*H*,3*H*)-pyrimidinedione (**6**, Fig. 1.1) is condensed with 3,4-dihydroxy-2-butanone 4-phosphate (**5**, Fig. 1.1), affording 6,7-dimethyl-8-ribityllumazine (**7**, Fig. 1.1) under the catalytic action of 6,7-dimethyl-8-ribityllumazine synthase. The lumazine derivative is subsequently dismutated by riboflavin synthase under formation of riboflavin and (**6** Fig. 1.1) (Plaut, 1963; Wacker et al., 1964; Beach and Plaut, 1970). In this bisubstrate reaction, one lumazine type substrate serves as the donor of a four carbon unit, and the second lumazine molecule serves as acceptor, whereby it is converted to riboflavin. The pyrimidine type product 5-amino-6-ribitylamino-2,4(1*H*,3*H*)-pyrimidinedione (**6**, Fig. 1.1) of riboflavin synthase can be recycled by lumazine synthase (Kis and Bacher, 1995). The reaction catalyzed by lumazine synthase affords 6,7-dimethyl-8-ribityllumazine (**7**, Fig. 1.1), water, and inorganic phosphate and is also thermodynamically irreversible (Kis et al., 1995). The dismutation reaction catalyzed by

riboflavin synthase results in the formation of an aromatic ring, and is again thermodynamically irreversible (Plaut, 1963). All reaction steps are carried out as a one-pot reaction involving 8 catalysts (Römisch et al., 2002). The final product, riboflavin, is obtained as a yellow solid that is harvested by centrifugation and is then purified by chromatography or recrystallization from dilute acetic acid.

The transfer of carbon atoms from glucose into riboflavin is shown in figure 1.1. Carbon atoms 2 - 4 and 6 of glucose become part of the xylene moiety of riboflavin. As a consequence of the dismutation reaction catalyzed by riboflavin synthase, a single-labeled glucose precursor diverts ^{13}C to two positions in the xylene ring of the riboflavin. Using this approach, a variety of [$^{13}C_2$]- and [$^{13}C_8$]- isotopomers of riboflavin can be obtained. In fact, by this method, all desired isotopomers can be synthesized since the reactant mixtures are all identical except for the ^{13}C-labeled glucose (Römisch et al., 2002). [$^{13}C_8$]Riboflavin can be prepared with [U-$^{13}C_6$]glucose as a starting material. Similarly, [6,8α-$^{13}C_2$]riboflavin, [5a,8-$^{13}C_2$]riboflavin, [7,9a-$^{13}C_2$]riboflavin, and [7α,9-$^{13}C_2$]riboflavin can be prepared with [2-$^{13}C_1$]glucose, [3-$^{13}C_1$]glucose, [4-$^{13}C_1$]glucose, [6-$^{13}C_1$]glucose as a starting material, respectively.

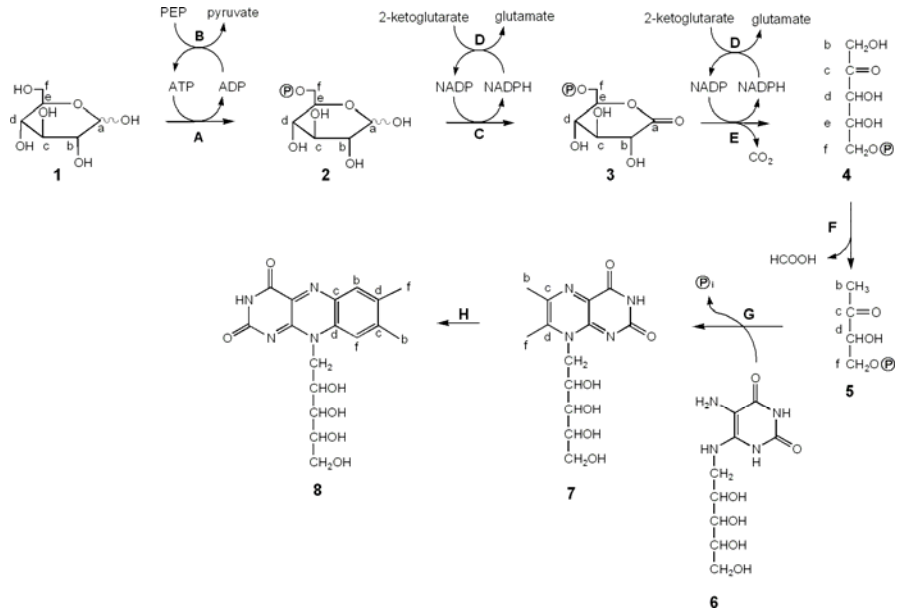

Figure 1.1 Enzyme assisted synthesis of riboflavin (8): (A) hexokinase; (B) pyruvate kinase; (C) glucose 6-phosphate dehydrogenase; (D) glutamate dehydrogenase; (E) 6-phosphogluconate dehydrogenase; (F) 3,4-dihydroxy-2-butanone 4-phosphate synthase; (G) 6,7-dimethyl-8-ribityllumazine synthase; (H) riboflavin synthase.

Riboflavin universally labeled with ^{13}C and/or ^{15}N is best obtained by biotransformation *in vivo*. A recombinant *Escherichia coli* strain carrying a plasmid for the efficient synthesis of the

ribABGH genes can convert [U-$^{13}C_6$]glucose into the riboflavin precursor, [U-$^{13}C_{13}$]-6,7-dimethyl-8-ribityllumazine, that can be converted into [U-$^{13}C_{17}$]riboflavin by treatment with riboflavin synthase. If the fermentation is conducted with culture medium containing $^{15}NH_4Cl$, the procedure can be adapted for the preparation of products, which are universally labeled with ^{15}N (Illarionov et al., 2004).

The *in vivo* biotransformation strategy is not limited to the use of universally ^{13}C-labeled glucose; in fact, any isotope-labeled glucose can be used as starting material. In that case, the labeled starting material is converted by intermediary metabolism into complex mixtures of carbohydrate isotopologues, which can be used by the cells as starting materials for coenzyme biosynthesis. The result is a mixture of coenzyme isotopologues (Fig. 1.2). Fermentation with [1-$^{13}C_1$]-, [2-$^{13}C_1$]-, or [3-$^{13}C_1$]glucose, respectively, affords mixtures of 6,7-dimethyl-8-ribityllumazine isotopologues (**7**, Fig. 1.1) and riboflavin (**8**, Fig. 1.1), predominantly with ^{13}C enrichment of single carbon atoms.

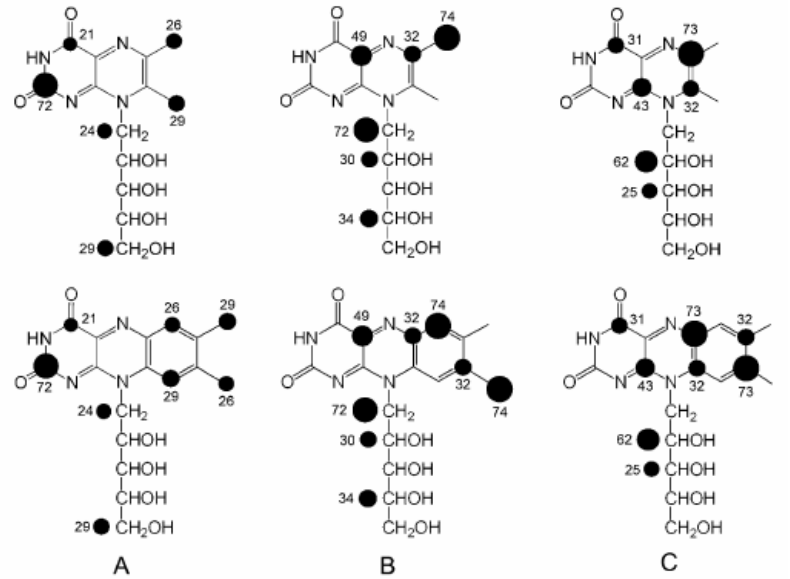

Figure 1.2 Labeling patterns of 6,7-dimethyl-8-ribityllumazine and riboflavin obtained by biotransformation of ^{13}C-labeled glucose samples with an *E. coli* strain M15[pREP4, pRFN4]. (A) From the experiment with [1-$^{13}C_1$]glucose. (B) From the experiment with [2-$^{13}C_1$]glucose. (C) From the experiment with [3-$^{13}C_1$]-glucose. ^{13}C enrichments are indicated by scaled dots. The numbers indicate ^{13}C abundances.

Among the different flavoproteins, most extensively studied and interesting are:

1. Phototropin.
2. DNA photolyase.
3. Flavodoxin.

These three flavoproteins were taken under the study.

1.1 Phototropin

1.1.1 General background

Perception, interpretation, and transduction of environmental light signals are critical for growth and development of higher plants throughout their life cycle. Among the many physiological processes under light control are seed germination, seedling growth, synthesis of the photosynthetic apparatus, and the timing of flowering. Such light-regulated growth and developmental responses are collectively known as photomorphogenesis. In fact, a majority of the photomorphogenesis occurring in plants is induced by UV/blue or red/far-red signals through three classes of photoreceptors: the cryptochromes (cry), the phototropins (phot) capable of operating in the UV/ blue light region (400–500 nm), and the phytochromes (phy) in the red/far-red region (600–800 nm) of the electromagnetic spectrum (Quail, 2002).

In 1995, Liscum and Briggs identified a genetic locus, designated NPH1 (non phototropic hypocotyl 1), which encodes a plasma membrane associated protein known to be essential for most phototropic responses in *Arabidopsis*. The non phototropic hypocotyl (nph) mutants of *Arabidopsis* showed impaired stem (or hypocotyl) phototropism to low intensities of unilateral blue light. In particular, one class of nph mutants, the nph1 mutant, was found to lack the activity of a plasma membrane associated protein that becomes phosphorylated upon irradiation with blue light. The encoded protein, originally designated NPH1, was therefore hypothesized to represent a phototropic receptor that undergoes autophosphorylation in response to blue light. Later experiments confirmed this hypothesis, and the NPH1 protein was named phototropin 1 (phot1) after its functional role in phototropism (Christie et al., 1999).

Phototropin is a 120-kDa flavoprotein that mediates phototropic responses to the direction of blue light, or UV light. The C-terminal region of phot1 contains the 11 signature domains found in serine/threonine protein kinases, whereas the N-terminal region of phot1 contains a repeated motif of 110 amino acids that belongs to the PER/ARNT/SIM (PAS) domain superfamily (Taylor and Zhulin, 1999). The PAS domains of phot1 are more closely related to a subset of proteins within the PAS domain superfamily that are regulated either by Light, Oxygen or Voltage. Hence, the PAS domains of phot1 were assigned the acronym LOV and named LOV1 and LOV2, respectively (Huala et al., 1997).

LOV1 and LOV2 domains are structurally very similar (Crosson and Moffat, 2001; Crosson and Moffat, 2002; Federov et al., 2003). Both LOV domains bind a single molecule of flavin mononucleotide (FMN). Nevertheless, differences in their sequences define them as

either LOV1 or LOV2 (Huala et al., 1997; Crosson and Moffat, 2001). They exhibit *in vitro* photocycle kinetics that is qualitatively identical but quantitatively distinct (Salomon, et al., 2000; Kasahara et al., 2002). LOV1 photoreactivity does not appear to be essential for phototropin function (Christie et al., 2002; Kagawa et al., 2004). The role of LOV1 is unclear, although size exclusion chromatography (Salomon et al., 2004) in addition to small angle X-ray scattering analysis (Nakasako et al., 2004) of purified LOV1 suggests that this domain may play a role in receptor dimerization.

Christie et al. (Christie et al., 1999) have first expressed the LOV domains from *Avena sativa* (oat) and *Arabidopsis* phototropin in *E. coli*. They also showed that the LOV domains of phy3, a putative photoreceptor from the fern, *Adiantum capillus-veneris* also bind FMN. *Adiantum* phy3 is an unusual protein in that it has a phytochrome-like N-terminal domain and a phototropin like C-terminal domain (Fig. 1.3B). Hence, phy3 displays the properties of both a red and a blue light photoreceptor (Nozue et al., 1998).

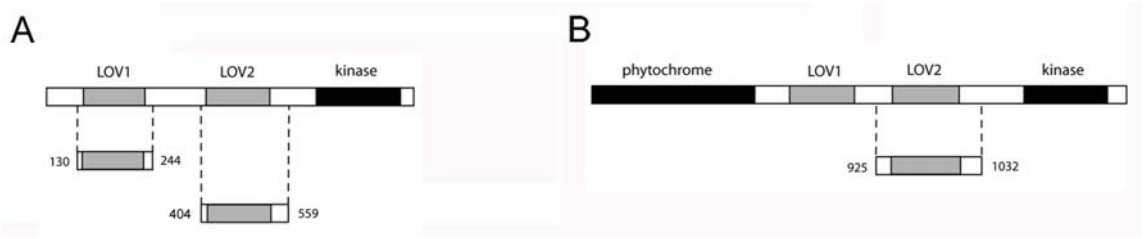

Figure 1.3 Phototropin structure of (A) *A. sativa* NPH1, (B) *A. capillus-veneris* phy3.

Alignments of the LOV1 and LOV2 domain sequences of nph1 from *A. sativa*, and phy3 from *A. capillus-veneris* (Fig. 1.4) shows that all LOV domains contain a conserved cysteine, which is part of the motif GRNCRFLQG, a conserved region found in all LOV domains of phototropin (the first R is not conserved in the LOV domains of phy3).

```
                                                                  ***  *
ASLOV1    130 -----GSALSAFQQTFVVSDASRPGHPIMYASAGFFNMTGYTSKEVVGRNCRFLQGSGTD
ASLOV2    404 GSEFLATTLERIEKNFVITDPRLPDNPIIFASDSFLQLTEYSREEILGRNCRFLQGPETD
ACVLOV2   925 --------GERIGKSFVITDPRLPDNPIIFASDRFLELTEYTREEVLGNNCRFLQGRGTD

                 *  **            *          * *                 *
ASLOV1    183 PAEIAKIRQALANGSNYCGRVLNYKKDGTAFWNLLTIAPIKDEEGRVLKFIGMQVEVSKY
ASLOV2    460 RATVRKIRDAIDNQTEVTVQLINYTKSGKKFWNLFHLQPMRDQKGDVQYFIGVQLDGTEH
ACVLOV2   976 RKAVQLIRDAVKEQRDVTVQVLNYTKGGRAFWNLFHLQVMRDENGDVQYFIGVQQEM---

ASLOV1    243 TE----------------------------------------
ASLOV2    520 VRDAAEREGVMLIKKTAENIDEAAKELPDANLRPEDLWAN
ACVLOV2       ----------------------------------------
```

Figure 1.4 Sequence alignment of *A. sativa* LOV1 (ASLOV1), *A. sativa* LOV2 (ASLOV2) and *A. capillus-veneris* LOV2 (ACVLOV2) domains. Asterisks indicate amino acid residues of protein from *A. capillus-veneris* that build an FMN binding site (Crosson and Moffat, 2002). Identical amino acid residues are drawn in black and similar amino acid residues are in grey shadow typeface.

1.1.2 LOV domain architecture and chromophore environment

X-ray crystallographic studies of maidenhair fern, *A. capillus-veneris* phy3 LOV2 (Crosson and Moffat, 2001) and *Chlamydomonas* phototropin LOV1 (Federov et al., 2003) reveal that LOV domains exhibit a prototypical PAS fold consisting of a five-stranded antiparallel β – sheet flanked by the helix-turn-helix motif αA/ αB, a single helical turn α' A and the 15 residue connector helix α C (Fig. 1.5).

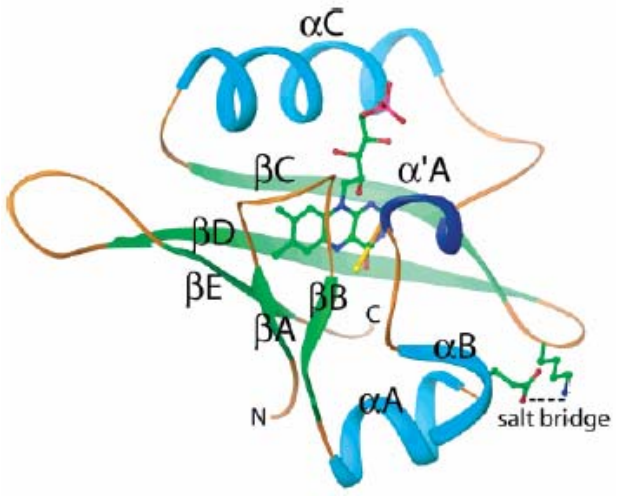

Figure 1.5 Ribbon diagram of *Adiantum* phy3 LOV2 structure. The FMN cofactor is shown in the chromophore binding of LOV2 and is coloured by elements: Carbon, green; nitrogen, blue; oxygen, red; phosphorous, pink. The conserved cysteine side chain is shown attached to the amino terminal end of helix α'A. The FMN is shown in the core of the domain (Source: Crosson et al., 2003).

Embedded in the PAS fold is a single molecule of flavin mononucleotide (FMN) that, in the dark state, is non–covalently bound to the core of protein by a series of polar interactions with the pyrimidine moiety and nonpolar interactions with the dimethylbenzene moiety of the isoalloxazine ring. Additional hydrogen-bond and charge–charge interactions stabilize the ribityl side chain, and terminal phosphate within the LOV fold (Crosson and Moffat, 2001).

1.1.3 Photoexcited–state structural dynamics of LOV domains

After illumination with blue light, recombinant LOV domains of phototropin undergo a transient, and fully reversible bleaching of their optical absorption at 400-500 nm accompanied by an increase of absorption at 390 nm (Salomon et al., 2000; Swartz et al., 2001). Based on the similarity of the spectral characteristics of the photoproduct (Salomon et al., 2000), and that of a kinetically competent intermediate in mercuric ion reductase (Miller et al., 1990), Vincent Massey suggested that the LOV photocycle comprises a light induced addition of a thiol group (cysteine 450 of phototropin in LOV2 domain from *A. sativa*) to the

C(4a) position of the flavin chromophore followed by the spontaneous fragmentation of the adduct in the dark.

Changes in LOV domain structure upon blue light illumination were first documented in a set of one dimensional ^{13}C, ^{15}N, ^{31}P NMR experiments using oat phototropin LOV2 containing an isotopically enriched FMN chromophore (Salomon et al., 2001). These experiments demonstrated that the photoproduct was indeed a cysteinyl-C(4a) adduct, and revealed changes in the chemical environments of the polypeptide backbone, the terminal phosphate, and the ribityl chain of FMN in response to photon absorption.

The three dimensional structure of a LOV domain in a photoexcited state was later solved by collecting X-ray diffraction data on a single crystal of fern phy3 LOV2 under continuous illumination at room temperature (Crosson and Moffat, 2002). While this steady state structure allowed the direct observation of a covalent bond between the conserved cysteine (C966), and the FMN C(4a) carbon, there were very few changes in the overall structure of the protein as evidenced by difference Fourier maps calculated against the dark state structure factor amplitudes (Crosson and Moffat, 2002) (Fig. 1.6 A).

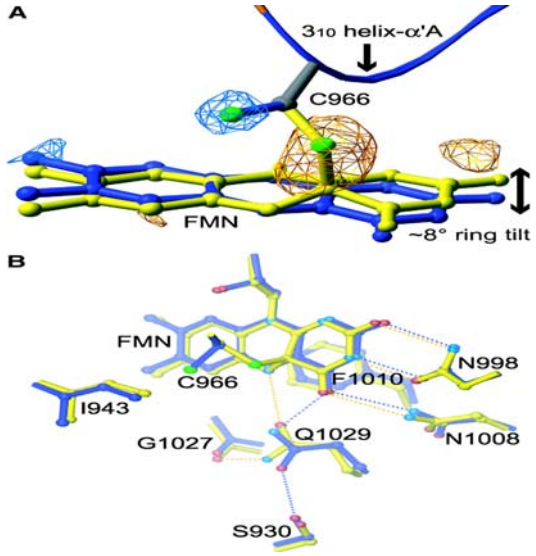

Figure 1.6 Conformational change in the FMN binding pocket of photoexcited LOV2, *A. capillus-veneris* (Source: Crosson and Moffat, 2002).

These data demonstrate that, in the context of the 104 amino acids visible in the phy3 LOV2 electron density maps, protein motion in response to photon absorption is small and is concentrated around the isoalloxazine ring of the FMN cofactor. The largest motion between the dark and illuminated state structures is in the conserved cysteine side chain, which

undergoes a simple chi1 rotation to bring the Sγ sulfur within an appropriate distance to form the covalent adduct with C(4a). Additionally, the flavin ring rotates ~8° so that residues with hydrogen bonds to the isolloxazine moiety can maintain these interactions (Fig. 1.6 B).

Yet, Fourier transform infrared spectroscopy (FTIR) and circular dichroism (CD) studies (Corchnoy et al., 2003) demonstrate that photoactivation of purified LOV2 in solution is accompanied by changes in the LOV-domain apoprotein (Iwata et al., 2003; Swartz et., al, 2002). In particular, the βE sheet region of *Adiantum* phy3 LOV2 exhibits a significant conformational change upon cysteinyl adduct formation (Nozaki et al., 2004). The βE sheet region contains a conserved glutamine residue (Gln1029) that when mutated to leucine results in a loss of these light-driven protein changes (Iwata et al., 2005; Nozaki et al., 2004). Gln1029 forms hydrogen bonds with the FMN chromophore and undergoes side chain rotation upon cysteinyl adduct formation (Crosson and Moffat, 2001; Crosson and Moffat, 2002). This residue therefore appears to be important for signal transmission from inside the chromophore-binding pocket to protein changes at the LOV2 surface.

A possible model that explains how adduct formation can signal through the surrounding LOV domain to result in kinase activation for this process has been provided by solution NMR experiments with phototropin of LOV2, *A. sativa* (Harper et al., 2004). These multidimensional NMR experiments were carried out on a construct of LOV2 containing an additional 40 amino acids after the last C-terminal residues evident in the crystal structure of phy3 LOV2. This C-terminal extension is conserved in all phototropin LOV2 domains, including phy3 LOV2. The conserved α-helix (designated Jα) is associated with the surface of LOV2 in the dark state is ampipathic in nature, consisting of polar and apolar sides, the latter of which docks against the five-stranded antiparallel β-sheet of the core LOV fold. Pulsed illumination of this LOV2 construct causes dramatic changes in $^{15}N/^{1}H$ HSQC and other spectra, indicating extensive blue light-induced structural changes. It was also shown that the adduct formation triggers the unfolding of the helical domain Jα, which serves as a linker between the LOV2 domain and the kinase domain in the LOV2 domain of *A. sativa* (Harper et al., 2004). That unfolding is believed to modulate the activity of the kinase domain, which is conducive to its autophosphorylation. Moreover, artificial disruption of the LOV2 Jα interaction through site directed mutagenesis results in activation of phot1 kinase activity in the absence of light (Harper et al., 2004), demonstrating that unfolding of Jα results in activation of the C-terminal kinase domain.

Two mechanisms of LOV2 signal transmission have been proposed. First, X-ray crystallography has revealed the presence of a conserved salt bridge at the surface of the LOV domain (Crosson and Moffat, 2001; Crosson and Moffat, 2002). Light-driven destabilization of this surface salt bridge has been hypothesized to play a role in coupling LOV domain photoexcitation to phototropin kinase activation (Crosson et al., 2003). The second mechanism involves a conserved glutamine residue within the LOV domain that interacts with the FMN chromophore via hydrogen bonding (Crosson and Moffat, 2001). This glutamine has recently been shown to be involved in propagating light-induced protein conformational changes associated with LOV2 protein fragments (Nozaki et al., 2005; Iwata et al., 2005), indicating that this residue may serve to transmit modifications from within the chromophore binding pocket to protein changes at the LOV domain surface.

1.1.4 Photochemistry of LOV domain/Reaction mechanism

Photocycle kinetics and structure of its intermediates: Studies of the photochemistry were carried out in the *E. coli* expressed oat phot1-LOV2 domain (Salomon et al., 2000; Swartz et al., 2001). Photoreactions of other FMN-binding LOV domains studied afterwards were shown to be qualitatively similar. Following light absorption, the LOV domains undergo a photocycle characterized by series of transient photo-intermediates (Swartz et al., 2001; Kottke et al., 2003; Losi et al., 2002). Presently, two excited states, and one metastable thermal intermediate have been kinetically resolved in the LOV domain photocycle. Briefly, at room temperature and slightly alkaline pH, light absorption at around 450 nm promotes the transition to the FMN singlet excited state that decays with a half-time around 2 ns into a red-absorbing species that absorbs maximally at 660 nm (Kennis et al., 2003). This species, labeled $LOV2_{660}$, has been shown to be an FMN triplet state (Swartz et al., 2001; Kottke et al., 2003; Losi et al., 2002). $LOV2_{660}$ decays in microseconds into the metastable intermediate, which absorbs maximally at 390 nm and is labeled $LOV2_{390}$ (Swartz et al., 2001). The $LOV2_{390}$ intermediate thermally relaxes back to the ground state, $LOV2_{447}$. The rate of return to the ground state varies from a few seconds to many minutes (Salomon et al., 2000; Kasahara et al., 2002; Losi et al., 2002; Schwerdtfeger and Linden, 2003; Imaizumi et al., 2003). This long-lived metastable intermediate involves the formation of protein-FMN covalent bond. Specifically S-C bond is formed between the sulfur of cysteine and C(4a) carbon of FMN (Fig.1.7). Because this bond forms in microseconds, and decays in seconds, continuous illumination of LOV2 sample with blue light converts most of the sample into $LOV2_{390}$; this property has conveniently allowed

for structural and spectroscopic studies of the $LOV2_{390}$ intermediate. Conformation of the C-S bond in $LOV2_{390}$ was obtained in this way by X-ray crystallography, and NMR (Salomon et al., 2001; Crosson and Moffat, 2002). Formation of the cysteine-C(4a) bond during the photocycle was also inferred from difference infrared-absorbance spectroscopy (FTIR) (Swartz et al., 2002; Ataka et al., 2003).

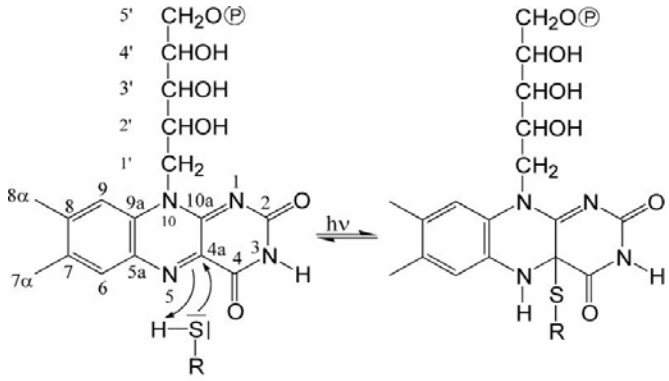

Figure 1.7 Proposed light induced formation of a covalent cysteinyl-C(4a) adduct of FMN and LOV2 apoprotein.

The flavin triplet state (^{3}FMN) has been proposed as a reactive intermediate in the primary blue-light induced reaction of LOV domains (Swartz et al., 2001). More specifically, ^{3}FMN has been suggested to be generated *via* intersystem crossing (ISC) from an excited singlet state precursor (Kennis et al., 2003), and to decay within a few microseconds by generating the FMN-cysteinyl photoadduct. The primary photoreaction has been claimed to proceed (i) *via* concerted mechanism (Crosson and Moffat, 2001) (ii) *via* an ionic mechanism, (Swartz et al., 2001) or (iii) *via* a radical-pair mechanism with a triplet-configured radical pair converting to a singlet-configured radical pair as a precursor for covalent-bond formation (Kay et al., 2003, Schleicher et al., 2004) (Fig. 1.8).

The concerted mechanism includes direct transfer of a proton from the cysteine thiol to N5 of the triplet state followed by formation of the S-C bond (Crosson and Moffat, 2001).

In the ionic mechanism, protonation of N5 either from cysteine C39 thiol (Crosson and Moffat, 2001; Kennis et al., 2003) or from an as yet unidentified acid group (Swartz et al., 2001), draws electronic density from the N5-C(4a) double bond, leaving C(4a) as a reactive carbo-cation that is attacked by the ionized sulphur or cysteine, forming the flavin–cysteinyl adduct.

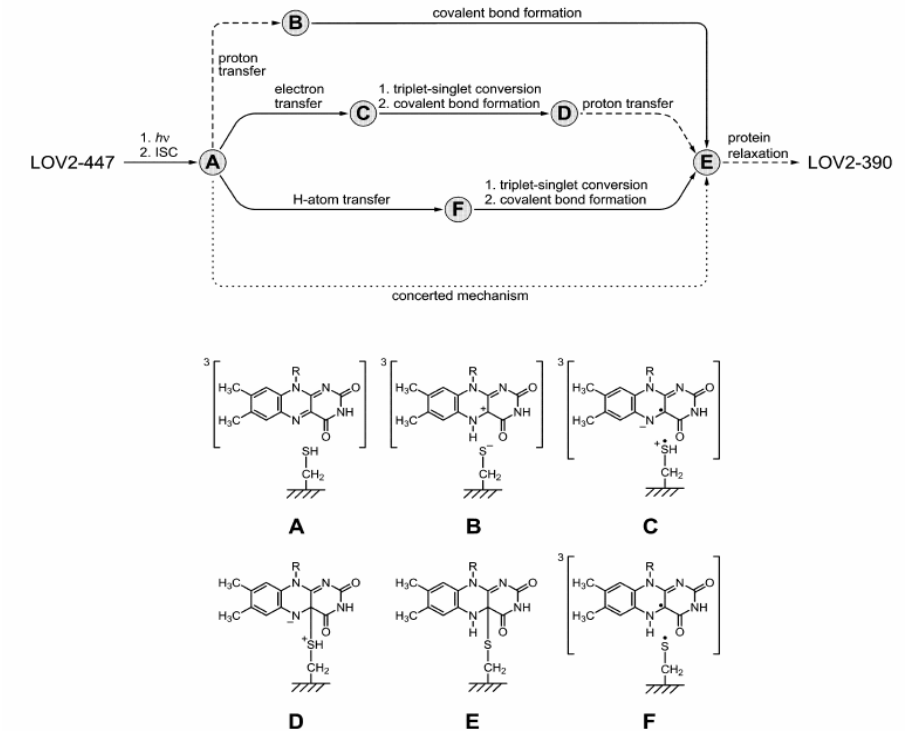

Figure 1.8 Suggested reaction pathway (top) and intermediates (bottom) of photoadduct (LOV-390) formation in wild-type LOV domains (Source: Schleicher et al., 2004).

The radical pair mechanism involves formation of a flavin semiquinone from the FMN triplet state in a one-electron photoreduction that may be followed by a proton transfer to give an anionic or neutral flavin radical. In this scenario, the sulfur donates either an electron (or then the proton) or a hydrogen atom resulting in formation of a sulfur radical and a neutral semiquinone radical. The adduct would form by recombination of the two radicals. The oat phot1-LOV2 triplet state absorption spectrum shows no evidence of a semiquinone (Swartz et al., 2001). It is possible that the triplet state is the rate limiting step, and that the rapid rate of disappearance of the semiquinone would not allow its transient accumulation and its detection in the absorption changes. Kay et al. (Kay et al., 2003) pointed out that protonation of the FMN triplet state is not necessarily the rate-limiting step in a radical-pair mechanism, whereas protonation of the triplet state should be a rate-limiting step in an ionic mechanism. The ionic mechanism would allow adduct formation in the triplet state, whereas the reaction-pair mechanism would require the reaction in a singlet state (antiparallel spins recombine to form a bond) (Kay et al., 2003).

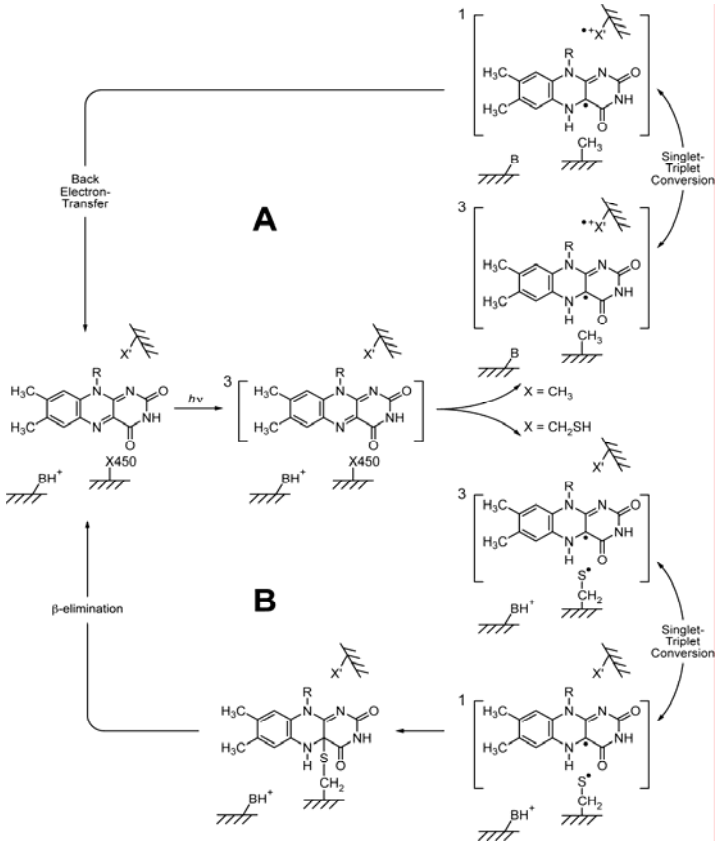

Figure 1.9 Hypothetical radical-pair mechanism for the formation of the $FMNH^{\bullet}$ radical in the LOV2 C450A mutant (A) or the FMN-C(4a)-cysteinyl adduct in wild-type LOV2 domains (B) after absorption of blue light by the FMN cofactor. (Source: Kay et al., 2003).

Blue light irradiation is conducive to the formation of a flavin radical instead of a photoadduct if the photoreactive cysteine residue is replaced by mutagenesis. The formation of the FMN-thiol adduct is not possible in the C450A mutant due to the absence of a thiol group. Upon irradiation with blue light, the LOV2 C450A mutant protein gives an optical absorption spectrum characteristic of a flavin radical characterized by absorption maxima at 570 and 605 nm. The radical state reverts spontaneously to the fully oxidized state of the FMN cofactor over a period of several minutes at room temperature.

Schleicher et al. (Schleicher et al., 2005) examined the photoreactivity of wild type and C450A mutant LOV domains of oat by optical spectroscopy and time resolved EPR at $T \leq 80$ K. The wild type proteins still formed an adduct *via* the photogenerated triplet state even at this non-physiological temperature. No paramagnetic species other than the photogenerated triplet FMN have been observed, implying that adduct formation does not require protonation of triplet FMN. So the radical pair mechanism (Fig. 1.9) can be considered as the most likely mechanism for adduct formation at low temperature. As the oxidising nature of triplet FMN is

virtually independent of the temperature, the generation of the photothioadduct *via* an electron transfer is active at ambient temperature as well.

1.2 DNA photolyase

1.2.1 General background

DNA photolyases are monomeric, 55 to 65 kDa flavoproteins widely found in microbes including bacteria, Archaea, and yeast (Sancar, 1994). Photolyase catalyze blue/UV-A light–dependent repair of DNA damage resulting from exposure to high-energy short-wavelength (<350 nm) UV light. There are two types of structurally related DNA photolyases, one called photolyase that repairs cyclobutane pyrimidine dimers and another called 6-4 photolyase that repairs pyrimidine-pyrimidone 6-4 photoproducts (Sancar, 1994; Sancar, 2000). Cyclobutane pyrimidine dimers (Pyr<>Pyr) and pyrimidine–pyrimidone (6–4) photoproducts are the predominant structural modifications resulting from exposure of DNA to ultraviolet light (Freidberg, 1995; Sancar, 1990) (Fig. 1.10). Both photoproducts result from 2π+2π cyclo-additions. The potentially mutagenic or lethal modifications (Otoshi et al., 2000) must be repaired in order to ensure cell survival and genetic stability. This can be affected by excision-repair or by photoreactivation mediated by DNA photolyases. Both enzymes have similar amino acid sequences (Nakajima et al., 1998; Todo, 1999).

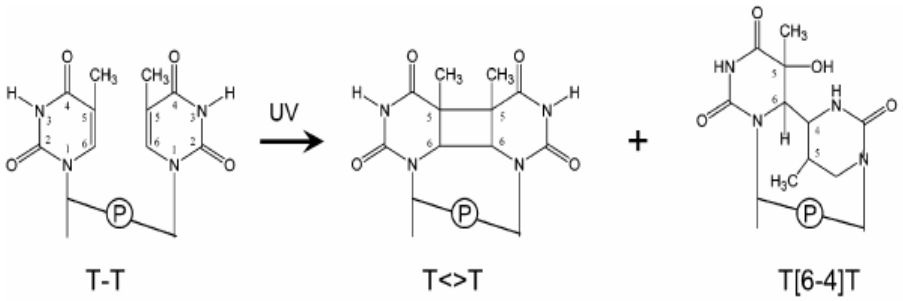

Figure 1.10 UV-induced DNA photoproducts. The two major lesions induced in DNA by ultraviolet irradiation are pyrimidine cyclobutane dimers and pyrimidine-pyrimidone (6-4) photoproducts. The figure shows the photoproducts that form between adjacent thymines. The same type of photoproducts may form between any type of adjacent pyrimidines T-T, T-C, C-T, and C-C except the (6-4) photoproduct does not form at C-T sites (Source: Sancar, 2003).

Photolyase contains two chromophores, a light-harvesting chromophore, which is either a folate (methenyltetrahydrofolate) or a deazaflavin, and a catalytic chromophore that is flavin adenine dinucleotide (FAD). Regarding the flavin cofactor of photolyases, a final point of interest is the redox status of the cofactor. FAD can be found in three redox states: oxidized,

one-electron-reduced (neutral blue radical or anionic red radical), and two-electron reduced (neutral or anionic) forms. The FAD is the essential cofactor both for specifically binding to damaged DNA and for catalysis (Sancar, 1994). The enzyme uses anionic reduced $FADH^-$ as redox-active cofactor (Jorns et al., 1987; Sancar et al., 1987; Payne et al., 1987). Subsequent to photoexcitation of the $FADH^-$ cofactor by direct absorption of near ultraviolet or visible light, the excited-state $FADH^-$ chromophore is believed to donate an electron to the pyrimidine dimer in the DNA, thus, generating a substrate radical anion and a neutral $FADH^\bullet$ radical (Payne et al., 1987; Kim et al., 1993; Kim and Sancar, 1993). The dimeric pyrimidine radical anion splits into pyrimidine monomers, and the excess electron is transferred back to the $FADH^\bullet$ cofactor to regenerate the initial redox state of the flavin, $FADH^-$ (Fig. 1.11).

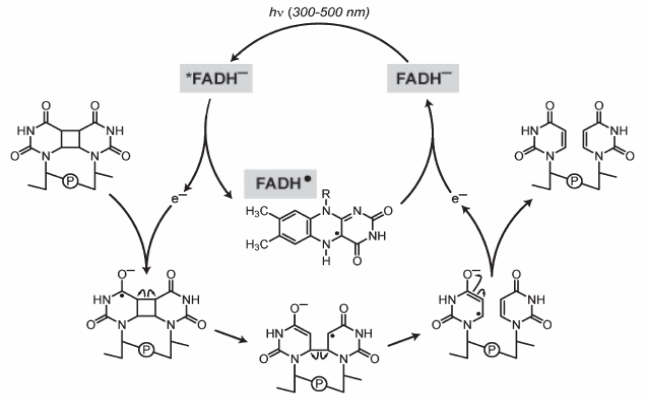

Figure 1.11 Putative repair reaction mechanism of DNA photolyase (Source: Sancar, 2003).

The "second chromophore" (MTHF or 8-HDF) is not necessary for catalysis and has no effect on specific enzyme-substrate binding. However, methenyltetrahydrofolate (MTHF) serves as light-harvesting cofactor in *E. coli* DNA photolyase (Sancar, 2003; Weber et al., 2005).

1.2.2 *Escherichia coli* DNA photolyase

The 3D structure of DNA photolyase from *E. coli* has been determined by X-ray crystallography.

Crystal structure: *E. coli* photolyase is composed of two well-defined domains: an N-terminal α/β domain (residues 1-131) and a C-terminal α-helical domain (residues 204-471), which are connected to one another with a long interdomain loop (residues 132-203) that wraps around the α/β domain (Fig. 1.12). The MTHF photoantenna is located in a shallow cleft between the two domains and partially sticks out from the surface of the enzyme. Two important contacts

are made with the apoenzyme. One is between the carbonyl side chain of Cys 292 and the other is between Lys 293 and the single Glu moiety of MTHF, which establishes a salt bridge that increases the affinity of the enzyme to the cofactor. The FAD cofactor is deeply buried within the α-helical domain and has an unusual U-shaped conformation with the isoalloxazine and adenine rings in close proximity. The FAD is held tightly in place by contact with 14 amino acids, most of which are conserved in the photolyase/cryptochrome family (Park et al., 1995; Komori et al., 2001). It should be noted that, even though the active form of flavin in photolyases is $FADH^-$, the crystal structures are those containing either the $FADH^\bullet$ blue-neutral radical or the FAD_{ox} form, and therefore, some subtle changes in the structure around flavin are expected in the active form of the enzyme. The flavin is accessible to the flat surface of α-helical domain through a hole in the middle of this domain (Fig. 1.12). The hole is too

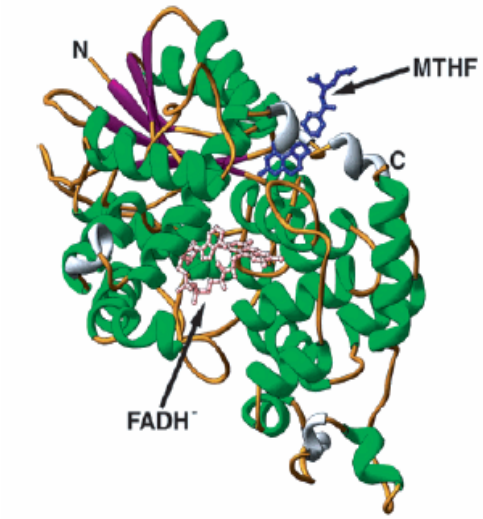

Figure 1.12 Crystal structure of *E. coli* photolyase: Ribbon diagram representation showing the N-terminal α/β domain, the C-terminal α-helical domain, and the positions of the two cofactors (Source: Sancar, 2003).

small to allow the diffusion of FAD in and out of the enzyme but allows easy accessibility to oxygen. This explains the relative ease with which $FADH^-$ is converted to $FADH^\bullet$ in most photolyase. A surface potential representation of the enzyme reveals a positively charged groove running the length of the molecule and passing through the entrance of the hole. These structural features led to the current model (Park et al., 1995) of binding to the DNA backbone through the positively charged groove, and flipping out the thymine dimer into the active site cavity lined with FAD and aromatic residues ("dinucleotide- flipping model"). In *E. coli* photolyase, the center to center distance between MTHF and FAD is 16.8 Å and the planes of the chromophores are nearly perpendicular to one another.

For DNA repair, the enzyme selectively binds to the damaged segment of the DNA in a light-independent step. Restoration of DNA functionality by enzymatic splitting of the CPD into the individual pyrimidine has been recognized as light induced electron transfer initiated by the absorption of near UV or visible light. DNA photolyase of *E. coli* is typically isolated as a blue-coloured protein carrying a neutral flavin radical, $FADH^{\bullet}$, as a chromophore. This catalytically inactive form can be converted to the active form ($FADH^{-}$) by photoreduction with the participation of the amino acid residue tryptophan 306, which is located approximately 14Å away, close to the surface of the enzyme (Kim et al., 1993; Gindt et al., 1999; Aubert et al., 1999; Aubert et al., 2000). It is believed to serve as the electron donor for this reaction, on the basis of site-specific mutagenesis studies (Li et al., 1991), time-resolved electron paramagnetic resonance (Kim et al., 1993) and transient optical absorption experiments (Heelis et al., 1993).

1.2.3 Reaction mechanism

Photolyase carries out catalysis by Michaelis-Menten kinetics. It binds S to form ES, which performs catalysis to yield EP, and then P dissociates. It differs from classic Michaelis-Menten kinetics in one important aspect, however, as the ES → EP transition is absolutely light dependent (Rupert, 1960; Rupert, 1962a,b; Harm and Rupert, 1968; Harm and Rupert, 1970; Harm and Rupert, 1976). The overall reaction may be summarized as follows. The enzyme binds a Pyr<>Pyr in DNA independent of light, and flips the dimer out of the double helix into the active site cavity to make a stable ES complex. The folate (or 8-HDF) then absorbs a near-UV/blue-light photon, and transfers the excitation energy (*via* dipole-dipole interaction) to flavin, which then transfers an electron to the Pyr<>Pyr; the 5-5 and 6-6 bonds of the cyclobutane ring are now in violation of Hückel rules, and therefore, the Pyr<>Pyr is split to form two pyrimidines. Concomitantly, an electron is transferred back to the nascently formed $FADH^{\bullet}$ to regenerate the $FADH^{-}$ form. To a first approximation, the reaction is a photon-powered cyclic electron transfer that does not result in a net gain or loss of an electron and hence, strictly speaking, is not a redox reaction.

1.2.4 *Escherichia coli* DNA photolyase E109A mutant

MTHF, the second cofactor of *E. coli* DNA photolyase, acts as a light-harvesting antenna. However, the protein has a relatively low affinity for this cofactor, which is therefore partially lost during purification (Hamm-Alvarez et al., 1990). Thus, individual wild-type enzyme

batches typically differ in their MTHF content. Heterogeneity of the enzyme with respect to the chromophores, however, is a serious handicap for spectroscopic studies. In order to obtain enzyme batches with reproducible absorption properties, a mutant protein was constructed that does not bind MTHF, but is nevertheless enzymatically active. X-ray structure analysis has shown that the position-2 amino group and the position-3 imino group of the pteridine moiety of MTHF form hydrogen bonds with the γ-carboxylic group of glutamic acid residue 109 (Park et al., 1995) (Fig. 1.13). Therefore the glutamic acid codon was replaced by a codon specifying alanine using PCR-driven site-directed mutagenesis (Schleicher et al., 2005).

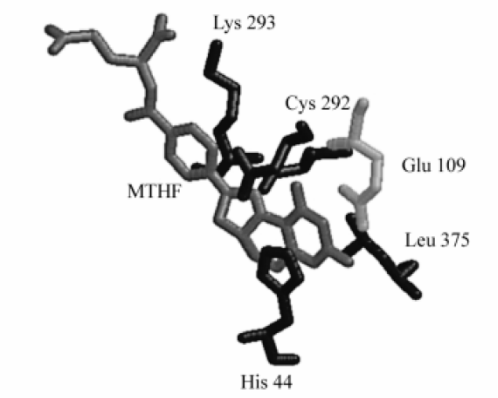

Figure 1.13 Protein environment to second chromophore MTHF. MTHF in dark grey, amino acids in black and the amino acid Glutamic acid 109 is represented in light grey (Source: Schleicher et al., 2005).

Replacement of the glutamic acid E109 with alanine results in a light harvesting cofactor - devoid enzyme which, however, has the same DNA substrate binding and EPR/ENDOR spectral properties as the wild – type protein (Weber et al., 2001).

1.3 Flavodoxin

1.3.1 General background

Flavodoxins are a group of relatively small flavoproteins (14 kDa - 23 kDa) consisting of one polypeptide chain, and containing a single molecule of noncovalently bound FMN (Mayhew and Ludwig, 1975). Flavodoxins are found in many microorganisms, where they serve to transfer electrons at low oxidation-reduction potentials. The flavin coenzyme can exist in three redox states, i.e., oxidized, one electron reduced or semiquinone, and two electron reduced or hydroquinone. During *in vivo* redox reactions the flavodoxins probably function only as one electron carriers, shuttling between the hydroquinone and the semiquinone states. *In vitro* the

flavin molecule shuttles between the oxidized, semiquinone and hydroquinone states. Flavodoxins act as redox mediators in the metabolism of pyruvate, hydrogen, nitrogen, sulfite, and pyridine nucleotides, transferring the reducing equivalents that are essential in these metabolic pathways. In some electron transfer reactions, such as that involving ferredoxin-$NADP^+$-reductase, flavodoxins are functionally interchangeable with ferredoxins, and can substitute for ferredoxins under iron limiting conditions (Mayhew and Tollin, 1992). Flavodoxins play a special role in several enzyme activation systems, where they are the required electron donors in essential priming or reactivation reactions. Flavodoxin dependent activations have been studied most thoroughly in *E. coli*, where flavodoxin provides reducing equivalents for the generation of protein radical intermediates in two key anaerobic enzymes, pyruvateformate lyase (Vetter and Knappe, 1971; Blaschkowski et al., 1982), and anaerobic ribonucleotide reductase (Bianchi et al., 1993). Physiologically, the semiquinone and the hydroquinone forms of FMN seem to be the most important oxidation states in flavodoxins (Mayhew and Tollin, 1992). However, there are indications that the semiquinone form of FMN in *E. coli* flavodoxin serves as an electron donor for the activation of methionine synthethase (Fujii et al., 1977).

1.3.2 Overall structure of *Escherichia coli* flavodoxin

Flavodoxin from *E. coli* contains 175 residues and has a molecular mass of 19.6 kDa (Osborne et al., 1991). It belongs to the class of long-chain flavodoxins, which are characterized by a loop inserted in the fifth β -strand.

Although *E. coli* flavodoxin interacts selectively with its acceptors in activation systems, the polypeptide fold of this flavodoxin is quite similar to several other “long-chain” flavodoxins that are 170-180 residues in length. All flavodoxins are α/β proteins with five parallel beta strands flanked on both sides by helices. The *E. coli* protein (Osborne et al., 1991) shares about 44% sequence identity with the long chain flavodoxins from *Anacystis nidulans* and *Anabena* 7120, which have been investigated both in single crystals by X-ray crystallography (Smith et al., 1983; Laudenbach et al., 1987; Rao et al., 1992; Burkhart et al., 1995), and in solution by NMR (Stockman et al., 1988a,b; Stockman et al., 1990; Clubb et al., 1991). Like homologous long-chain flavodoxins, *E. coli* flavodoxin contains a five-stranded parallel β-sheet and five α-helices. The β-strands were found to comprise the residues 3-8, 29-34, 48-56, 80-89, 114-116 and 141-145. The helices comprise residues 12-25, 40-45, 62-73, 98-108 and 152-166. In the long-chain flavodoxins, the final strand is broken into two sections

by an insertion of approximately 20 residues, and the insert itself is organized around a small antiparallel sheet (Ponstingl and Otting, 1997). In addition to the four long helices, a short helix is found before the start of β-strand 3 in *E. coli* and most other flavodoxins. Hydrogen bonded residues that comprise the small antiparallel sheet in the antiparallel hairpin beneath the flavin is formed by hydrogen bonding of residues 56-57 and 60-61. The C-terminus of *E. coli* flavodoxin extends for an extra seven residues beyond the termini found in the structures of *Synthecoccus 7942* or *Anabaena 7120*. The first part of this C-terminal extension has been modeled as a short helix that lies across the "top" of the molecule, and appears to be stabilized by a hydrophobic cluster involving Leu 168, Leu 170, Ile 173, Leu 174, and residues from the N-terminal end of the β-sheet (Hoover and Ludwig, 1997).

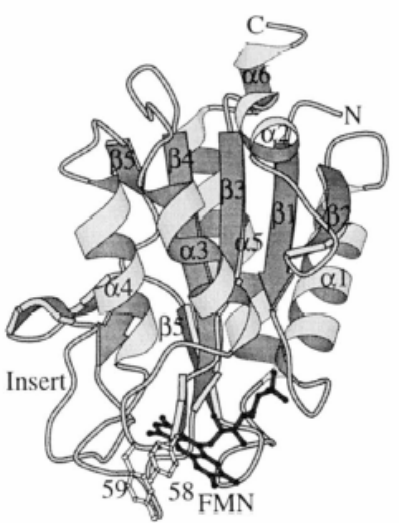

Figure 1.14 Ribbon drawing of *E, coli* flavodoxin (Kraulis, 1991). The five central parallel β-strands represented as arrows are covered by the major helices (α1, α3, α4, α5*)*. A small antiparallel sheet (on the left) is formed by residues from the insert that breaks strand five of the parallel sheet, and a short helix at residues 41-45 *(*α2*)* precceds β3*,* The helical portion of the C-terminal tail can be seen at the top of the drawing (Source: Hoover and Ludwig, 1997).

Flavodoxins bind FMN very tightly. Polypeptide segments connecting secondary structural elements are involved in binding of the isoalloxazine ring, and phosphate group of the FMN cofactor. The conserved sequence in the loop between β1 and α1 make a number of N-H···0 and O-H···O hydrogen bonds to phosphate oxygens of the cofactor. The conformation of this loop is the most invariant feature of the flavodoxin fold.

2 Materials and Methodology

2.1 Materials

2.1.1 Instruments

Acrylamide Gel Electrophoresis	Chamber and casting conditions for SE 250 Mighty Small II (Hoefer Scientific Instruments, San Francisco, USA)
Agarose Gel Electrophoresis	Chamber and gel carrier (Appligene, Heidelberg)
Autoclave	Sanoclav (Wolf, Geislingen)
Balance	1602 MP, Sartorius (Göttingen)
Centrifuges	high speed refrigerated centrifuge: RC2B, RC5B, and RC5B with GS3, GSA and SS34 rotors (Sorvall, Connecticut, USA)
Cuvette	Hellma-Quarzküvetten QS 1 cm (Hellma, Müllheim)
Eppendorf-Centrifuge	A14 (Jouan, Unterhaching)
Electroporator	Gene Pulse with pulse controller (Biorad, Munich)
Fermenter	BioFlo3000 (New Brunswick Scientific, Edison NJ, USA)
French Press	Cell Disruption Equipment Basic Z Model (Constant Systems LTD, Warwick, GB)
FPLC-Station	Control unit Gp-10, Fraction collector RediFrac, optical unit monitor Uvicord SII, Conductivity monitor, pumps P-500, mixer 0.6 ml, gradient valve Psv-50, injection valve V-7 and two-channel writer REC 102, (Pharmacia, Freiburg)
Heat block	Techne DRI-Block DB-2A
Hiprep 26/10 Desalting column	Amersham Biosciences Europe GmBH
HPLC Instrumentation	Pump: Pumpe 64 (Knauer, Bad Homburg, Germany); UV absorbance detector 440 (Waters), Fluroescence detector RF 530 (Shimadzu, Duisburg, Germany), dual pen recorder PM 8222(Philips), Preparative HPLC system with UV detector (Du Pont, Bas Homburg, Germany)

Incubator	Innova 4230 (New Brunswick Scientific Co., New Brunswick, NJ, USA)
NMR-Spectrometer	Bruker AC 250, AM 360 and DRX 500 (Bruker, Karlsruhe)
Photometer	Ultraspec 2000 UV/visible Spectrophotometer (Amersham Pharmacia Biotech, Freiburg)
pH-Meter	E603 with Standard glass electrode (Deutsche Metrohm, Filderstadt)
Peristaltic Pump	Braun, Melsungen, Germany
Rotation evaporator	Membrane pump-Vaccum pump (Vaccum brand GmbH & Co., Wertheim) Rotavapor RE 120 (Büchi, Germany), Water bath (Köttermann, Germany)
Table Vibrator	IKA-Vibrax-VXR (Goeddecke, Ingolstadt)
Ultrasonicator	Branson Sonifier 250 (Branson SONIC Power Company, Danbury, USA)
Ultrafiltration Chamber	Ultrafiltration cell 50 ml and 10 ml (Amicon, Witten, Westphalia)
Vaccum pump	MZ 2C (Vaccum Brand GmbH&Co./Wertheim)
Vaccum centrifuge	Roto-Vac 3 (Biotech-Fischer, Reiskirchen)
Video documentation	Fröbel Labortechnik, Wasserburg

2.1.2 Chromatographic materials

HPLC: Nucleosil 10-C18, Nucleosil, Nucleosil 100-7C-18 (Macherey Nagel, Düren, Germany), Lichrosorb 10-C-18 Merck, Damrstadt, Germany).

TLC: Cellulose, Kieselgel 40 (Merck, Damrstadt, Germany)

2.1.3 Chemicals and enzymes

Chemicals: FMN, FAD, Riboflavin, Sodium dithionite were purchased from Sigma (Deisenhofen). Labeled glucoses: [1-$^{13}C_1$]-, [2-$^{13}C_1$]-, [3-$^{13}C_1$]- and [U-$^{13}C_6$]glucose were purchased from Omicron (South Bend, Indiana,USA), and [U-$^{13}C_{11}$]tryptophan from Cambridge Isotope Laboratories (Andover, MA, USA).

Solvents for NMR Spectroscopy were purchased from: D_20 (99.9%, Isotec Inc. Ohio, USA), $CDCl_3$ (Aldrich, Steinheim).

Enzymes: Thrombin, Lysozyme, Pyruvate kinase was purchased from Sigma (Deisenhofen). DNaseI was purchased from Boehringer (Mannheim).

2.1.4 Culture medium

The components of media were dissolved in 1 litre of deionised water. The medium was sterilized by autoclaving (121°C, 1.3 bar, 20 min). For LB agar plates, 20 g/l agar was added to LB medium. Sterile antibiotics were added to cooled autoclaved medium. Medium marked with asterisk is sterile filtered.

LB (Luria Bertani)-Medium	10 g	Peptone
	5 g	Yeast Extract
	5 g	NaCl
LB Amp-Medium	1 l	LB-Medium autoclaved
	180 mg	Ampicilin
LB Amp-Kana-Medium	1 l	LB-Medium autoclaved
	180 mg	Ampicilin
	15 mg	Kanamycin
LB Kan-Ery-Medium	1l	LB-Medium autoclaved
	15 mg	Kanamycin
	10 mg	Erythromycin
SOC-Medium	20 g	Peptone
	5 g	Yeast Extract
	20 mM	Glucose
	10 mM	$MgSO_4$
	10 mM	NaCl
	10 mM	$MgCl_2$
	2.5 mM	KCl

Glycerin-Medium	70 %	LB-Medium
	30 %	Glycerin

M9-Mineral-Medium for *E. coli*:
10 % (v/v) M9-Salt concentrate
0.4 % (v/v) Vitamin-Mix
0.1 % (v/v) Spurenelement-Mix
5 g/l Glucose (Stock solution 500 g/l), ^{13}C glucose – 4g/l
1 g /l NH_4Cl (Stock solution 200 g/l), ^{15}N NH_4Cl – 5g/l
0.138 g/l $MgSO_4.H_2O$ (Stock solution 138 g/l; 1M)
5.5 mg/l $CaCl_2$ (Stock solution 5.5 g/l; 50 mM)

M9-Salt concentrates (10x):
120 g Na_2HPO_4
30 g KH_2PO_4
5 g NaCl
pH 7.5

Vitamin-Mix (250x)*:
20 mg/l Pyridoxamin-Hydrochloride
10 mg/l Thiamin-Hydrochloride
20 mg/l para-Aminobenzoic acid
20 mg/l Calcium-Pantothenat
5 mg/l Biotin
10 mg/l Folic acid
100 mg/l Cyanocobalamin (1/1000 Mannit-mixing)
20 mg/l Riboflavin for unlabeled culture

Spurenelemente-Mix (1000x)*:
16 g/l $MnCl_2 \cdot 4H_2O$
15 g/l $CuCl_2 \cdot 2H_2O$
27 g/l $CoCl_2 \cdot 6H_2O$
37.5 g/l $FeCl_3$
40.8 g/l Na-citrat
84 mg Zn-accetat $\cdot 2H_2O$
50 mg Na_2-EDTA

TSS:	3.5 g/l K_2HPO4
	60 g/l Tris-Base
	pH 7.4

2.1.5 Buffers and solution

Saline	0.9 % (w/v) NaCl in deionised water

SDS-polyacrylamide gel electrophoresis:

Acrylamide solution	194 g Acrylamide
(T=40 %; C=3 %):	6 g N, N´-Methylene-bisacrylamide
	in 500 ml Water
Ammonium peroxide sulphate solution (APS)	10 % (w/v)
Bromphenol blue solution	0.25 % (w/v)
Coomassie blue colouring solution	0.25 % (w/v) Coomassie-Blue R-250 45 % (v/v) Methanol
	9 % (v/v) Acetic acid
Electrophoresis buffer	25 mM Tris-HCl, pH 8.3
	192 mM Glycine
	0.1 % (w/v) SDS
Destaining solution I	50 % (v/v) Methanol
	10 % (v/v) Acetic acid
Destaining solution II	15 % (v/v) Methanol
	7.5 % (v/v) Acetic acid
SDS-PAGE sample buffer	5 % SDS
	30 % Glycerine
	60 mM Tris-HCl, pH 6.8
	10 % Saccharose
	3 % 2-Mercaptoethanol
	0.02 % Bromophenol blue
Stacking gel buffer	0.25 M Tris-HCl, pH 6.8
	0.2 % (w/v) SDS
Separating gel buffer	1.5 M Tris-HCl, pH 8.8
	0.4 % (w/v) SDS

Agarose gel electrophoresis:

Ethidium bromide-solution	1 µg/ml
Sample buffer for DNA-Gel	50 % (v/v) Glycerine 0.25 % (w/v) Xylencyanol 0.25 % (w/v) Bromophenol in TE-buffer
TAE-Puffer 50x	2 M Tris-Ac, pH 8.2 0.1 M EDTA
TE-Puffer 10x	100 mM Tris-HCl, pH 8.2 10 mM Na_2EDTA

Peqlab E.Z.N.A. Plasmid Miniprep Kit:

Solution I for resuspension:	50 mM Tris-HCl, pH 8.0 10 mM EDTA 40 µg/ml RNase A
Solution II for Lysis:	200 mM Natrium hydroxide 1 % (w/v) Natriumdodecylsulphate (SDS)
Solution III for Neutralization:	3 M Potassium acetate, with acetic acid adjusted pH 5.5
HB-buffer:	Washing for HiBind®-DNA-column
DNA-Wash buffer:	Washing for HiBind®-DNA-column

Protein determination:

Bradford-buffer:	2 g secondary Sodium phosphate 0.6 g primary Sodium phosphate 7 g Sodium chloride 0.2 g Sodium azide in 1 l Water, pH 7.2
Bradford-Reagent:	0.1 g Coomassie Blue G-250 100 ml 85 % Phosphoric acid 50 ml Ethanol in 1 l Water Overnight shaking, filtration and in 4°C storage.

Protein purification (phototropin, LOV domain):

Buffer A	50 mM Sodium dihydrogen phosphate
(Washing and equilibrating	300 mM Sodium chloride
buffer)	10 mM Imidazole
	0.02 % (v/v) Sodium azide
	pH 8.0
Buffer B	50 mM Sodium dihydrogen phosphate
(Elution buffer)	300 mM Sodium chloride
	1 M Imidazole
	0.02 % (v/v) Sodium azide
	pH 8.0
Buffer A'	50 mM Sodium dihydrogen phosphate
(Denaturating buffer)	300 mM Sodium chloride
	10 mM Imidazole
	0.02 % (v/v) Sodium azide
	8 M urea (for wild type)
	6 M guanidine hydrochloride (for mutant)
	pH 8.0
Buffer C	50 mM Tris
(Buffer for cleavage of	200 mM KCl
hisactophilin from LOV domain)	2.5 mM $CaCl_2$
	pH 7.5
Buffer D	25 mM Sodium dihydrogen phosphate
(Buffer for equilibration of LOV domain)	25 mM Potassium dihydrogen phosphate pH 7.0

Protein purification (DNA photolyase):

Buffer A (Breaking buffer)	50 mM	HEPES, pH 7.0
	10 mM	DTT
	100 mM	NaCl
	10 % (w/v)	Saccharose
Buffer B	50 mM	HEPES, pH 7.0
	100 mM	KCl
	10 mM	DTT

	10 % (v/v)	Glycerine
Buffer C	50 mM	HEPES, pH 7.0
	2 M	KCl
	10 mM	DTT
	10 % (v/v)	Glycerine
Buffer D	50 mM	HEPES, pH 7.0
	50 mM	NaCl
	10 mM	DTT
	10 % (v/v)	Glycerine
Buffer E	50 mM	HEPES, pH 7.0
	0.1 mM	KCl
	10 mM	DTT
	10 % (v/v)	Glycerine
Buffer F	50 mM	HEPES, pH 7.0
	1 M	KCl
	10 mM	DTT
	10 % (v/v)	Glycerine

Protein purification (flavodoxin):

Buffer A	100 mM Tris Hydrochloride
(Washing and equilibrating	500 mM Sodium chloride
buffer)	20 mM Imidazole
	0.02 % (v/v) Sodium azide
	pH 8.0
Buffer B	100 mM Tris Hydrochloride
(Elution buffer)	500 mM Sodium chloride
	500mM Imidazole
	0.02 % (v/v) Sodium azide
	pH 8.0
(Buffer C)	100 mM Tris Hydrochloride
(Dialysis buffer)	pH 8.0

2.1.6 Bacterial strain and plasmid

Table 2.1 Bacterial strain and plasmid (phototropin LOV domain)

Strain/plasmid	Relevant characteristics	Source
E. coli strain		
XL1-Blue	recA1, endA1, gyrA96, thi-1, hsdR17, supE44, relA1, lac[F', proAB, lacI^{q}ZΔM15, Tn10(tet^{r})]	Bullock et al., 1987
M15[pREP4]	lac, ara, gal, mtl, recA^{+}, uvr^{+}, [pREP4, Kan^{R}, lacI]	Stueber et al., 1990
E. coli ATCC 49980 (WP2)	genetic locus WP2 (trp^{-}, uvrA^{-}, malB^{-})	Minks et al., 1999; Budisa et al., 2001
Expression plasmids		
pNCO113	Expression vector for *E. coli*	Stueber et al., 1990
pNCO113-hisactophilin	pNCO113 vector with the gene coding for hisactophilin of *Dictyostelium discoideum* with 3´-*Bam*HI and *Hind*III cloning sites	Kay et al., 2003
pNCO113-hisactophilin (C49S mutant)	pNCO113 vector with a gene coding for a cystein-free mutant of hisactophilin of *D. discoideum* and a thrombin cleavage site with 3´-*Bam*HI and *Hind*III cloning sites	Prof. Dr. Markus Fischer, for this study
pNCO-HISACT-ASLOV1-syn	pNCO-HISACT-(C49S)-BH vector with the LOV1 domain (aa 130-244) of phototropin NPH1-1 of *A. sativa*	Prof. Dr. Markus Fischer, for this study
pNCO-HISACT-ASLOV2-syn	pNCO-HISACT-(C49S)-BH vector with the LOV2 domain (aa 404-559) of phototropin NPH1-1 of *A. sativa*	Prof. Dr. Markus Fischer, for this study
pNCO-HISACT-ACVLOV2-syn	pNCO-HISACT-BH vector with the LOV2 domain (aa 925-1032) of phototropin phy3 of *A. capillus-veneris*	Prof. Dr. Markus Fischer, for this study
pNCO-HISACT-ASLOV2C450A-syn	pNCO-HISACT-ASLOV2-syn with mutation C450A	Prof. Dr. Markus Fischer, for this study
pNCO-HISACT-ASLOV2C450A/W491A-syn	pNCO-HISACT-ASLOV2 C450A -syn with mutation W491A	Prof. Dr. Markus Fischer, for this study
pNCO-HISACT-ASLOV2C450A/W557A-syn	pNCO-HISACT-ASLOV2 C450A -syn with mutation W557A	Prof. Dr. Markus Fischer, for this study
pRFN4	Vector containing the rib-operon of *B. subtilis*	Illarionov et al., 2004

Table 2.2 Oligonucleotides used for the construction of the synthetic genes coding for *A. sativa* LOV1 and LOV2 domains, and *A. capillus-veneris* LOV2 domain.

Designation	Sequence (5´ to 3´)*
ASLOV1-1	ttcctccaaggttccggcacggatccagctgagattgccaagatccgtcaggctctggcaaatggttcgaac
ASLOV1-2	gcggtaccgtctttcttgtagttgaggacacggccgcagtagttcgaaccatttgccagagcctgacggatc
ASLOV1-3	caacatgaccggttacacatccaaggaagtggtaggtcgtaactgtcgtttcctccaaggttccggcacggatc
ASLOV1-4	cttcatccttgattggtgcaatggtcaggagattccagaatgcggtaccgtctttcttgtagttg
ASLOV1-5	ccaggtcacccaatcatgtacgcaagcgctggtttcttcaacatgaccggttacacatccaag
ASLOV1-6	ccttacttccacttgcatgccgatgaacttgaggacacgaccttcttcatccttgattggtgcaatgg
ASLOV1-7	gcactgtccgcattccaacagaccttcgtagtttcggacgccagccgtccaggtcacccaatcatgtacgcaag
ASLOV1-8	cttattataagcttattcagtgtatttacttacttccacttgcatgccgatgaa
ASLOV1-9	ataataataagatctgcactgtccgcattccaacagaccttc
ASLOV2-1	gcgcaaaattcgtgatgccatcgataaccaaacagaggtcactgtacagctgattaattatacaaag
ASLOV2-2	aggctgcaagtgaaagaggttccagaacttttttaccactctttgtataattaatcagctgtacagtgac
ASLOV2-3	aactgccgttttcttcaaggtcctgaaaccgatcgcgcgacagtgcgcaaaattcgtgatgccatcgataac
ASLOV2-4	ggacaccaataaagtactggacatcacccttctgatcacgcataggctgcaagtgaaagaggttccag
ASLOV2-5	agtttcttgcagttgacagaatattcgcgagaagaaattctgggtcgtaactgccgttttcttcaaggtcc
ASLOV2-6	cacgctcggccgcatcacggacatgttcggtaccatccaactggacaccaataaagtactggacatc
ASLOV2-7	gtcattactgacccacgtttgccagataatcccattatcttcgcgtccgatagtttcttgcagttgacagaatattc
ASLOV2-8	catcaatattttctgcagttttcttaatcagcatgacaccctcacgctcggccgcatcacggacatg
ASLOV2-9	ataataggatccgaatttcttgctactacacttgaacgtattgagaagaactttgtcattactgacccacgtttgccag
ASLOV2-10	cctctggacgcagattagcatctggaagttcttttgccgcctcatcaatattttctgcagttttcttaatc
ASLOV2-12	tattattataagcttagttagcccacaaatcctctggacgcagattagcatctgg
ACVLOV2-1	gaggaagtcctaggtaacaactgccgtttcctgcagggccgcggtactgatcgtaaagcagtgcag
ACVLOV2-2	gacatcgcgctgctccttgactgcatcacggatcagctgcactgctttacgatcagtaccgcggcc
ACVLOV2-3	catcttcgcgagtgaccggtttctggagctcacggagtatacacgtgaggaagtcctaggtaacaactgc
ACVLOV2-4	ccaaaaggcgcgcccacctttgtatagtttaaaacctgtacagtgacatcgcgctgctccttgactgc
ACVLOV2-5	aagtctttcgtgatcacagatcctcgtttaccagacaaccctatcatcttcgcgagtgaccggtttctg
ACVLOV2-6	ggacgtcgccatttttcatcacgcatgacttgaagatggaagagattccaaaaggcgcgcccacctttg
ACVLOV2-7	ataataggatccggtctggtaccacgcggtgagcgtatcggtaagtctttcgtgatcacagatcctc
ACVLOV2-8	tattattataagcttacatctcctgctgaactccgatgaaatattggacgtcgccattttcatcacgcatg

*recognition sites used for cloning are underlined

Table 2.3 Bacterial strain and plasmid (DNA photolyase)

Strain/plasmid	Relevant characteristics	Source
Strain		
Bacillus subtilis		
BR151[pBL1]	trpC2,lys-3,metB10 [pBL1,lacI,ery^r]	Williams et al., 1981
Expression Plasmids		
pBl1	Erythromycin resistant, 5.27 Kbp	Henner, 1990
p602E109A	p602-CAT with the phr gene of *E. coli* with mutation Glu109Ala	Schleicher et al., 2005
p602	Kanamycin resistant, 5.8 Kbp	Henner, 1990
p602-CAT	Expression vector for *B. subtilis*	Le Grice, 1990

Table 2.4 Bacterial strain and plasmid (*E. coli* flavodoxin)

Strain/plasmid	Relevant characteristics	Source
Strain		
E. coli strain		
M15[pQE30]	ac,ara,gal,mtl,recA$^+$,uvr$^+$,[pQE30,lacI,bla^r]	Rohdich et al., 2003
Expression plasmid		
pQEfldA	Expression vector of flavodoxin from *E. coli*	Rohdich et al., 2003

2.2 Molecular-biological method

2.2.1 Isolation of plasmid with PeQlab Plasmid Isolation Miniprep Kit

10 ml of fresh overnight culture with the plasmid was centrifuged (4000 RPM, 15 min, RT) and the supernatant discarded. The pellet was resuspended in 250 µl of solution I by vortexing and transferred to a microcentrifuge tube. No cell clumps should be visible after resuspension of the pellet. In order to lyse the cells, 250 µl solution II was added, mixed gently by repeatedly inverting the tube until the solution became viscous and slightly clear. Violent agitating, and vibrating were avoided, since this result in shearing of genomic DNA. The lysis reaction was not allowed to proceed for more than 5 min at ambient temperature. Afterwards 350 µl of solution III was added, and mixed by gentle and thorough inverting the tube. The

solution became cloudy. Subsequently the microcentrifuge tube was centrifuged (13000 RPM, 10 min, RT). The supernatant was pipetted carefully in a spin column and centrifuged again (13000 RPM, 1 min, RT). The flow through was discarded. The spin column was washed by adding 500 µl of HB buffer on a top of it and subsequent centrifugation (13000 RPM, 1 min, RT). Thereafter it was washed with 750 µl of DNA wash buffer, centrifuged (13000 RPM, 1 min, RT), and flow through was discarded. For complete removal of residual DNA wash buffer, the spin column was centrifuged for additional 1 min at 13000 RPM. For elution of plasmid DNA, spin column was placed in a clean microcentrifuge tube, 50 µl of bidistilled water was added to the top of the spin column and centrifuged (13000 RPM, 1 min, RT). By this method up to 20µg of plasmid DNA could be isolated from 10 ml of cell culture.

2.2.2 Agarose gel electrophoresis

For the analytic and preparative separation of DNA fragments, the agarose gel electrophoresis is used. Due to its negative charge, DNA molecules move in the electrical field towards the anode, whereby small molecules move faster in agarose gels than large molecules. Thus, this method can be used for determination of the size of DNA fragments, as well as DNA concentration in a sample and its purity. A determination of the fragment size becomes possible by the use of a DNA molecular weight standard (peqgold, Peqlab biotechnology GmbH). Agarose gel is used at concentrations of between 1 % to 3 %. Agarose gels were prepared by suspending agarose powder in TAE buffer and boiling the mixture until a clear solution is formed. The solution was cooled down to 45–50°C and poured onto the gel carrier, which is provided with a gel comb. After rigid agarose gel was formed (15–20 minutes at room temperature), it was placed in an electrophoresis chamber that was filled with TAE buffer so that the gel was completely submerged. The gel comb was removed from the gel and DNA samples (5 - 20 µl), as well as suitable molecular weight marker were pipetted into the wells of the gel. The electrophoresis chamber electrodes were connected to a constant current power supply (80 - 120 V) and the gel was run for 45–90 minutes. The colour marker bromophenol blue present in the sample buffer makes the progress of electrophoresis visible. The gel was then incubated 20 minutes in ethidium bromide solution (1 µg/ml), washed with distilled water. Ethidium bromide, which strongly intercalates within DNA, becomes highly fluorescent in UV light. That makes visible DNA bands containing ethidium bromide under illumination with UV light. The lower detection limit is about 10 ng of DNA per band.

DNA-Marker with following bands 10kb, 8kb, 6kb, 5kb, 4kb, 3.5kb, 3kb, 2.5kb, 2kb, 1500bp, 1200bp, 1031bp, 900bp, 800bp, 700bp, 600bp, 500bp, 400bp, 300bp, 200bp, 100bp was used.

2.2.3 Competent cells and transformation

Electrical competent cells were made according to protocol of Dower and coworker (Dower et al., 1988). Preculture, which was incubated at 37°C, not longer than 16 h, was inoculated into 1000 ml LB medium in 1:100. As soon as, the culture had achieved an optical density of 0.5-0.7 (with 600 nm), which corresponds to the middle logarithmic growth phase, it was placed on ice for 15 min. The cells should not warm up over 4°C throughout the experiment in order to avoid a reduction of the transformation rate. Afterwards the cells were centrifuged in 4°C precooled rotor with 4000 RPM for 20 minutes. The supernatant was discarded, and the pellet was resuspended in 10% ice-cold, sterile glycerine. This procedure was repeated twice, whereby first time the pellet was resuspended in 500 ml, the second time in 20 ml 10 % ice-cold, sterile glycerin. Then, centrifuged again (20 mins, 4000 RPM), the supernatant was discarded and the pellet was suspended in a final volume of 2 ml 10 % ice-cold, sterile glycerin. The suspension was aliquoted into sterile kryotubes and frozen in liquid nitrogen. This procedure results the cell concentration of 1-3x10^{10} cells/ml and the transformation rate approximately 3x10^{7} transformants/µg DNA.

Electroporation method of *E.coli* transformation

For the electrical transformation, following parameter was adjusted:

Capacity: 25 µF

Resistance: 200 Ω

Tension: 2,5 kV for cuvette with 2 mm gap width

1.8 kV for cuvette with 1 mm gap width

40 µl electrical competent cells was thawed in ice, and transferred into a sterile, precooled 1.5 ml eppendorf cap. To this, 2 µl plasmid DNA between 100 ng and 10 pg was added. Then the mixture of competent cells and DNA were transferred into the precooled electroporation cuvette, (gap width 0.2 cm). The well dried cuvette was put into the electroporation chamber, so that contact existed to the electrodes and parameters applied as specified above. The cells were removed immediately from the cuvette and suspended in 1 ml SOC medium. For

expression, the cells were incubated one hour at 37°C. Subsequently, the cell suspension was plated on LB medium with selective antiobiotics and incubated over night at 37°C.

2.2.4 Construction of an expression plasmid for LOV domain

Expression plasmid for *A. sativa* LOV1 domain, *A. sativa* LOV2 domain (wild type, C450A, C450A/W491A and C450A/W557A) and *A. capillus-veneris* phy3 LOV2 domain were constructed by Prof. Dr. Markus Fischer for this study.

2.2.4.1 Construction of expression plasmid for *Avena sativa* LOV1 NPH1-1 domain

The partially complementary oligonucleotides ASLOV1-1 and ASLOV1-2 were annealed and treated with a mixture of deoxyoligonucleotide triphosphates and DNA polymerase. The resulting 112 bp segment was elongated by a series of four PCR amplifications using pairwise combinations of oligonucleotides according to table 2.2 (oligonucleotides ASLOV1-3/ASLOV1-4, ASLOV1-5/ASLOV1-6, ASLOV1-7/ASLOV1-8, and ASLOV1-9/ASLOV1-8). The resulting 376 bp DNA fragment was digested with *Bgl*II and *Hind*III, and ligated into the plasmid pNCO113-hisactophilin(C49S mutant), which had been treated with *Bam*HI and *Hind*III affording the expression plasmid pNCO-HISACT-ASLOV1-syn (Table 2.1).

2.2.4.2 Construction of an expression plasmid for *Avena sativa* LOV2 NPH1-1 domain

The open reading frame coding for the LOV2 domain of *A. sativa* was constructed in analogy to the LOV1 gene described above. The synthesis was performed using pairwise combinations of oligonucleotides given in table 2.2 (ASLOV2-1/ASLOV2-2, ASLOV2-3/ASLOV2-4, ASLOV2-5/ASLOV2-6, ASLOV2-7/ASLOV2-8, ASLOV2-9/ASLOV2-10, and ASLOV2-9/ASLOV2-12). The resulting 501 bp DNA fragment was digested with *Bam*HI and *Hind*III and ligated into the plasmid pNCO113-hisactophilin(C49S mutant), which had been treated with the same restriction endonucleases affording the expression plasmid pNCO-HISACT-ASLOV2-syn (Table 2.1).

2.2.4.3 Construction of expression plasmid for *Adiantum capillus-veneris* phy3 LOV2 domain

The open reading frame coding for the LOV2 domain of *A. capillus-veneris* was constructed in analogy to the LOV1 gene described above. The synthesis was performed using pairwise combinations of oligonucleotides given in table 2.2 (ACVLOV2-1/ACVLOV2-2,

ACVLOV2-3/ACVLOV2-4, ACVLOV2-5/ACVLOV2-6, and ACVLOV2-7/ACVLOV2-8). The resulting 369 bp DNA fragment was digested with *Bam*HI and *Hind*III and ligated into the plasmid pNCO113-hisactophilin which had been treated with the same restriction endonucleases affording the expression plasmid pNCO-HISACT-ACVLOV2-syn (Table 2.1).

2.2.5 Construction of recombinant *Bacillus subtilis* strain expressing DNA photolyase E109A mutant

Recombinant *B. subtilis* strain; BR151 [pBl1] [p602E109A] expressing DNA photolyase E109A mutant was constructed by Dr. Erik Schleicher (Schleicher et al., 2005).

2.2.6 Construction of recombinant *Escherichia coli* strain expressing flavodoxin

Recombinant *E. coli* strain; M15[pQEfldA] expressing fldA was constructed by Dr. Felix Rohdich (Rohdich et al, 2003).

2.3 Protein-chemical methods

2.3.1 Culture preservation

Bacterial cultures were streaked on agar plates with appropriate antibiotics and stored at 4°C. In every four weeks, the new subcultures were prepared on fresh medium. For longer time storage, cultures were stored in liquid nitrogen or in -80°C. For stock culture, 8 ml over night culture was centrifuged, supernatant discarded, and cell pellete was resuspended in 1 ml 30 % Glycerin LB medium, which was transferred to sterile kryotubes, and stored in liquid nitrogen or in -80°C.

2.3.2 Microbial culture

Luria Bertani (LB) medium and minimal medium with the appropriate antibiotics were used as culture media. Culture medium supplemented with appropriate antibiotics was inoculated with an over night culture of bacterial strain in the ratio 1:100 and incubated at 30°C or 37°C in the incubator with shaking. With an OD_{600} of 0.5-0.7, IPTG in a final concentration of 1 mM was induced, and incubated further at 30°C for 5 h or at 37°C for overnight. The culture was harvested by centrifugation (20 min, 4000 RPM, 4°C), the cell pellete was washed with 0.9 % saline, recentrifuged (30 min, 4000 RPM, 4°C), and stored at -20°C till protein purification.

2.3.3 Expression test

A single colony from transformed cells was inoculated in LB medium with appropriate antibiotics and was grown over night at 37°C. 20 µl of this over night culture was inoculated into 200 ml mainculture with appropriate antibiotics. The culture was incubated at 37°C under shaking. After an OD_{600} of 0.5-0.7, IPTG was induced to a final concentration of 1 mM and further incubated 5 h at 37°C. The culture was then harvested by centrifugation (20 min, 5000 RPM). The cell pellete was then disrupted by ultrasonication, centrifuged, and supernatant checked for protein expression by means of SDS polyacrylamide gel electrophoresis.

2.3.4 SDS-polyacrylamide gel electrophoresis

The determination of the purity of protein fractions was measured using discontinuous sodium dodecylsulfate polyacrylamide gel electrophoresis (SDS-PAGE) according to the system of Laemmli (1970). SDS is an anionic detergent, which solubilizes and denatures proteins; SDS confers net negative charges to proteins. The proteins have then mobility, which is inversely proportional to their size or molecular mass.

The gel was prepared using the SDS-PAGE discontinuous buffer system. The components of the separating gel solution were mixed together, and then loaded into the slab deposited between two glass plates on the gel caster. The top of the gel was overlayed with isopropanol. The polymerisation of acrylamide was completed after 1 h. The stacking gel solution was prepared, and loaded on top of the separating gel (air bubbles avoided) in the presence of 10 wells comb. The polymerisation of stacking gel was completed after 20 min. The slab gel was placed on the SE 250 Mighty Small II electrophoresis system, which was connected to a cooling system. Proteins sample were mixed with SDS-sample buffer in ratio of 1:1. The mixtures were heated at 95°C for 10 min. Then the protein samples were loaded into the wells. Standard proteins were used as weight markers. The electrophoresis system was powered from a power supply with 20 mA per gel. After running for 2 h, the gel was removed carefully and stained in staining solution for 30 min. The gel was then destained with destaining solution for 1 hour.

Table 2.5 SDS-PAGE recipe (using the SDS-PAGE discontinuous buffer system)

Stock solution	Stacking Gel (4 %)	Separating Gel (15 %)
Acrylamide (40 %T, 3%C)	0.5 ml	3.5 ml
Stacking gel buffer	2.5 ml	-
Separating gel buffer	-	2.5 ml
Water	2.0 ml	3.75 ml
10% w/v APS	75 µl	100 µl
TEMED	5 µl	5 µl

As protein standard, protein marker with following bands protein was used: 66, 45, 36, 30, 20 and 13 kDa.

2.3.5 Protein expression

The genes of interest were cloned and overexpressed in the high copy vector pNCO113 or pQE30 (Qiagen) under the control of a T5 promoter, and a *lac* operator in *E. coli* host strains. The T5 promoter is a strong promoter, which is recognized by the RNA polymerase of *E. coli*. Expression of recombinant proteins encoded by these vectors is rapidly induced by the addition of isopropyl-β-D-thiogalactoside (IPTG), which binds to the *lac* repressor protein and inactivates it. Once the *lac* repressor is inactivated, the host cell's RNA polymerase can transcribe the sequences downstream from the promoter. The *E. coli* host cells strain M15[pREP4] contain multiple copies of the plasmid pREP4, which confers kanamycin resistance and carries the *lacI* gene (encoding the lac repressor). The *E. coli* host strain K12 XL1-Blue contains a mutated *lacI* gene ($lacI^q$) (encoding the lac repressor). For overexpression, the recombinant bacterial strains were grown as described below.

2.3.5.1 Expression of LOV domain

The recombinant *E. coli* strain was cultured in baffled 2 liter Erlenmeyer flasks containing 800 ml LB medium supplemented with appropriate antibiotics (for eg.15 mg/l Kanamycin and 180 mg/l ampicillin for *E. coli* M15 strain, and 180 mg/l ampicillin for *E. coli* Xl1 strain). The main culture was inoculated with an over night culture of bacterial strain in the ratio of 1:100, and incubated at 37°C in the incubator with shaking. With an OD_{600} of 0.5-0.7, final concentration of 1 mM IPTG was induced, and incubated further for overnight at 30°C. The culture was harvested by centrifugation (20 min, 4000 RPM, 4°C), afterwards the cell pellete

was washed with 0.9 % saline, recentrifuged (30 min, 4000 RPM, 4°C), and cell pellete was stored at -20°C till protein purification. ^{13}C labeling of the protein was obtained by cultivating *E. coli* (wild type/mutant) in minimal medium supplemented with components of minimal medium and appropriate antibiotics together with [U-$^{13}C_6$]-or [1-$^{13}C_1$]- or [2-$^{13}C_1$]– or [3-$^{13}C_1$]glucose or [U-$^{15}N_4$]NH_4Cl as carbon or nitrogen source, respectively.

For ^{13}C-tryptophan labeling of the protein, plasmid constructs specifying mutant LOV domains were transformed into the tryptophan auxotrophic *E. coli* ATCC 49980 (WP2) (Minks et al., 1999,; Budisa et al., 2001). The recombinant strains were grown in new minimal medium (NMM) (Budisa et al., 1997) containing [U-$^{13}C_{11}$]tryptophan.

2.3.5.2 Expression of DNA photolyase E109A mutant

The recombinant *B. subtilis* strain harbouring plasmids pBL1 and p602E109A was cultured in baffled 2 liter Erlenmeyer flasks containing 700 ml LB medium supplemented with 15 mg/l kanamycin, 10 mg/l erythromycin and 3 mg/l isotope labeled Riboflavin. The cultures were incubated at 32°C with shaking. At an optical density of 0.7 (600 nm), isopropylthio-β-d-galactopyranoside was added to a final concentration of 1 mM, and incubation was continued overnight. The cells were harvested by centrifugation and stored at -20°C.

2.3.5.3 Expression of *Escherichia coli* flavodoxin

The recombinant *E. coli* strain M15[pQEfldA] was cultured in baffled 2 litre Erlenmeyer flasks containing 800 ml LB medium supplemented with 150 mg/l ampicilin and 50 mg/l kanamycin. The cultures were incubated at 37°C with shaking. At an optical density of 0.7 (600 nm), isopropylthio-β-d-galactopyranoside (IPTG) was added to a final concentration of 1 mM, and incubation was continued further for 5 hours. The cells were harvested by centrifugation and stored at -20°C.

2.3.6 Protein extraction

The first step of a typical protein isolation procedure consists of cell disruption method, which releases the protein in soluble form from its intracellular compartment. For cell disruption, thawed cell pellete (5-10 gm wet mass) were suspended in respective buffer (10 ml per wet mass). Lysozyme (1 mg/g *E. coli* cells) and DNaseI (0.1 mg/g of *E. coli* cells) were added. The mixture was incubated at room temperature for 30 min with stirring. The French Pressure Cell (French Press) was performed for cell lysis. French Press achieves cell lysis by

subjecting the sample to high pressure (1.8 Kbar for *E. coli*) followed by sudden release to atmospheric pressure. The rapid change in pressure causes cells to burst. The extract obtained after lysis, termed homogenate was centrifuged (SS3 rotor, 15000 RPM, 4°C for 30 mins). The subsequent supernatant, called the crude extract was used for protein purification.

2.3.7 Protein purification

2.3.7.1 Purification of LOV domain

Nickel chelating chromatography: LOV Protein was purified by column chromatography, more specifically by immobilized metal affinity chelating chromatography (IMAC). To immobilize the metal ion on Chelating Sepharose Fast Flow, solution of 100 mM $NiSO_4$ was passed through the column, washed with distilled water to remove excess $NiSO_4$. The column was equilibrated with 10 column volumes of equilibrating buffer; Buffer A with the flow rate of 2 ml/min.

'As isolated LOV domain': The crude extract was applied to the column of Nickel Chelating Sepharose Fast flow (column volume – 15 ml), which had been equilibrated with buffer A (50 mM sodium phosphate, pH 8, containing 300 mM NaCl, 10 mM imidazole and 0.02 % sodium azide). The column was washed with 5 column volumes of buffer A, and was then developed with a linear gradient of 10 mM (buffer A) to 1000 mM imidazole (buffer B).

'Reconstituted LOV domain': The crude extract was passed through a column (volume – 15 ml), which had been equilibrated with buffer A. The column was washed with buffer A containing 8 M urea for Wild type protein, and 6 M guanidine hydrochloride for mutant protein until the flow through was colourless (to visual inspection), and then with buffer A containing 0.3-0.4 mM universally or selectively ^{13}C-labeled FMN or 0.4 mM 5-Deaza-FMN. The column was subsequently washed with buffer A, and the reconstituted protein was eluted with a linear gradient of 10 mM (buffer A) to 1000 mM imidazole (buffer B). The possible fusion protein (Hisactophilin domain and LOV domain) fractions as noted by UV absorption at 280 nm were analyzed by SDS PAGE.

After each purification, the column was regenerated by washing with 0.05 M EDTA/ 0.5 M NaCl followed by 0.2 M NaOH, and subsequently regeneration with 100 mM nickel sulphate.

Desalting and cleavage of fusion protein (Hisactophilin domain and LOV domain): Pre-packed columns of Sephadex™ G-25 gel filtration media; HiPrep™ 26/10 Desalting column

(10 × 2.6 cm, Amersham Biosciences) was used for cleavage of fusion protein. In a single step, the sample was desalted, exchanged into a new buffer, and low molecular weight materials were removed. The combined fractions of Hisactophilin fusion protein from the nickel-chelating Sepharose column were desalted, and transferred to a buffer C containing 50 mM Tris hydrochloride, pH 7.5, 200 mM KCl and 2.5 mM $CaCl_2$. Thrombin (5 units per mg of protein) was added, and the mixture was incubated overnight at room temperature with gentle shaking. Thrombin recognises the consensus sequence Leu-Val-Pro-Arg-Gly-Ser, cleaving the peptide bond between Arginine and Glycine. This is utilised in many vector systems, which encode such a protease cleavage site allowing removal of an upstream domain.

Nickel chelating chromatography: The Hisactophilin cleaved LOV protein was applied to nickel-chelating Sepharose column, which was then developed with buffer A. Cleaved LOV protein was collected in flow through, whereas hisactophilin protein and uncleaved fusion protein remained bound to the column. Yellow fluorescent fractions of cleaved LOV protein were combined and concentrated by ultrafiltration to a volume of 8 ml.

Desalting and equilibration of LOV protein by phosphate buffer: The LOV protein was transferred to buffer D containing 25 mM sodium/potassium phosphate, pH 7, on a HiPrep 26/10 desalting column. The possible protein fractions as noted by UV absorption at 280 nm were analyzed by SDS PAGE.

2.3.7.2 Purification of DNA photolyase E109A mutant

DNA Photolyase is an unstable enzyme, which is inclined to the self aggregation under oxidative conditions. The catalytic cofactor FAD can be present in three different oxidation states, which can be converted into one another dependent upon light and oxygen. All the purification work with this enzyme was therefore accomplished under argon atmosphere in order to prevent a change of oxidation stages.

The recombinant DNA photolyase E109A mutant (blue radical form) was isolated by a sequence of three chromatographic steps. The entire purification procedure was carried out in a single day.

Coloring material affinity chromatography: The principle of the coloring material affinity chromatography is based on the interaction of coloring materials with protein, which is responsible mostly for the binding of cofactors such as ATP, NADH, and NADPH. Since the reciprocal effects decrease with the salt concentration, protein can be eluted from the column with rising salt gradients. The column of Blue Sepharose (Cibacron coloring material) (Pharmacia, Freiburg; Column volume: 45 cm^3) was first equilibrated with 3 column volume of buffer B and the crude cell extract applied to the column. The column was washed with 10 column volumes of buffer B and protein then eluted with increasing salt (potassium chloride) gradients (buffer C). All steps were accomplished with flow rate of 4 ml/min. The fractions, which contained the protein, were combined. For the exchange of the buffer two different methods were used: first of all the Ammonium sulphate precipitation and secondly a desalting column.

Ammonium sulphate precipitation: The solubility of a protein in the aqueous environment depends strongly on the concentration of dissolved salts. With high ionic strength, the solubility of a protein lowers due to competition between salt ions and protein around the solvated molecules. Thus a simple and fast concentration and a simultaneous exchange of buffer of a protein solution can be achieved easily through 'salting out'. Most frequently due to its good solubility in water and high ionic strength, ammonium sulphate is used. The combined photolyase fraction was incubated with ammonium sulphate solution (0.43 g/ml) with stirring for 2 minutes and centrifuged (6000 RPM, 10 min, 4°C). The precipitate was harvested by centrifugation and dissolved in 5 ml buffer D containing 50mM NaCl for the next desalting step.

Desalting column: Desalting column; HiPrep 26/10 Desalting was used with an exclusion volume of 5 kDa. The column was equilibrated with 2 column volume of buffer D. The protein sample was applied into column maximally 10 ml and eluted with flow rate of 5 ml/min. Protein containing fractions were combined.

Affinity chromatography: For affinity chromatography the column material used was Heparin Sepharose CL-6B (Pharmacia, Freiburg). The material consists of 6% transverseinterlaced Agarose, which contains 3 mg Heparin/ml column volume. This material exhibits an affinity for oligonucleotide binding material. The column was equilibrated first

with 3 column volume buffer E. The protein solution in buffer D was applied to column. Column was washed with 10 column volume of buffer E, and then eluted with increased salt gradient of 0.1-1 M of KCl (buffer F). All steps were accomplished with flow rate of by 5 ml/min. Protein containing fractions, as shown by chromatogram were combined. The enzyme can be stored without loss of activity at -80°C.

Recovery of riboflavin: The non metabolized isotope-labeled riboflavin was recovered as described below. After cell harvesting, the collected supernatant was applied on a Florisil column (V = 100 ml) and washed with water (3 times column volume). Subsequently isotope labeled riboflavin was eluted with a mixture of 50% (v/v) acetone, 50 % (v/v) water. The eluate was concentrated under reduced pressure to approximately half volume and neutralized with HCl. Then the solution was completely dehydrated in the lyophilization unit. Riboflavin was then recovered by recrystalisation with water.

2.3.7.3 Purification of *Escherichia coli* flavodoxin

The crude cell extract (supernatant) was applied to a column of Ni-chelating Sepharose FF (Amersham Pharmacia Biotech; column volume, 20 ml), which had been equilibrated with 100 mM Tris hydrochloride, pH 8.0, containing 0.5 M sodium chloride and 20 mM imidazole (flow rate, 2 ml/min). The column was washed with 100 ml of 100 mM Tris hydrochloride, pH 8.0, containing 0.5 M sodium chloride and 20 mM imidazole, and was then reconstituted with 0.5 mM of isotope labeled FMN. The column was subsequently washed with buffer A, and the reconstituted protein was eluted with a linear gradient of 20 mM (buffer A) to 500 mM imidazole (buffer B) in 100 mM Tris hydrochloride, pH 8.0, containing 0.5 M sodium chloride (total volume, 100 ml). Purity of flavodoxin was determined by SDS-PAGE. Pure fractions were combined, and dialyzed overnight against 100 mM Tris hydrochloride, pH 8.0.

2.3.8 Protein concentration determination

The amount of protein was determined by the Commassie Brilliant Blue Dye (Bradford) method modified by Read and Northcote (1981). 50 µl protein sample was added to 950 µl of Bradford reagent in a 1 ml cuvette. As a reference, 50 µl of buffer without protein was mixed with 950 µl of Bradford reagent. The absorbance was measured at 595 nm after 2 minutes incubation at room temperature. The amount of protein was estimated from a standard curve using bovine serum albumin as standard protein.

Protein concentration was determined photometrically by optical spectroscopy in UV/vis range obeying Beer-Lambert's law;

$A = \varepsilon\lambda cl$,

where A is absorbance (no units, since A = log10 P_0/P), ε is the molar extinction coefficient at wavelength λ with units of M^{-1} cm^{-1} c is the path length of the sample that is, the path length of the cuvette in which the sample is contained, expressed in cm. l is the concentration of absorbing solution, expressed in mol l^{-1}.

Determination of concentration of LOV domain:

The concentration of protein was determined using molar extinction coefficient for LOV1 of *A. sativa* (ε_{449} = 12,200 $M^{-1}cm^{-1}$), LOV2 of *A. sativa* (ε_{447} = 13,800 $M^{-1}cm^{-1}$) (Salomon et al., 2000) and LOV2 of *A. capillus-veneris* (ε_{450} = 11,200 $M^{-1}cm^{-1}$) (Christie et al., 1999).

Determination of concentration of DNA photolyase:

The UV/vis spectrum of $FADH^{\bullet}$ in DNA photolyase exhibits characteristic absorption bands at 500, 580 and 625 nm, rendering the enzyme blue at higher concentrations. Blue fractions; neutral radical form of photolyase was measured photometrically at 580 nm (molar extinction coefficient = 4800 $M^{-1}cm^{-1}$) (Jorns et al., 1990).

Determination of concentration of *E. coli* flavodoxin:

Flavodoxin concentration was determined by measuring the absorbance at 464 nm (molar extinction coefficient = 8420 $M^{-1}cm^{-1}$) (Jenkins, 1994).

2.3.9 Concentrating protein solution through ultrafiltration

Concentration of protein by ultrafiltration proceeds by forcing the liquid in a protein solution through a membrane which retains the protein of interest. Agitating cells of 10 ml and 50 ml volumes (Amicon, Witten, Westphalia), and concentrator with C30 membrane of the company Pall Gelman (Ann Arbour, USA) were used for this purpose. The exclusion limit of the membrane was selected in order to hold the target protein above membrane. LOV domain and flavodoxin was concentrated by agitaiting cell and stored at -80°C. Photolyase was concentrated using concentrator. The photolyase sample was stored in oxygen free, dark kryotube at -80°C.

2.3.10 Preparation of cofactor

2.3.10.1 Preparation of random isotpologue libraries of 6,7-dimethyl-8-ribityllumazine by *in vivo* biotransformation

Random isotopologue libraries of 6,7-dimethyl-8-ribityllumazine was prepared by *in vivo* biotransformation (Illarionov et al., 2004).

6,7-dimethyl-8-ribityllumazine universally labeled with ^{13}C, and/or ^{15}N is obtained by biotransformation *in vivo*. A recombinant *E. coli* strain; M15[pREP4, pRFN4] carrying a plasmid for the efficient synthesis of the ribABGH genes converts glucose into the riboflavin precursor, 6,7- dimethyl-8- ribityllumazine. Fermentation of $[U^{13}C_6]$glucose affords $[U^{13}C_{13}]$lumazine that can be converted into $[U^{13}C_{17}]$riboflavin by treatment with riboflavin synthase. Not only $U^{13}C$ labeled glucose, the use of single labeled glucose substrates specifically carrying ^{13}C in position 1, 2 or 3 can be used as starting material. In such case, the labeled starting material is converted by intermediary metabolism into complex mixtures of carbohydrate isotoplogues, which can be used by the cells as starting material for coenzyme biosynthesis. The product mixtures constitute random isotopologue libraries.

Bacterial Culture - Recombinant *E. coli* strains were grown overnight at 37°C in shaking flasks containing 100 ml of LB medium supplemented with 50 mg of ampicillin and 15 mg of kanamycin per liter. Cells were collected by centrifugation (5000 RPM, 4°C, 10 min), and were resuspended in 0.8 l of M9 medium supplemented with vitamins, trace elements, and ampicillin (50 mg per liter), as well as ^{13}C-labeled glucose (4 g/l) and/or $^{15}NH_4Cl$ (2 g/l). The suspensions were incubated at 37°C with shaking. After incubation for 13 h, cell suspensions were centrifuged; the cells were discarded.

Isolation of 6,7-Dimethyl-8-ribityllumazine - Supernatants of bacterial cultures were passed through columns of Florisil, which were then washed with 2 column volume of water, and developed with a mixture of 50 % (v/v) acetone, 50 % (v/v) water. Eluates were evaporated to a small volume under reduced pressure and were then lyophilized. The residue was dissolved in 2 ml of 50 mM hydrochloric acid and applied to a column of Hypersil RP 18 (20 x 250 mm), which was developed with a mixture of methanol/formic acid/water (25:1:288, v/v). The retention volume of 6,7-dimethyl-8-ribityllumazine was 160 ml.

HPLC- Analytical high performance liquid chromatography was performed with an RP18 column (5 µm, 4 x 250 mm), which was developed with a mixture of methanol/formic acid/water (25:1:288, v/v). The flow rate was 1.5 ml/min. The effluent was monitored photometrically at 408 and 470 nm.

2.3.10.2 Preparation of random isotopologue libraries of riboflavin by enzymatic synthesis

A solution (total volume, 20 ml) containing 100 mM Tris, pH 8, 10 mM $MgCl_2$, 3 mg (0.8 mM) of [2-$^{13}C_1$]- or [3-$^{13}C_1$]glucose, 3.5 mg (0.8 mM) of phosphoenol pyruvate, 0.5 mg (0.05 mM) of ATP, 6 mg (2.1 mM) of 2-oxoglutaric acid, 0.6 mg of NAD (0.04 mM), 2.5 mg (2.3 mM) of NH_4Cl, 5 mg (0.8 mM) of a ^{13}C-isotopologue mixture of 6,7-dimethyl-8-ribityllumazine obtained by biotransformation of [2-$^{13}C_1$] or [3-$^{13}C_1$]glucose, 5 units of hexokinase, 5 units of pyruvate kinase, 5 units of glucose 6-phosphate dehydrogenase, 5 units of glutamate dehydrogenase, 5 units of 6-phosphogluconate dehydrogenase, 2 mg of 3,4-dihydroxy-2-butanone 4-phosphate kinase, 2 mg of lumazine synthase and 4 mg of riboflavin synthase was incubated at 37°C for 4h. The reaction was monitored by TLC (Cellulose F, Merck AG, Darmstadt, Germany; eluent, 3% (w/v) ammonium chloride).

2.3.10.3 Preparation of ordered isotopologue libraries of riboflavin

Selectively labeled riboflavin: [xylene-$^{13}C_8$]Riboflavin; [6,8α-$^{13}C_2$]riboflavin; [5a,8-$^{13}C_2$]riboflavin; [7,9a-$^{13}C_2$]riboflavin; [7α,9-$^{13}C_2$]riboflavin; [4,10a-$^{13}C_2$]riboflavin; [4a-$^{13}C_1$]riboflavin were obtained from Dr. Werner Römisch (Römisch et al., 2002).

2.3.10.4 Preparation of flavin mononucleotide (FMN)

A solution (total volume of 20 ml) containing 100 mM Tris, pH 8.0, 10 mM $MgCl_2$, riboflavin (20 mg), ATP (1.5 mg), PEP (15 mg), Pyruvate kinase (10 units), and Flavokinase from *Schizosacharomyces pombe* (2 mg) was incubated at 37°C. The completion of the reaction (typically after about 16 h) was monitored by TLC (Cellulose F, Merck AG, Darmstadt, Germany; eluent, 3 % (w/v) ammonium chloride. Often the solution could be used for the reconstitution for flavoprotein directly. If further purification of the FMN was necessary, protein was precipitated by addition of trichloroacetic acid and centrifuged. Subsequently, the solution was neutralized and applied on Sep Pak C18-cartridge (Waters, Milford, USA). The column was washed with water and flavin was eluted with methanol. The yellow fractions of the eluate was combined and evaporated under reduced pressure.

2.3.10.5 Preparation of 5-deaza-FMN

5-deazariboflavin was prepared by Dr. Stefan Hecht. A reaction mixture containing 100 mM Tris buffer, pH 8, 10 mM magnesium chloride, 1.5 mg ATP, 20 mg 5-deazariboflavin, 15 mg

phosphoenol pyruvate, 10 units of pyruvate kinase, and 2 mg of Flavokinase from *S. pombe* was incubated at 37°C for 16 h. The conversion to 5-deaza-FMN was monitored by Thin layer Chromatography (Cellulose F, Merck AG, Darmstadt, Germany; eluent, 3 % (w/v) ammonium chloride). The mixture was used without purification for the reconstitution procedure.

2.3.10.6 Preparation of tetraacetylriboflavin (TARF)

Tetraacetylriboflavin (TARF) was prepared according to a published procedure (Müller, 1971). 5 mg of riboflavin was suspended in 10 ml of a mixture of glacial acetic acid, and acetic anhydride (1:1; v/v); 0.5 ml of 1 M perchloric acid was added carefully with stirring within 10 minutes. A 4-fold volume of water was added to the clear solution, and the reaction mixture was extracted with chloroform. The separated organic phase was washed three times with water and dried with anhydrous sodium sulphate. The suspension was then filtered, and the filtrate evaporated to dryness under reduced pressure at 30°C. The compound was dissolved in 0.5 ml deuterated chloroform.

2.3.11 Isolation of tryptophan

Bacterial cell mass was suspended in 2 M barium hydroxide and was boiled under reflux for 24 h. The solution was neutralized with gaseous carbon dioxide, and the precipitate of barium carbonate was removed by centrifugation. The residue was dissolved in 100 mM ammonium formate. The solution was applied to a reversed phase HPLC column (250 × 16 mm) that was developed with 100 mM ammonium formate**.** The eluent was monitored photometrically at 278 nm. Aliquots were also spotted on cellulose thin layer plates that were developed with a mixture of butanol:acetic acid:water (30/20/10; v/v) and viewed by ninhydrin reaction. The retention volume of tryptophan was 192 ml. Fractions were combined, and concentrated to dryness under reduced pressure and dissolved in 5 ml of water. The solution was applied to a reversed phase HPLC column (250 × 16 mm) that was then developed with 5 % aqueous methanol. The retention volume of tryptophan was 88 ml. Fractions were combined and concentrated to dryness under reduced pressure.

2.4 Spectroscopic method

2.4.1 Optical spectroscopy

Protein concentrations were controlled by optical absorption spectroscopy using Ultraspec 2000 UV/visible spectrometer (Amersham Pharmacia Biotech, Frieburg).

2.4.2 NMR spectroscopy

NMR spectra were measured at 17°C with a 500 MHz spectrometer from Bruker Instruments, Karlsruhe, Germany. Precision NMR tubes (5 mm; Wilmad) were used for the acquisition of the spectra. ^{13}C NMR chemical shifts were referenced to internal dioxane (67.84 ppm relative to tetramethylsilane). ^{15}N NMR chemical shifts were referenced to external [5-^{15}N] 6, 7-dimethyl-8-ribityllumazine (327 ppm relative to liquid ammonia), and ^{31}P NMR chemical shifts were referenced to external 85 % (v/v) phosphoric acid (0 ppm). The acquisition of ^{13}C and ^{31}P NMR spectra required 5-20 hours; the acquisition of ^{15}N NMR spectra required more than 60 h.

For irradiation of LOV protein, samples were irradiated with blue light emitted by a photodiode (455 nm, 175 mW, Luxeon Star/O Batwing, Lumileds Lighting, San Jose, CA) inside the magnet via a flexible quartz optical fiber, whose conical tip was immersed into the solution of the NMR tube 1.5 cm above the magnetic center. Typical NMR samples were completely bleached within a period of 5 min. Spectra were recorded after that time with continuous illumination.

The solvent for LOV protein was 25mM sodium/potassium phosphate, pH 7.0, containing 10 % (v/v) D_2O for the ^{2}H signal to lock the magnetic field and the sample volume of 0.5ml with sample concentration ranging from 0.8 to 1.5 mM.

Flavodoxin samples for ^{15}N and ^{13}C-NMR measurements contained 100 mM Tris buffer pH 8.0. Protein concentrations ranged from 0.8 to 1.5 mM. The samples contained 10% D_2O (v/v) for the ^{2}H signal to lock the magnetic field. Precision NMR tubes (5 mm; Wilmad) were used for the acquisition of the spectra. Reduction of the protein was conducted by the addition of sodium dithionite solution to the anaerobic protein solutions. Anaerobic protein was obtained by dialysing protein solution against the anaerobic dialysis buffer (100 mM Tris buffer pH 8.0) overnight. Anaerobic condition was maintained by working under the glove box and using the special air tight NMR tube.

2.4.3 Circular dichroism

The circular dichroism (CD) spectra were recorded on a Jasco J-715 spectropolarimeter with temperature controller PFD-350S connected to the software program J-700 for Windows. The spectra were taken at 20°C in quartz glass cuvettes with a path length of 0.1 cm. The spectra were collected between 200 and 400 nm, with a scanning speed of 500 nm/min, the response of 0.5 sec, the band width of 1.0 nm, and the average of 5 scans was reported.

3 Results and Discussion

3.1 Phototropin LOV domain

3.1.1 Carbon isotopologue editing of FMN bound to LOV domain

3.1.1.1 Isolation of LOV domain

Isotopologue mixtures of 6,7-dimethyl-8-ribityllumazine were prepared by *in vivo* biotransformation of ^{13}C-labeled glucose using a recombinant *E. coli* strain (Illarionov et al., 2004). These isotopologue mixtures were then used as starting material for the preparation of isotopologue mixtures of FMN by enzyme-assisted synthesis. More specifically, the transformation of 6,7-dimethyl-8-ribityllumazine (**3**, Fig. 3.1) into riboflavin catalyzed by the enzyme, riboflavin synthase, proceeds as a dismutation, whereby two equivalents of 6,7-dimethyl-8-ribityllumazine (**3**, Fig. 3.1) are transformed into one equivalent each of riboflavin (**5**, Fig. 3.1), and 5-amino-6-ribitylamino-2,4(1H,3H)-pyrimidinedione (**4**, Fig. 3.1).

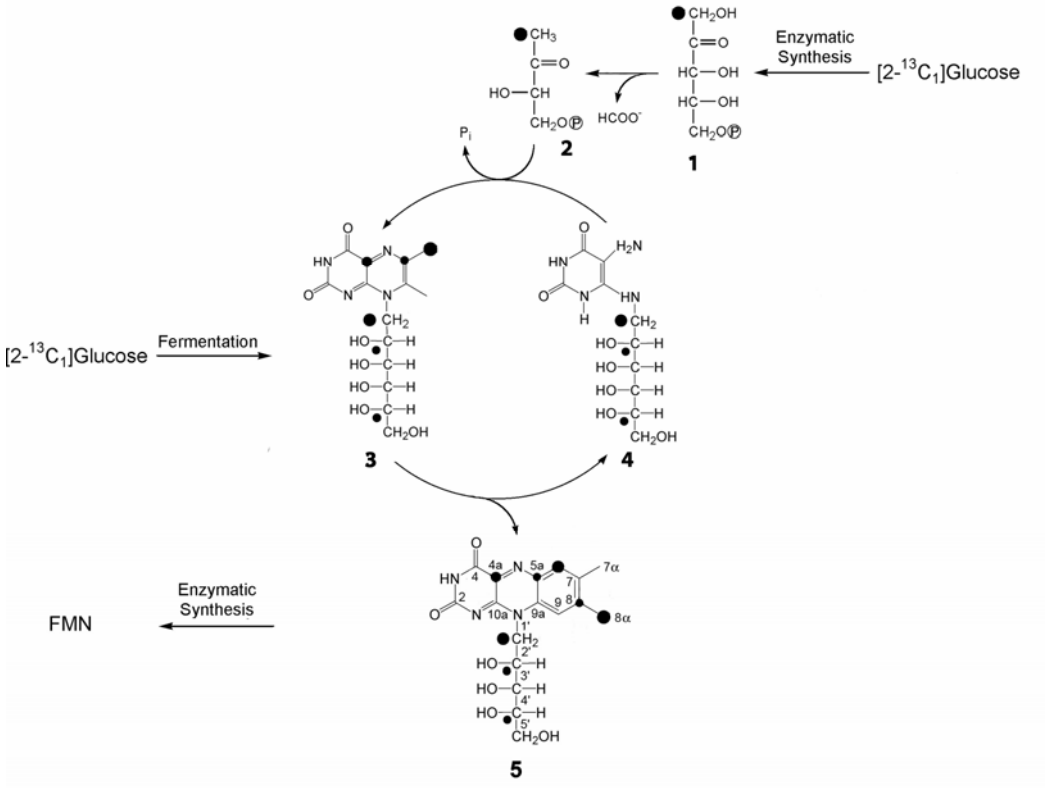

Figure 3.1 Synthesis of isotopologue libraries of FMN from [2-^{13}C$_1$]glucose. 1) Ribulose 5-phosphate; 2) 3,4-dihydroxy-2-butanone 4-phosphate; 3) 6,7-dimethyl-8-ribityllumazine; 4) 5-amino-6-ribitylamino-2,4(1*H*,3*H*)-pyrimdinedione; 5) riboflavin.

In order to avoid the inherent loss of isotope-labeled precursor, the second product 5-amino-6-ribitylamino-2,4(1*H*,3*H*)-pyrimidinedione (**4**, Fig. 3.1) resulting from the dismutation can be

reconverted into 6,7-dimethyl-8-ribityllumazine (**3**, Fig. 3.1) by treatment with lumazine synthase using 3,4-dihydroxy-2-butanone 4-phosphate as cosubstrate. The cosubstrate can be prepared in appropriately ^{13}C-labeled form by enzymatic conversion of ^{13}C-labeled glucose. By that approach, the yield of riboflavin based on isotope-labeled 6,7-dimethyl-8-ribityllumazine (**3**, Fig. 3.1) can be optimized.

The riboflavin arising by *in vitro* biotransformation can be converted into FMN by treatment with riboflavin kinase; ATP required as kinase substrate can be conveniently recycled using phosphoenol pyruvate as phosphate donor. The FMN isotopologue mixtures were used to reconstitute the recombinant LOV domains from phototropins of *A. sativa* and *A. capillus-veneris*.

Synthetic genes specifying the LOV1 and LOV2 domains of phototropin NPH1-1 from *A. sativa* and the LOV2 domain of phototropin phy3 from *A. capillus-veneris*, were optimized for hyperexpression in *E. coli* host strains. The assembled DNA fragments were cloned into an expression vector specifying fusion proteins comprising hisactophilin from *Dictyostelium discoideum* and a thrombin cleavage site. The cognate fusion proteins were expressed efficiently in recombinant *E. coli* strains and could be bound to nickel-chelating Sepharose due to the large number of histidine residues present in the hisactophilin domain. The column was washed with buffer containing 8 M urea to release the protein-bound FMN, and the resulting apoprotein was reconstituted on the column with isotope-labeled FMN. The protein was then eluted with imidazole. The solution was treated with thrombin and passed again through a nickel-chelating column in order to remove the cleaved hisactophilin domain that was retained, whereas the LOV2 domains were not retained. The SDS page of the purified protein is shown in figure 3.2.

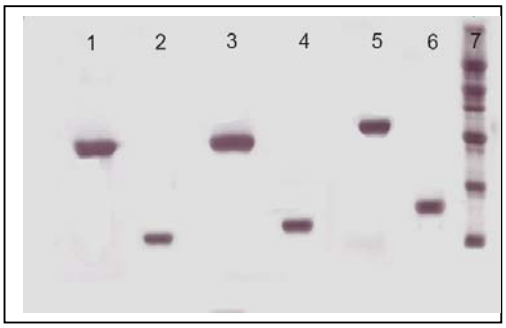

Figure 3.2 SDS polyacrylamide gel: 1. Fusion protein of hisactophilin and LOV domain from LOV2 *A. capillus-veneris* (27 kDa); 2. LOV2 domain from *A. capillus-veneris* (13 kDa); 3. Fusion protein of hisactophilin and LOV domain from LOV1 *A. sativa* (26 kDa); 4. LOV1 domain from *A. sativa* (14 kDa); 5. Fusion protein of hisactophilin and LOV domain from LOV2 *A. sativa* (33 kDa); 6. LOV2 domain from *A. sativa* (18 kDa); 7. Protein marker (66 kDa, 45 kDa, 36 kDa, 30 kDa, 20 kDa, 13 kDa).

3.1.1.2 Optical spectroscopy

Spectroscopic analysis of LOV2 *A. capillus-veneris* - The recombinant LOV2 domain of *A. capillus-veneris* (fern) has absorbance maxima at 375 and 450 nm, chararacteristic of FMN in the oxidised redox state (Fig. 3.3). Shoulders at 422 and 474 nm are vibrational contributions that are well resolved. This is indicative of tight binding between the noncovalently bound FMN, and the highly ordered protein structure, as well as of the nonpolar nature of the flavin-binding pocket.

Spectroscopic analysis of LOV1 and LOV2 *A. sativa* - The absorption spectra of LOV1 and LOV2 are similar but not identical (Fig. 3.3). The absorption spectrum of LOV1 has double peak structure at 361 and 370 nm, while in LOV2, the major absorption maximum occurs at 378 nm in the UV region. The absorption maximum in the blue region of the spectrum is at 449 nm for LOV1 and 447 nm for LOV2.

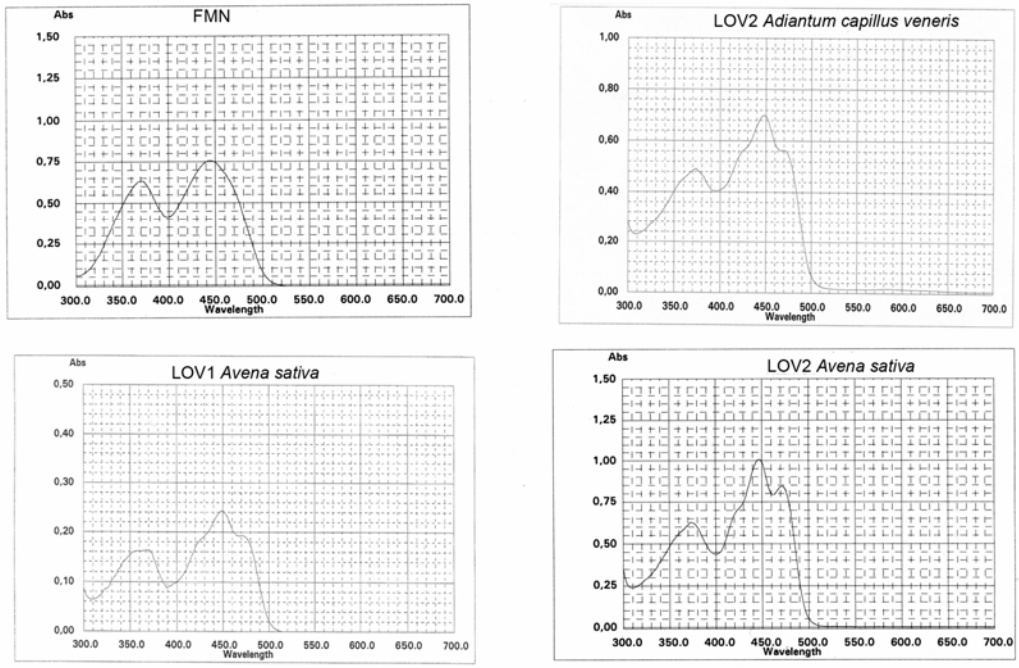

Figure 3.3 UV/vis absorption spectra of FMN and FMN bound to LOV domain.

3.1.1.3 NMR spectroscopy

The recombinant LOV protein from *A. capillus-veneri*s and *A. sativa* were reconstituted with various isotope-labeled FMN samples. The absorption spectrum of the reconstituted protein was virtually identical to that of the native recombinant protein before reconstitution. ^{1}H, ^{13}C

and ^{31}P NMR spectra are recorded without illumination, and subsequently with continuous blue-light illumination of the sample.

Signal assignments were based on comparison of proteins reconstituted with selectively isotope-labeled FMN samples, uniformly labeled FMN sample and $^{13}C^{13}C$ coupling patterns of the universally ^{13}C-labeled ligand in complex with the protein and on the basis of protein samples reconstituted with isotoplog mixtures obtained by biotransformation of two differently labeled glucoses. This study for the first time shows that all 17 carbons of FMN bound to LOV domains can be assigned with [U-$^{13}C_{17}$]FMN and two isotopologue mixtures of FMN (i.e. obtained by biotransformation of [2-$^{13}C_1$]- or [3-$^{13}C_1$]glucose) as shown in figure 3.4 for LOV2 *A. capillus-veneris* (fern).

In the spectrum of protein reconstituted with universally ^{13}C-labeled FMN (Fig. 3.4A), all signals with the exception of C(2) (159.4 ppm) appear as broadened multiplets due to $^{13}C^{13}C$ coupling of directly adjacent carbon atoms. In the samples reconstituted with the isotopologue mixtures, the carbon signals of the bound FMN appear as singlet, and their apparent intensities vary over a wide range (Fig. 3.4B and 3.4C). This intensity variation is due to the presence of the single ^{13}C-labeled isotopologues at different abundances in the random FMN isotopologue libraries. The relative intensities of the individual carbon signals observed in the protein sample reflect the relative abundances of the different FMN isotopologues, and constitute the basis for an unequivocal signal assignment. For example, the position 8α methyl group but not the position 7α methyl group is significantly labeled in the sample of 6,7-dimethyl-8-ribityllumazine obtained by biotransformation of [2-$^{13}C_1$]glucose, and therefore, the signal detected at 23.2 ppm in the spectrum with the isotopologue library from [2-$^{13}C_1$]glucose can be clearly assigned to C(8α). The methyl atom C(7α) is not ^{13}C-enriched from either [2-$^{13}C_1$]- or [3-$^{13}C_1$]glucose, and therefore, no signal can be detected in the ^{13}C-NMR spectra of the corresponding protein samples (Fig. 3.4B and 3.4C). On the other hand, a second methyl signal (doublet with a coupling constant of 44 Hz) is observed at 21.9 ppm in the spectrum with [U-$^{13}C_{17}$]FMN as a cofactor. It is obvious that this signal has to be assigned to C(7α).

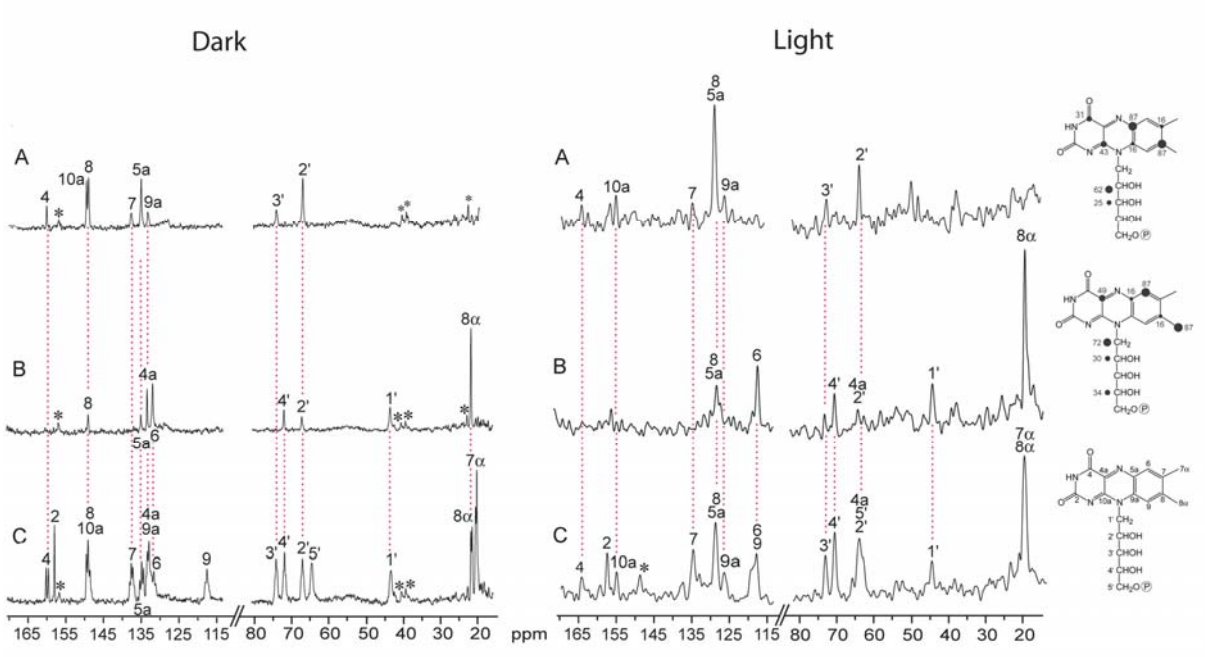

Figure 3.4 ^{13}C NMR spectra of ^{13}C-labeled FMN with LOV2 domain from *A. capillus-veneris* under dark conditions (left part) or irradiated with blue light (right part). (A) FMN obtained from [3-$^{13}C_1$]glucose. (B) FMN obtained from [2-$^{13}C_1$]glucose. (C) [U-$^{13}C_{17}$]FMN. Asterisks indicate impurities.

Due to the specific ^{13}C-enrichments in the ribityl moiety of the FMN samples, the signals for C(1'), C(2') and C(4') were observed in the isotopologue mixture from [2-$^{13}C_1$]glucose, whereas only the signals for C(2') and C(3') are detected in the spectrum of the isotopologue mixture from [3-$^{13}C_1$]glucose with higher intensity of the C(2') signal. On this basis, all ribityl signals can be unequivocally assigned (Table 3.1 and Fig. 3.4).

Table 3.1 NMR chemical shifts, and coupling constants of free FMN, FMN bound to LOV2 domain from *A. capillus-veneris* in dark and light condition. Coupling patterns are indicated in parenthesis where'd' denotes doublet and 't' denotes triplet and 'q' denotes quartet.

FMN atom	NMR Chemical Shifts, ppm				$^{13}C^{13}C$ Coupling Constants, Hz		
	Free TARF	Free FMN	LOV-2 bound FMN		Free FMN	LOV-2 bound FMN	
			dark	light		dark	light
2	154.4	159.8	159.4	159.2		(s)	(s)
4	159.2	163.7	161.3	165.9	76 (4a)	74(d)	nd [e]
4a	135.1	136.2	134.2	65.7	50 (4), 76 (10a)	nd [a]	nd [e]
5a	134.5	136.4	136.2	130.1	60, 66 (6, 9a)	60(t)	nd [e]
6	132.5	131.8	133.1	119.1	60, 66 (7,5a)	nd [a]	nd [e]
7	137.2	140.4	138.9	136.0	44, 66, 47 (7α, 6, 8)	47(q)	nd [e]
7α	19.5	19.9	21.9	21.8	44 (7)	43(d)	44(d)
8	148.7	151.7	150.2	130.1	64, 42, 49 (8α, 9,7)	nd [a]	nd [e]
8α	21.6	22.2	23.2	22.2	42 (8)	42(d)	47(d)
9	115.8	118.3	118.9	119.6	62, 64 (8, 9a)	60(t)	nd [e]
9a	131.4	133.5	134.4	127.7	62, 53 (5a, 9)	nd [a]	nd [e]
10a	150.8	152.1	150.8	156.7	52 (4a)	nd [a]	nd [e]
1'	45.0	48.8	44.8	46.8	39 (2')	45(d)	nd [e]
2'	70.2	70.7	68.1	66.7	40 (1', 3')	39(t)	nd [e]
3'	70.0	74.0	75.1	75.5	42 (2', 4')	41(t)	nd [e]
4'	69.5	73.1	72.9	73.0	42 (3', 5')	39(t)	nd [e]
5'	62.1	66.4	65.8	66.7	41 (4')	32(d)	nd [e]
P		5.1	4.8	4.1			

nd [a] - not determined because of signal overlapping; nd [e] - not determined because of broad signal

Table 3.2 ^{13}C abundance of LOV2 domain from *A. capillus-veneris* bound to FMN obtained from [2-$^{13}C_1$]glucose, and FMN obtained from [3-$^{13}C_1$]glucose under dark and light conditions.

Carbon position	^{13}C abundance (%)					
	[2-$^{13}C_1$]glucose			[3-$^{13}C_1$]glucose		
	free FMN	LOV2-bound FMN		free FMN	LOV2-bound FMN	
		dark	light		dark	light
4				31	31 [c]	+ [b]
4a	49	nd [a]	nd [a]			
5a	16	26	nd [a]	87	70	nd [a]
6	87	nd [a]	+ + [b]			
7				16	26	+ [b]
8	16	nd [a]	nd [a]	87	nd [a]	nd [a]
8α	87	+ + [b]	+ + [b]			
9a				16	nd [a]	+ [b]
10a				43	nd [a]	+ [b]
1'	72	90	+ + [b]			
2'	30	27	nd [a]	62	81	+ + [b]
3'				25	28	+ [b]
4'	34	34 [c]	+ [b]			

[a] - not determined because of signal overlapping; [b] - peak present at high intensity (+) and very high intensity (++); [c] - reference value.

Using the same isotopologue editing approach, unequivocal signal assignments can be obtained for the carbon atoms of the isoalloxazine ring. [2-$^{13}C_1$]glucose transfers the label to the ring carbon atoms 4a, 5a, 6, and 8 with ^{13}C-enrichments of 6 > 4a > 5a = 8. The carbon atoms 4, 5a, 7, 8, 9a and 10a acquire ^{13}C-label from [3-$^{13}C_1$]glucose with enrichments of 5a = 8 > 10a > 4 > 9a = 7. Indeed, in the signal region for aromatic carbon atoms (115 – 165 ppm), four signals were observed in the protein samples with FMN from [2-$^{13}C_1$]glucose (Fig. 3.4B), and six signals were detected with FMN from [3-$^{13}C_1$]glucose (Fig. 3.4C). The signal intensities were found to be different as predicted from the different ^{13}C-enrichments in the isotopologue libraries (Table 3.2), and thus provided the basis for the assignments.

The validity of the signal assignment obtained by the isotopologue editing method was confirmed by signal assignments using an ordered library of ^{13}C-labeled FMN isotopologues. More specifically, the ^{13}C NMR chemical shifts of 7 selectively ^{13}C-labeled FMN isotopologues bound to the LOV2 domain of *A. capillus-veneris* was measured (Fig. 3.5).

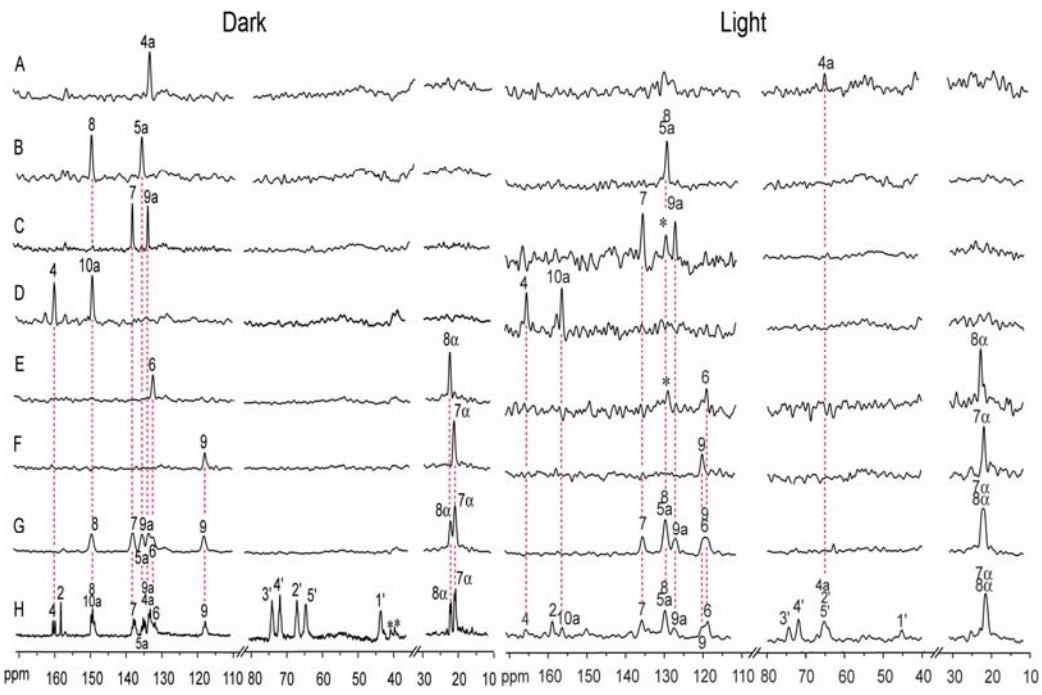

Figure 3.5 ^{13}C NMR spectra of ^{13}C-labeled FMN with LOV2 domain from *A. capillus-veneris* under dark condition, and under blue light irradiation. (A) [4a-$^{13}C_1$]FMN. (B) [5a,8-$^{13}C_2$]FMN. (C) [7,9a-$^{13}C_2$]FMN. (D) [4,10a-$^{13}C_2$]FMN. (E) [6,8α -$^{13}C_2$]FMN. (F) [7α,9-$^{13}C_2$]FMN. (G) [xylene-$^{13}C_8$]FMN. (H) [U-$^{13}C_{17}$]FMN. Asterisks indicate impurities.

The chemical shifts observed with ordered library of ^{13}C-labeled FMN samples were in perfect agreement to the signal assignments made on the basis of the random isotopologue libraries (Fig. 3.4).

The same isotopologue editing method was used to assign all ^{13}C NMR signals of bound FMN in the LOV2 domain of *A. capillus-veneris* under constant blue light irradiation. Specifically, the sample was irradiated by a blue light emitting photodiode via a quartz fibre. To avoid photo-damage of the protein that was noticed after prolonged sample irradiation, the acquisition times were typically lowered under blue light than under dark conditions. As a consequence, the signal-to-noise ratios of the NMR spectra of the illuminated samples were lower than those of the corresponding spectra in the dark. However, even with this limitation, the observed signal amplitudes were taken as a basis for the assignment of all signals. As an example, signals for C(2') > C(3') were seen in the ribityl region of the spectrum with FMN from [3-$^{13}C_1$]glucose, whereas signals for C(1') > C(4') > C(2') were detected with FMN from [2-$^{13}C_1$]glucose. The expected signal for C(2') was broadened, and partially overlapped with the signal of C(4a) that displayed only low intensity under light conditions. Again, the signal assignments obtained from the random isotopologue libraries matched those from the selectively labeled FMN samples. Notably, the overlapping signals for C(8) and C(5a) were confirmed with a sample reconstituted with [5a, 8-$^{13}C_2$]FMN, and the signal of C(4a) at 65.7 ppm was also observed with protein carrying [4a-$^{13}C_1$]FMN as cofactor.

Using the experimental approach described above, the ^{13}C signals of FMN in complex with recombinant LOV1 and LOV2 domain of phototropin from *A. sativa* (oat) were assigned in the dark and light state (Fig. 3.6 and 3.7). The modulation of the signal amplitude was taken as the basis for the unequivocal signal assignments (Tables 3.3 and 3.4).

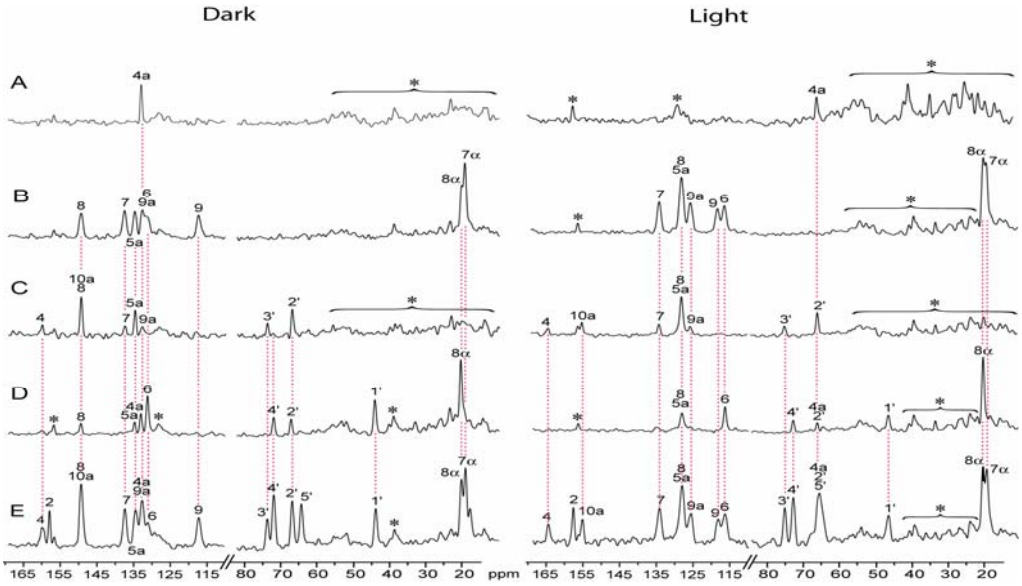

Figure 3.6 ^{13}C NMR spectra of ^{13}C labeled FMN with LOV1 domain from *A. sativa* under dark condition and under blue light irradiation. (A) [4a-$^{13}C_1$]FMN. (B) [xylene-$^{13}C_8$]FMN. (C) FMN obtained from [3-$^{13}C_1$]glucose. (D) FMN obtained from [2-$^{13}C_1$]glucose. (E) [U-$^{13}C_{17}$]FMN. Asterisks indicate impurities.

Table 3.3 ^{13}C NMR chemical shifts and coupling constants of free FMN, FMN bound to LOV1 domain from *A. sativa* under dark and light conditions. Coupling patterns are indicated in parenthesis where'd' denotes for doublet and 't' denotes for triplet.

Carbon Position	^{13}C NMR Chemical Shifts, ppm				$^{13}C^{13}C$ Coupling Constants, Hz		
	Free TARF	Free FMN	LOV-1 bound FMN		Free FMN	LOV-1 bound FMN	
			dark	light		dark	light
2	154.4	159.8	159.3	161.0		(s)	(s)
4	159.2	163.7	161.2	166.6	76 (4a)	75(d)	nd [e]
4a	135.1	136.2	134.6	66.1	50 (10a), 76 (4)	nd [a]	nd [e]
5a	134.5	136.4	136.3	130.2	60, 66 (6, 9a)	nd [a]	nd [e]
6	132.5	131.8	133.4	118.7	60, 66 (7, 5a)	nd [a]	nd [e]
7	137.2	140.4	139.0	136.2	44, 66, 47 (7α, 6, 8)	nd [a]	nd [e]
7α	19.5	19.9	21.5	21.4	44 (7)	44(d)	44(d)
8	148.7	151.7	150.8	130.2	64, 42, 49 (8α, 9, 7)	nd [a]	nd [e]
8α	21.6	22.2	22.5	21.9	42 (8)	40(d)	40(d)
9	115.8	118.3	119.2	120.5	62, 64 (8, 9a)	70,55(t)	nd [e]
9a	131.4	133.5	134.4	127.9	62, 53 (5a, 9)	nd [a]	nd [e]
10a	150.8	152.1	150.6	157.0	52 (4a)	nd [a]	nd [e]
1'	45.0	48.8	45.6	47.2	39 (2')	31(d)	nd [e]
2'	70.2	70.7	68.0	66.2	40 (1', 3')	38(t)	nd [e]
3'	70.0	74.0	74.6	75.2	42 (2', 4')	m	nd [e]
4'	69.5	73.1	72.8	72.9	42 (3', 5')	m	nd [e]
5'	62.1	66.4	65.5	65.9	41 (4')	36(d)	nd [e]

nd [a] - not determined because of signal overlapping; nd [e] - not determined because of broad signal; m - coupling of high order

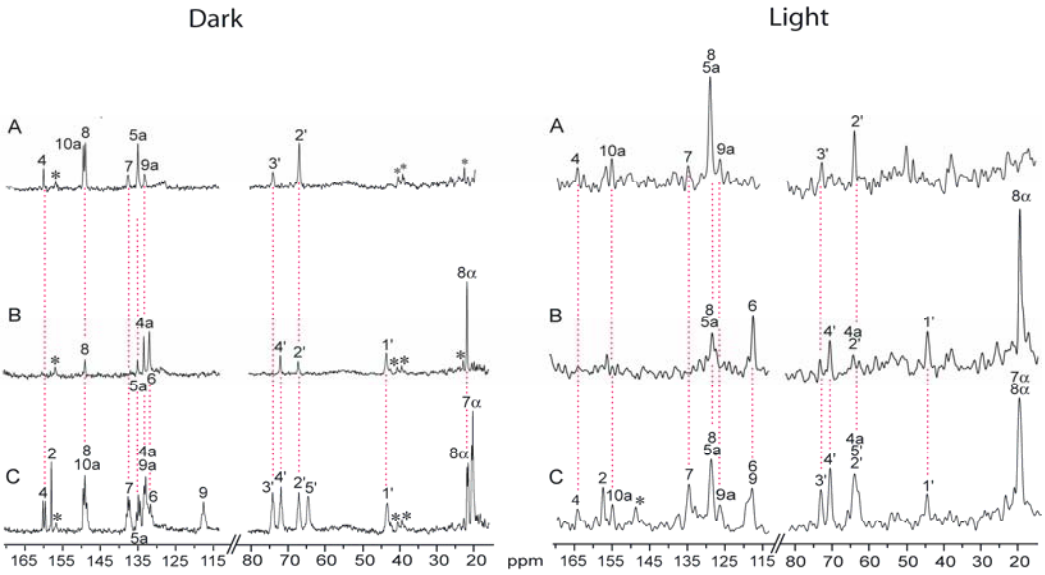

Figure 3.7 ^{13}C NMR spectra of ^{13}C labeled FMN with LOV2 domain from *A. sativa* under dark condition (left) and under blue light irradiation (right). (A) FMN obtained from [3-$^{13}C_1$]glucose. (B) FMN obtained from [2-$^{13}C_1$]glucose. (C) [U-$^{13}C_{17}$]FMN. Asterisks indicate impurities.

Table 3.4 ^{13}C NMR chemical shifts and coupling constants of free FMN, FMN bound to LOV2 domain from *A. sativa* under dark and light conditions. Coupling patterns are indicated in parenthesis where'd' denotes for doublet, 't' denotes for triplet and 'q' for quartet.

FMN atom	NMR Chemical Shifts, ppm				$^{13}C^{13}C$ Coupling Constants, Hz		
	free TARF	free FMN	LOV-2 bound FMN		free FMN	LOV-2 bound FMN	
			dark	light		dark	light
2	154.4	159.8	159.3	159.4		(s)	(s)
4	159.2	163.7	161.2	165.9	76 (4a)	75(d)	52(d)
4a	135.1	136.2	134.5	66.0	50 (10a), 76 (4)	65(t)	nd [e]
5a	134.5	136.4	136.3	130.2	60, 66 (6, 9a)	60(t)	nd [e]
6	132.5	131.8	132.9	118.7	60, 66 (7, 5a)	65(t)	60(t)
7	137.2	140.4	139.1	136.2	44, 66, 47 (7α, 6, 8)	55(q)	nd [e]
7α	19.5	19.9	21.6	21.9	44 (7)	47(d)	47(d)
8	148.7	151.7	150.8	130.2	64, 42, 49 (8α, 9, 7)	55(q)	55(q)
8α	21.6	22.2	22.5	21.9	42 (8)	44(d)	44(d)
9	115.8	118.3	119.3	120.5	62, 64 (8, 9a)	70(t)	65(t)
9a	131.4	133.5	134.5	127.8	62, 53 (5a, 9)	65(t)	70(t)
10a	150.8	152.1	150.8	156.9	52 (4a)	45(d)	45(d)
1'	45.0	48.8	45.6	47.4	39 (2')	40(d)	nd [e]
2'	70.2	70.7	68.1	66.0	40 (1', 3')	40(t)	nd [e]
3'	70.0	74.0	74.7	75.2	42 (2', 4')	40(t)	nd [e]
4'	69.5	73.1	72.8	73.0	42 (3', 5')	40(t)	40(t)
5'	62.1	66.4	65.7	66.7	41 (4')	40(d)	nd [e]
P		5.1	4.75	4.15			

nd [e] - not determined because of broad signal

Besides, the aim of the study was to assign all ^{13}C signals of the protein-bound cofactor (including the ribityl side chain signals) in the dark as well as the blue-light irradiated state using the isotopologue editing method, the modulation in the chemical shift of LOV domain of different origin were also taken into consideration. A correlation diagram of the chemical shifts for all proteins investigated is shown in figure 3.8.

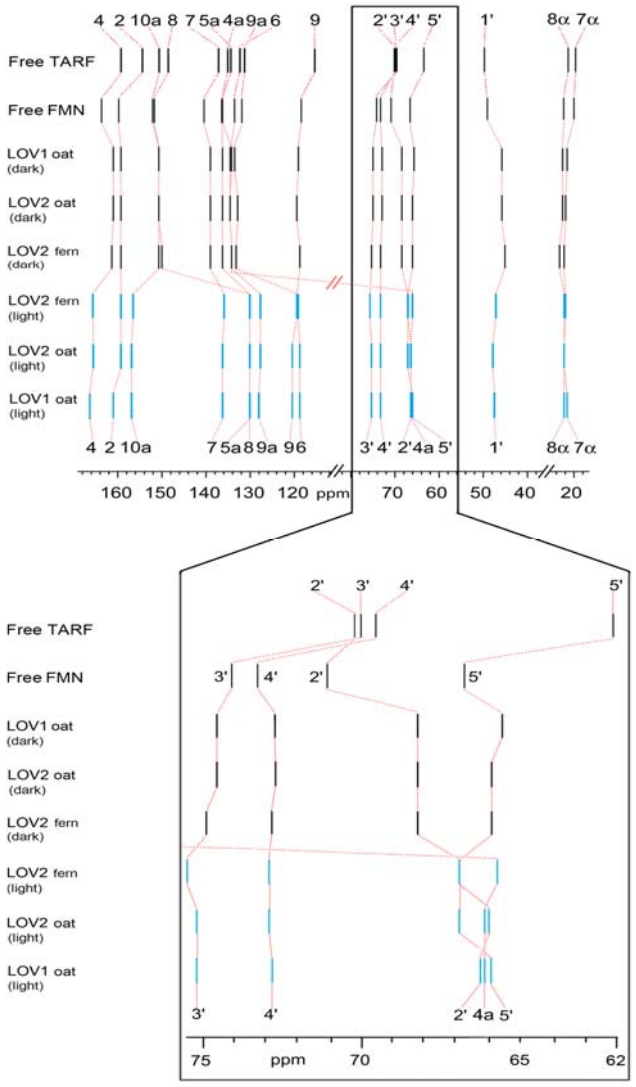

Figure 3.8 Chemical shifts of ^{13}C-labeled FMN in complex with LOV domains: black strips, dark conditions; blue strips, irradiated with blue light.

3.1.1.4 Discussion

The isotopologue editing method allows the rapid and unequivocal assignment of all carbon atoms (including all ribityl signals) in ^{13}C NMR spectra of protein-bound flavin cofactors using no more than three FMN samples, i.e. a uniformly labeled and two partially labeled flavin samples that can be biosynthetically obtained by *in vivo* biotransformation of [2-$^{13}C_1$]-

and [3-$^{13}C_1$]glucose. Since, in the latter two cases, the degree of ^{13}C enrichment of a given carbon atom in the flavin samples differs, the ^{13}C NMR signal strength (amplitude) of a given carbon atom provides an additional constraint in the signal assignment procedure. The assignment of ribityl chain can provide important information about the binding interaction between the hydroxyl groups of the side chain of flavin and the apoprotein and could also report possible conformational changes of the side chain, for example due to reduction of a flavoprotein.

In the dark state, the chemical shifts of the isoalloxazine moiety of flavin from LOV1 domain of *A. sativa* (oat) are very similar to those observed with LOV2 of the same species, and of different strains (Fig. 3.8). Most of the differences (± 0.3 ppm) between the two sets are within the accuracy limits of chemical shift determination except for C(8) of $LOV2_{fern}$ which is upfield shifted by 0.6 ppm, and C(8α) of $LOV2_{fern}$ which is downfield shifted by 0.7 ppm, respectively as compared to $LOV1_{oat}$ and $LOV2_{oat}$. The chemical shift of the side chain carbon atoms 1' and 3' of $LOV2_{fern}$ show significant differences, which may be ascribed to variation in the strength of the hydrogen bond of the corresponding hydroxyl groups with the proteins, and/or to conformational changes in the side chain (Fig. 3.8). A similar effect is shown by the proteins in the blue light irradiated state. The greatest difference in chemical shifts is observed for C(2) of $LOV1_{oat}$, which is downfield shifted by 1.6 ppm as compared to the LOV2 molecules. Similarly the C(4) and C(7α) of $LOV1_{oat}$ are downfield shifted by 0.7 ppm and upfield shifted by 0.5 ppm, respectively, as compared to $LOV2_{oat}$ and $LOV2_{fern}$. A significant difference is also observed for C(9), and C(1') of $LOV2_{fern}$ which are upfield shifted by 0.9 and 0.6 ppm, respectively, and C(2') which is downfield shifted by 0.7 ppm, as compared to $LOV1_{oat}$, and $LOV2_{oat}$.

Based on extensive ^{13}C-, and ^{15}N-NMR studies on free flavins in aprotic, and protic media (Müller, 1971), which have shown that a direct correlation exists between the π-electron density, and the ^{13}C chemical shift of a particular atom of the flavin molecule, the observed chemical shifts can be interpreted in terms of the electronic structure of the protein-bound flavin, and its perturbation by binding interaction, and chemical reactions. Thus, the dark state interaction between FMN and the LOV domains under study is characterized by strong hydrogen bonding with the C(2) atom of flavin. The strength of the hydrogen bond corresponds approximately to that of free FMN in water, indicating polarization of the flavin along the axis C(8)-C(6)-C(9a)-N(5)-C(10a)-C(2). This is manifested by the observed downfield shifts of the corresponding C atoms (Tables 3.1, 3.3 and 3.4). Although there exists

a hydrogen bond between the protein and the flavin at C(4), its strength is considerably weaker than that observed in free FMN in water. These observations are in good agreement with recent X-ray data showing a distance of 0.31 nm between the N_δ group of N998, and the oxygen atom of the C(2) group (Fig. 3.9 and Table 3.5).

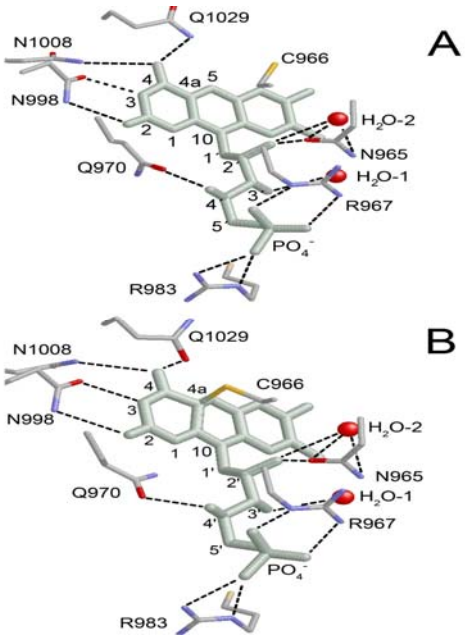

Figure 3.9 *Adiantum* phy3 LOV2 structures, (A) dark, and (B) light state (PDB ID code 1G28 and 1JNU respectively) (Crosson and Moffat, 2001; Crosson and Moffat, 2002). Atoms in amino acid residues are colored by elements: carbon, *white*; oxygen, *red*; nitrogen, *blue*; sulfur, *yellow*.

To the C(4)O group, two hydrogen bonds (N_ε group of Q1029, N_δ group of N1008) have been suggested by X-ray data, however the distance between the bond-forming atoms is larger than that observed at C(2)O, supporting our interpretation. A strong hydrogen bond to C(4)O would have influenced the chemical shift of the C(4a) atom by a downfield shift as compared to that of FMN (Salomon et al., 2001). The even slightly upfield shifted resonance of the C(4a) atom in comparison to TARF indicates extra π-electron density allocation to this position, released from the N(10) atom, which is downfield shifted compared to TARF, as shown previously (Salomon et al., 2001). The resonance position of C(4a) is thus in full agreement with the weak hydrogen bond observed at C(4)O. The partial positive charge created on N(10) (Vervoort et al., 1986b) by the release of electron density onto C(4a) is distributed mainly onto the C(5a), and the C(9) atom, and to a lesser extent onto the C(7) atom, in agreement with the fact that the latter atom experiences a smaller downfield shift than the other two atoms. The data demonstrate that, with regard to the isoalloxazine moiety

of flavin, there are only minor electronic differences of the prosthetic group of the different proteins investigated in this study.

Table 3.5 Distances between FMN atoms (Ligand) and amino acid residues of LOV2 from *Adiantum* phy3 (Crosson et al., 2001; Crosson et al., 2002). For comparison, ^{13}C chemical shifts of bound FMN atoms are given.

Atom		Dark state		Light state	
Ligand	Protein	Distance, Å	^{13}C NMR chemical shifts, ppm	Distance, Å	^{13}C NMR chemical shifts, ppm
C(4a)	S_γ [C(966)]	4.2	134.2	1.8	65.7
	O_ε [Q(1029)]	4.7		4.0	
O(4)	N_ε [Q(1029)]	3.5	161.3 [C(4)]	3.1	165.9 [C(4)]
	N_δ [N(1008)]	3.4		3.4	
N(3)	O_δ [N(998)]	2.8		3.0	
O(2)	N_δ [N(998)]	3.1	159.4 [C(2)]	3.3	159.2 [C(2)]
N(5)	C_ε [F(1010)]	3.2	136.2 [C(5a)]	3.8	130.1 [C(5a)]
	O_δ [N(965)]	2.7		2.9	
O(2')	N_δ [N(965)]	3.9	68.1 [C(2')]	3.9	66.7 [C(2')]
	O (H_2O-2)	3.4		3.4	
	O (H_2O-1)	3.6		3.6	
O(3')	O (H_2O-1)	3.1	75.1 [C(3')]	3.1	75.5 [C(3')]
O(4')	O_ε (Q970)	3.3	72.9 [C(4')]	3.7	73.0 [C(4')]
	N_ε (Q970)	3.2		3.0	
O(1) (on P)	N_ε [R(967)]	2.6		2.5	
O(2) (on P)	N_η [R(967)]	2.6	4.8 (P)	2.7	4.1 (P)
O(3) (on P)	N_η [R(983)]	2.8		3.0	
O(3) (on P)	N_ε [R(983)]	2.6		2.7	

The chemical shifts of the C(3') and C(4') atoms of the side chain of protein-bound flavin resemble those of FMN in water indicating stronger hydrogen bonding interactions with the hydroxyl group of C(3'), and a somewhat weaker one with that of C(4') in strength as compared to those observed in FMN. This hydrogen bonding pattern agrees with that observed by X-ray crystallography (Harper et al., 2004). The resonance position due to C(1') reflects the increased sp^2 hybridization of N(10) (Vervoort et al., 1986b). Both, C(2') and C(5'), are upfield shifted by more than 1 ppm compared to those of FMN. Whereas the X-ray

data indicate no hydrogen bond between C(5'), and the protein, but a strong one at C(2'), the NMR data do not indicate hydrogen bonding at these atoms. It is suggested that the apparent absent hydrogen bond at C(2'), as revealed by ^{13}C NMR, may be masked by a counteracting factor like a conformational change.

Upon blue light irradiation of the proteins, rather drastic changes are observed in the NMR spectra (Salomon et al., 2001). The most obvious one is the large upfield shift (-68.5 ppm) of the C(4a) resonance. This proves the conversion of the C(4a) atom from sp^2 to sp^3 hybridization, in line with the formation of a covalent bond between this atom of flavin, and the sulfur atom of C966 in LOV2 of *A. capillus-veneris*. The other carbon atoms of flavin most affected by conversion of the protein by light are: C(8) (-19.9 ppm), C(6) (-14.0 pm), C(9a) (-6.7 ppm), and C(10a) (+5.9 ppm). All these atoms are involved in the possible mesomeric structures of oxidized flavin (Vervoort et al., 1986a), that are disturbed by the C(4a) substitution. The upfield shifts of the resonances of these atoms, with the exception of C(10a), which shows a downfield shifted signal, demonstrates the allocation of the incoming electron density at these positions. The downfield shift of the resonance line due to C(10a) is caused by the higher electron density withdrawal from this atom by the further polarization of the C(2)O group, as compared to that of the molecule under dark conditions. Overall, with regard to the chemical shifts of the carbon atoms of the isoalloxazine ring, the electronic structure of the different proteins investigated is very similar, if not almost identical. Only the chemical shifts of the C(2), C(4), and C(4a) atoms of the adduct of LOV1, and LOV2 proteins differ considerably from each other. The chemical shifts of the former protein are downfield from those due to LOV2 indicating stronger hydrogen bonding in LOV1 than in LOV2 at these positions. The hydrogen bond pattern as observed by NMR of the oxidized proteins are also observed in the adduct forms. Whereas the chemical shifts of the resonance line due to C(4a) in $LOV2_{oat}$, and $LOV1_{oat}$ are very similar, that due to $LOV2_{fern}$ is upfield shifted with respect to the former ones. This observation suggests some structural difference(s) at the C(4a) position between the proteins from oat and that from fern.

The hydrogen bonding pattern observed for the C(3') and the C(4') atoms of the ribityl side chain in the oxidized proteins are also observed in the corresponding adducts, but the strength of hydrogen bonding with the C(3') is considerably increased, especially that in $LOV2_{fern}$. With regard to C(5') atom the LOV2 proteins exhibit similar chemical shift for this atom, whereas that of LOV1 is upfield shifted by 0.5 ppm. The chemical shift for the C(2')

atom increases in the order: $LOV2_{oat}$, $LOV1_{oat}$, and $LOV2_{fern}$, possibly reflecting variations in the strength of hydrogen bonding interactions at this position.

In summary, the ^{13}C NMR data show that there exist some subtle differences between the proteins studied, as far as the isoalloxazine moiety of the flavin in the ground and photo-adduct state is concerned. The largest difference among the three proteins is observed for the resonance line of the C(2)O group (downfield shift) of LOV1 in the photo-adduct state. However there are some resonances of ribityl side chain carbon atoms, which differ to a greater extent among the three proteins (Fig. 3.8), indicating variations in the interaction with the proteins and/or conformational differences.

3.1. 2 CIDNP study on *Avena sativa* LOV2 domain C450A mutant

Blue light irradiation is conducive to the formation of a flavin radical instead of a photoadduct, if the photoreactive cysteine residue is replaced by mutagenesis. The formation of the FMN-thiol adduct is not possible in the C450A mutant due to the absence of a thiol group. The optical absorption spectra of the LOV2 C450A domain shows absorption maxima at 363 and 447 nm, characteristic of an FMN chromophore in the oxidized redox state. Upon irradiation with blue light, the LOV2 C450A mutant protein gives an optical absorption spectrum characteristic of a flavin radical characterized by absorption maxima at 570 and 605 nm.

A recombinant LOV2 domain comprising amino acid residues 409-525 and carrying a C450A mutation that had been reconstituted with [U-$^{13}C_{17}$]FMN was recorded in the dark and under continuous blue-light irradiation (Richter et al, 2005). Based on comparison of chemical shift with that of free FMN, and the coupling patterns in samples containing [U-$^{13}C_{17}$]FMN, all ^{13}C NMR signals of FMN in the C450A mutant, LOV2 domain could be unequivocally assigned (Fig. 3.10A).

In the NMR spectra of recombinant LOV2 C450A domain recorded in the dark, most of the ^{13}C-enriched carbon atoms of the FMN chromophore appeared as multiplets and revealed only minor differences of chemical shift compared to wild type.

Blue-light illumination of the protein samples did not affect the chemical shifts of the observed signals, however, some of the signals appeared with negative signal amplitude, whereas other signals remained in absorption, either with attenuated or enhanced intensity indicating the observation of photochemically induced dynamic nuclear polarization (photo CIDNP) in an integral cofactor-protein system. CIDNP (Chemically Induced Dynamic

Polarization Transfer) is a phenomenon, which refers to non-Boltzmann nuclear spin-state distributions detected as enhanced absorptive or emissive NMR signals.

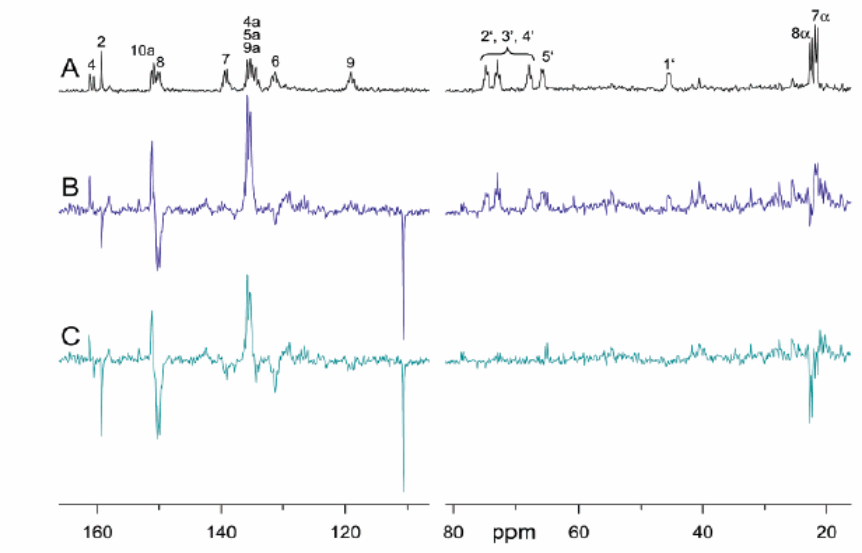

Figure 3.10 ^{13}C NMR spectra of [U-$^{13}C_{17}$]FMN–reconstituted LOV2 C450A domain. (A) Dark spectrum. (B) Light Spectrum. (C) Difference spectrum: light-minus-dark (Richter et al., 2005).

In addition to the emissive signals attributed to the FMN chromophore, a strongly emissive NMR line was observed at 110.6 ppm (Fig. 3.10B). This signal is not due to the resonance of any of the carbons within the FMN chromophore as it was not observed in the NMR spectrum recorded in the dark (Fig. 3.10A). Hence, it must be assigned to a ^{13}C atom of the C450A apoprotein, although the amino acid carbon atoms are not ^{13}C-enriched. Apparently, the signal of this atom becomes strongly polarized as a result of the photoreaction of the mutant domain. The NMR signal polarization was attributed to polarization transfer during the decay of the photoinduced radical state of the FMN chromophore that has been generated by the blue light irradiation.

At the time of preliminary studies, Harper and coauthors reported the NMR structure of the LOV2 domain of *A. sativa*, and showed that blue light irradiation caused a significant conformational change in a helix region extending from residue 522 – 560 that was proposed to serve as the optomechanical switch involved in LOV domain signalling (Harper et al., 2003). So it was decided to include that C-terminal helix region into the recombinant construct for a more detailed CIDNP study. For simplicity, the proteins with and without the C-terminal helix will be designated as “long” and “short” LOV2 domains. Their sequences

are shown in figure 3.11. Whereas the short clone contains one tryptophan residue (W491), the long clone contains two tryptophan residues (W491 and W557). Notably, both proteins carry a C450A mutation.

```
Long LOV2 domain  404 LATTLERIEKNFVITDPRLPDNPIIFASDSFLQLTEYSREEILGRNARFLQGPETDRATVR
Short LOV2 domain 409 -----ERIEKNFVITDPRLPDNPIIFASDSFLQLTEYSREEILGRNARFLQGPETDRATVR

Long LOV2 domain       KIRDAIDNQTEVTVQLINYTKSGKKFWNLFHLQPMRDQKGDVQYFIGVQLDGTEHVRDAA
Short LOV2 domain      KIRDAIDNQTEVTVQLINYTKSGKKFWNLFHLQPMRDQKGDVQYFIGVQLDGTEHVRDAA

Long LOV2 domain       EREGVMLIKKTAENIDEAAKELPDANLRPEDLWAN 559
Short LOV2 domain      EKLN-------------------------------- 525
```

Figure 3.11 Sequence alignment of *A. sativa* long LOV2, C450A domain and short LOV2, C450A domain.

The long LOV2 domain reconstituted with [U-$^{13}C_{17}$]FMN, when recorded in the dark and under continuous blue-light irradiation, showed similar pattern of NMR spectra as the short LOV2 domain, except that of emissive signal at 110.6 is offset to 113.5 ppm.

In order to increase the sensitivity of the experiment and to assign the 113.5 ppm signal to a specific amino acid residue, ^{13}C-labeled LOV2 C450A protein was prepared. More specifically, the *E. coli* hyperexpression strain was grown in medium containing [U-$^{13}C_6$]glucose as carbon source affording totally ^{13}C-labeled protein. Universally ^{13}C-labeled short and long LOV domains under blue light irradiation showed emissive multiplets at 110.6 ppm and 113.5 ppm, respectively. They also showed a number of less intense emissive multiplets in the range of 110 – 140 ppm. This supported the hypothesis that the optically excited state of the flavin chromophore could decay under formation of a radical pair, where one of the non-paired electrons is located on the FMN chromophore, which is thereby converted into a neutral blue radical form, and that the other electron is located on amino acid side chain.

The emissive signals in the range of 110 – 140 ppm showed fine structure arising by $^{13}C^{13}C$ coupling and were tentatively interpreted as the CIDNP signature of a photochemically induced tryptophan radical. In order to test this hypothesis, mutant proteins were constructed by site directed mutagenesis, where one of the two tryptophan residues in 491 position and 557 position of the LOV2 C450A domain of *A. sativa* was replaced by alanine. The photodynamic properties of these C450A/W491A and C450A/W557A double mutants were similar to those of the C450A mutant protein as judged by UV/vis spectroscopy (Fig. 3.12 and 3.13).

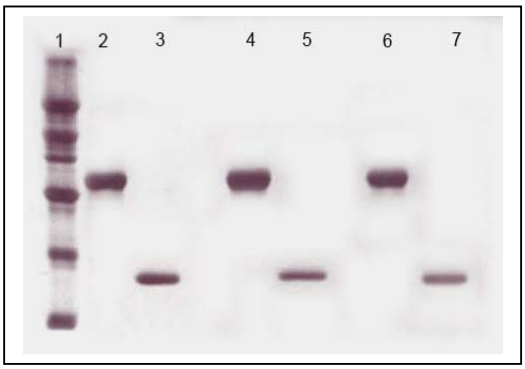

Figure 3.12 SDS polyacrylamide gel of mutant LOV domains: 1. Protein marker (66 kDa, 45 kDa, 36 kDa, 30 kDa, 20 kDa, 13 kDa); 2. Fusion protein of hisactophilin and LOV domain from LOV2 C450A mutant (32 kDa); 3. LOV2 domain C450A mutant (18 kDa); 4. Fusion protein of hisactophilin and LOV domain from LOV2 C450A/W491A mutant (32 kDa); 5. LOV2 domain C450A/W491A mutant (18 kDa); 6. Fusion protein of hisactophilin and LOV domain from LOV2 C450A/W557A mutant (32 kDa); 7. LOV2 domain C450A/W557A mutant (18 kDa).

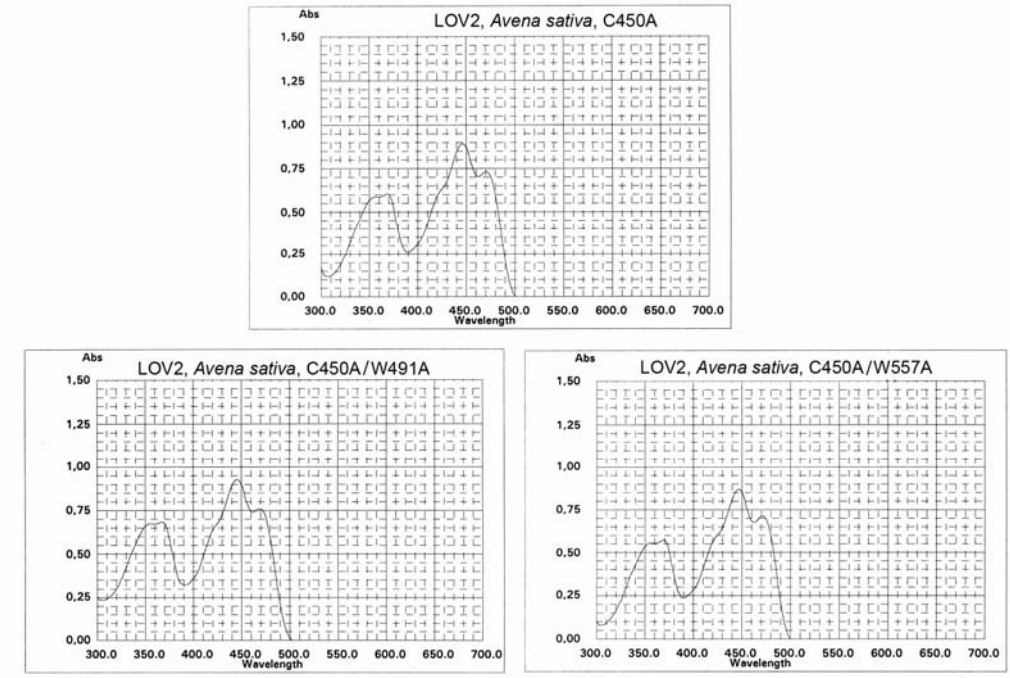

Figure 3.13 UV/vis spectroscopy of LOV2 C450A, LOV2 C450A/W491A and LOV2 C450A/W557A mutant.

Figure 3.14 shows ^{13}C NMR spectra of unlabeled protein samples obtained under blue light irradiation. As mentioned above, the short LOV2 domain shows an emissive signal at 110.6 ppm (Fig. 3.14 A). The long LOV2 domain shows a similar line that is offset to 113.5 ppm (Fig. 3.14 B). The replacement of tryptophan 557 by alanine in the long protein version did not change the NMR pattern (Fig. 3.14 C); on the other hand, the replacement of tryptophan

491 by alanine quenched the emissive signal (Fig. 3.14 D). These observations suggest that tryptophan 491 and the FMN chromophore jointly form a radical pair upon blue light irradiation.

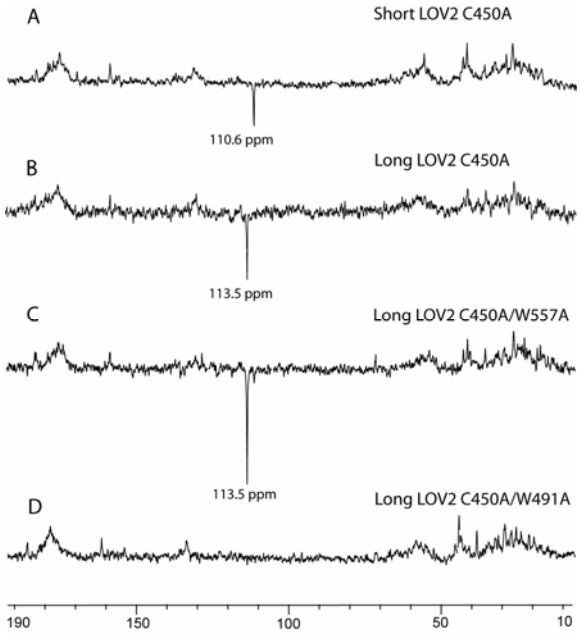

Figure 3.14 Overlay of ^{13}C NMR spectra of unlabeled samples from *A. sativa* under blue light irradiation. A) Short LOV2 domain C450A mutant. B) Long LOV2 domain C450A mutant C) Long LOV2 domain C450A/W557A double mutant. D) Long LOV2 domain C450A/W491A double mutant.

For further confirmation, a series of specifically ^{13}C-labeled protein samples were prepared by growth of tryptophan-auxotrophic *E. coli* hyperexpression strain [*E. coli* ATCC 49980 (WP2)] with a supplement of [U-$^{13}C_{11}$]-tryptophan. Figures 3.15A and 3.15B show ^{13}C NMR spectra of the tryptophan-labeled C450A/W557A double mutant and the C450A/W491A double mutant (long LOV2 domain) obtained under dark conditions, respectively. Both spectra show doublets at low field, which are easily, assigned as the carboxylic groups of tryptophan 491 and 557, respectively, on basis of chemical shift and multiplicity arguments (coupling constants are about 52 and 54 Hz, respectively; Tables 3.6 and 3.7). The signals for α and β side chain carbon atoms of the respective tryptophan moieties are also easily assigned on basis of chemical shift and $^{13}C^{13}C$ coupling multiplicity. Due to signal overlapping, the multiplets in the range of 110–140 ppm are less easily assigned. In detail, the signals for C(3) and C(7) are both expected at the high-field end of the aromatic signal cluster. In case of the C450A/W491A double-mutant, C(3) and C(7) can be easily distinguished on basis of their respective pseudotriplet C(7) and pseudoquartet C(3)

signatures, whereas they appear to overlap in case of the C450A/W557A double-mutant. The signal of C(7a) can be easily assigned on basis of its pseudotriplet appearance at the low-field end of the aromatic signal clusters. The signals of C(2) and C(3a) can be identified by their respective doublet and pseudoquadruplet signatures. The remaining aromatic carbon atoms, C(4), C(5) and C(6) should appear as pseudotriplets.

^{13}C NMR spectra of the tryptophan-labeled C450A/W557A and C450A/W491A double mutants obtained under blue light irradiation show multiplets that appear with the same chemical shifts and coupling patterns as in the dark state, whereas the intensities of the tryptophan signals show dramatic differences by comparison with the dark state (Fig. 3.15A and 3.15B). Most notably, certain tryptophan signals appear with negative amplitude, i.e. in emissive mode, but even those tryptophan signals that continue to appear with positive amplitude in figures 3.15C and 3.15D show significantly modulated amplitude ratios. More specifically, the signals of the carboxylic groups and α side chain carbons are absorptive in each case, but the signal of the β side chain carbon atom is emissive in case of the C450A/W557A double mutant. The indole ring carbon atom 3 of tryptophan 557 also appears in emissive mode in the light spectrum of the C450A/W491A spectrum in figure 3.15D albeit with a relatively low negative amplitude. The most dramatic changes are observed with the indole carbon atoms of tryptophan 491 (C450A/W557A double mutant), which are all emissive (Fig. 3.15C). Most notably, the signal of C(3) appears with very large negative intensity as a pseudo-quadruplet with an apparent coupling constant of 58 Hz, and can therefore be unequivocally distinguished from C(7), which should have the appearance of a pseudotriplet. Additional evidence for the assignment of the emissive 113.5 ppm signal in figure 3.15C as C(3) is available from CIDNP data obtained with partially ^{13}C-labeled proteins produced by fermentation with single-labeled [$^{13}C_1$]-glucose isotopologue. A minor emissive signal at 110.8 ppm (indicated by * in Fig. 3.15C) with the same multiplet signature as that of C(3) at 113.5 ppm does not correspond to any tryptophan signal in the dark spectrum. Time-resolved blue light irradiation spectra showed that this signal represents a protein species that is formed by photodamage due to protracted blue light irradiation; the signal can therefore be ignored in the subsequent analysis.

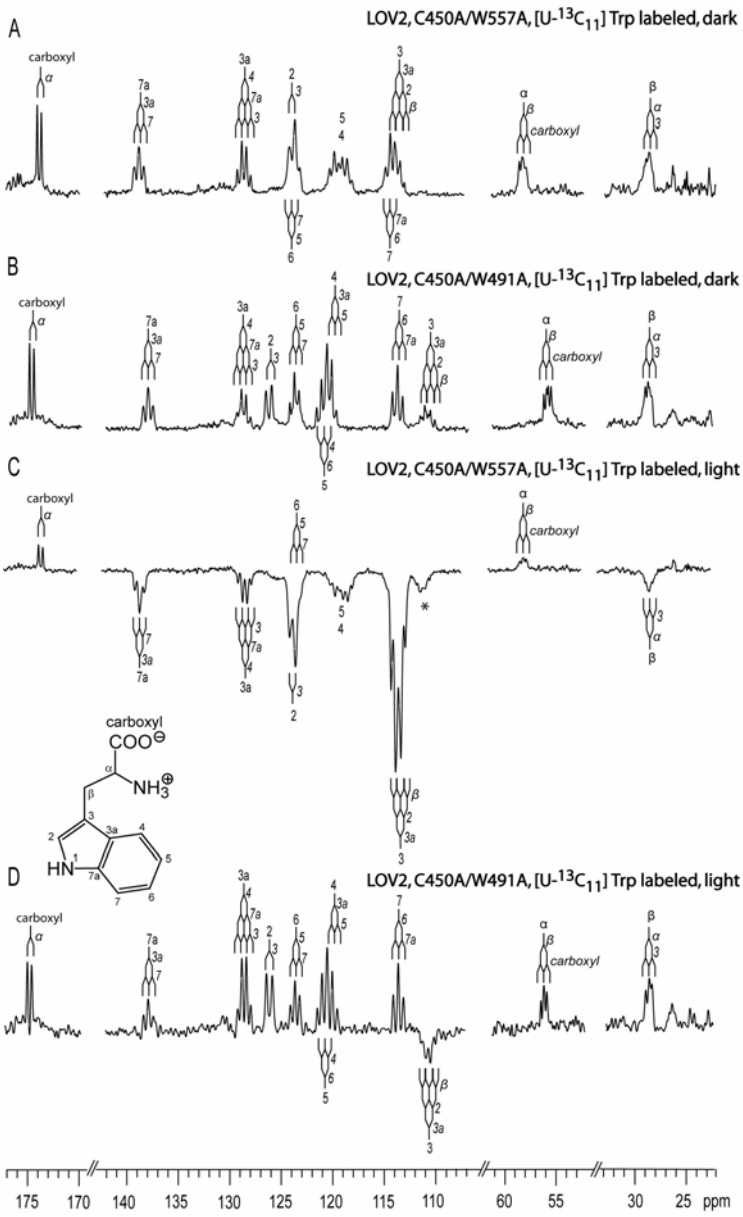

Figure 3.15 ^{13}C NMR spectra of long LOV2 domain from C450A/W491A and long LOV2 domain from C450A/W557A double mutants labeled with [U-$^{13}C_{11}$]tryptophan. A) C450A/W557A under dark condition. B) C450A/W491A under dark condition. C) C450A/W557A under blue light irradiation. D) C450A/W491A under blue light irradiation. Asterisks indicate a photodamage product.

The chemical shifts of all tryptophan carbon signals observed under dark conditions are summarized in figure 3.16 and tables 3.6 and 3.7 below.

Table 3.6 ^{13}C NMR chemical shifts of LOV2, C450A/W491A double mutant labeled with [$U^{13}C_{11}$]tryptophan.

Carbon Position	Chemical Shift of Free tryptophan (ppm)	Chemical shift		Relative intensity		Coupling constant	
		Dark	Light	Dark	Light	Dark	Light
Carboxyl	176.4	174.7	174.7	1.0[a]	1.0[a]	53 (d)	54 (d)
7a	138.2	137.9	137.9	0.74	0.43	59 (t)	60 (t)
3a	128.3	128.6	128.5	0.79	1.40	54, 56 (q)	53, 54 (q)
2	126.9	126.1	126.1	0.85	1.07	69 (d)	70 (d)
6	123.8	123.6	123.6	1.13	0.82	55 (t)	55 (t)
5	121.2	120.5	120.5	2.17	1.85	nd[b]	nd[b]
4	120.2	120.5	120.5	2.17	1.85	nd[b]	nd[b]
7	113.7	113.6	113.6	1.05	0.91	61 (t)	62 (t)
3	109.2	110.7	110.6	0.50	- 0.87	54, 58 (q)	56, 58 (q)
α	56.9	55.8	55.8	1.09	0.96	36 (t)	44 (t)
β	28.2	28.5	28.4	1.37	1.30	34 (t)	40 (t)

[a] - reference value; nd[b] – not determined because of overlapping signals

Table 3.7 ^{13}C NMR chemical shifts of LOV2, C450A/ W557A double mutant labeled with [$U^{13}C_{11}$]tryptophan.

Carbon Position	Chemical Shift of Free tryptophan (ppm)	Chemical shift		Relative intensity		Coupling constant	
		Dark	Light	Dark	Light	Dark	Light
Carboxyl	176.4	173.6	173.3	1.0[a]	1.0[a]	52 (d)	52 (d)
7a	138.2	138.6	138.3	0.91	-1.83	56 (t)	57 (t)
3a	128.3	128.4	128.1	0.96	-1.38	54, 54 (q)	54, 52 (q)
2	126.9	123.5	123.5	1.85	-5.85	nd[b]	nd[b]
6	123.8	123.5	123.5	1.85	-5.85	nd[b]	nd[b]
5	121.2	118.9	118.3	1.88	-3.23	nd[b]	nd[b]
4	120.2	118.9	118.3	1.88	-3.23	nd[b]	nd[b]
7	113.7	114.0	113.5	1.87	-14.99	nd[b]	nd[b]
3	109.2	114.0	113.5	1.87	-14.99	nd[b]	nd[b]
α	56.9	58.0	57.7	1.08	1.03	42 (t)	38 (t)
β	28.2	28.4	28.2	1.42	-0.81	39 (t)	45 (t)

[a] - reference value; nd[b] – not determined because of overlapping signals

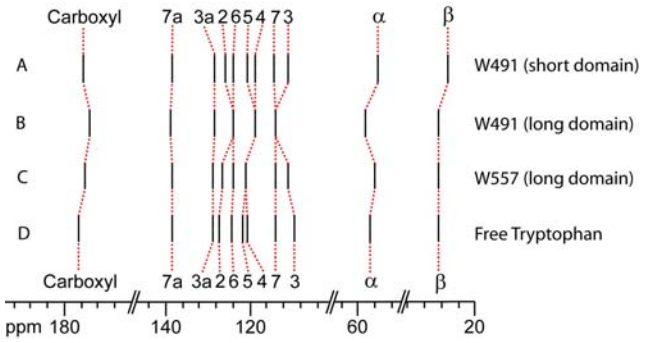

Figure 3.16 ^{13}C chemical shifts of LOV2 domain as detected in: A) W491 (short domain) - C450A, [U-$^{13}C_6$]glucose labeled, short LOV2 domain. B) W491 (long domain) – C450A/W557A, [U-$^{13}C_{11}$]tryptophan labeled, long LOV2 domain. C) W557 (long domain) – C450A/W491A, [U-$^{13}C_{11}$]tryptophan labeled, long LOV2 domain.

As shown below, the CIDNP spectra of protein samples prepared by fermentation with single or multiple ^{13}C-labeled glucose support the tentative assignments shown with [U-$^{13}C_{11}$]tryptophan labeling. Emissive ^{13}C NMR signals can also be observed under blue light irradiation of LOV2 domain samples prepared by *in vivo* labeling with singly or multiply ^{13}C-labeled glucose as carbon source, which strongly support the assignment of tryptophan obtained.

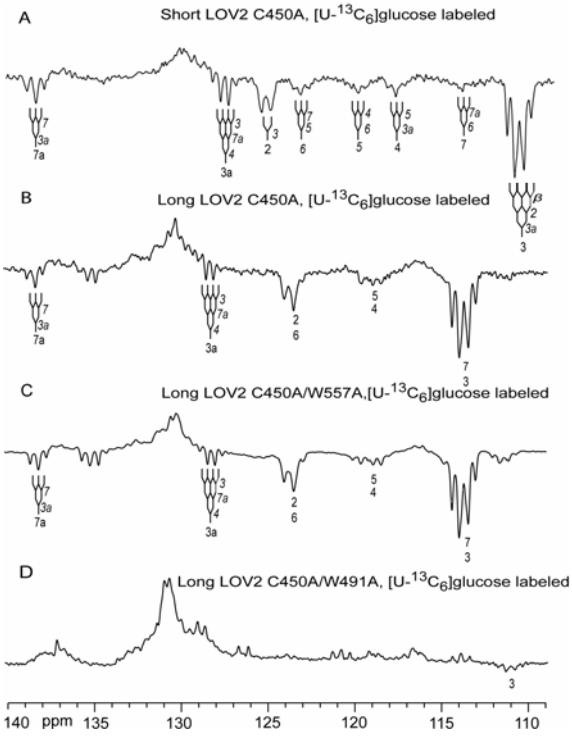

Figure 3.17 ^{13}C NMR spectra of LOV2 domain from C450A mutant and double mutants labeled with [U-$^{13}C_6$]glucose under blue light irradiation. A) Short LOV2 domain C450A mutant. B) Long LOV2 domain C450A mutant C) Long LOV2 domain C450A/W557A double mutant. D) Long LOV2 domain C450A/W491A double mutant.

Figure 3.17C shows the light spectrum of a sample of the C450A/W557A double mutant ("long version") obtained by *in vivo* labeling with [U-$^{13}C_6$]glucose. In the blue light irradiation spectrum of the C450A/W557A double mutant labeled with [U-$^{13}C_6$]glucose, the indole region is closely similar to that of the protein labeled with [U-$^{13}C_{11}$]tryptophan in figure 3.15C. Obviously, the emissive signals in the globally labeled protein in that region are predominantly or exclusively due to emission from the side chain of tryptophan 491.

Light spectra for partially ^{13}C-labeled protein samples that were obtained by growth of the *E. coli* strains hyperexpressing the long or short LOV2 domains in the presence of [1-$^{13}C_1$]-, [2-$^{13}C_1$]- or [3-$^{13}C_1$]glucose are shown in figure 3.18 and figure 3.19, respectively.

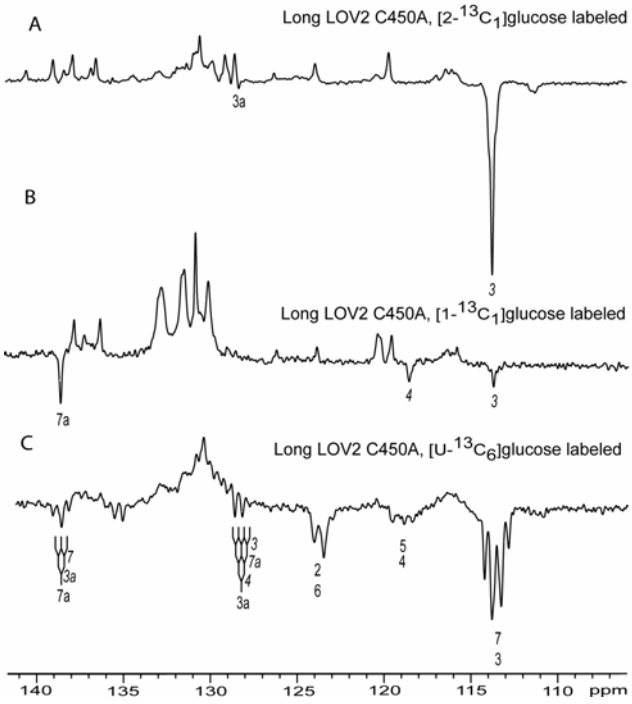

Figure 3.18 ^{13}C-NMR signals of long LOV2 C450A domain. Light spectrum of ^{13}C-labeled sample from A) [2-$^{13}C_1$]glucose. B) [1-$^{13}C_1$]glucose. C) [U-$^{13}C_6$]glucose.

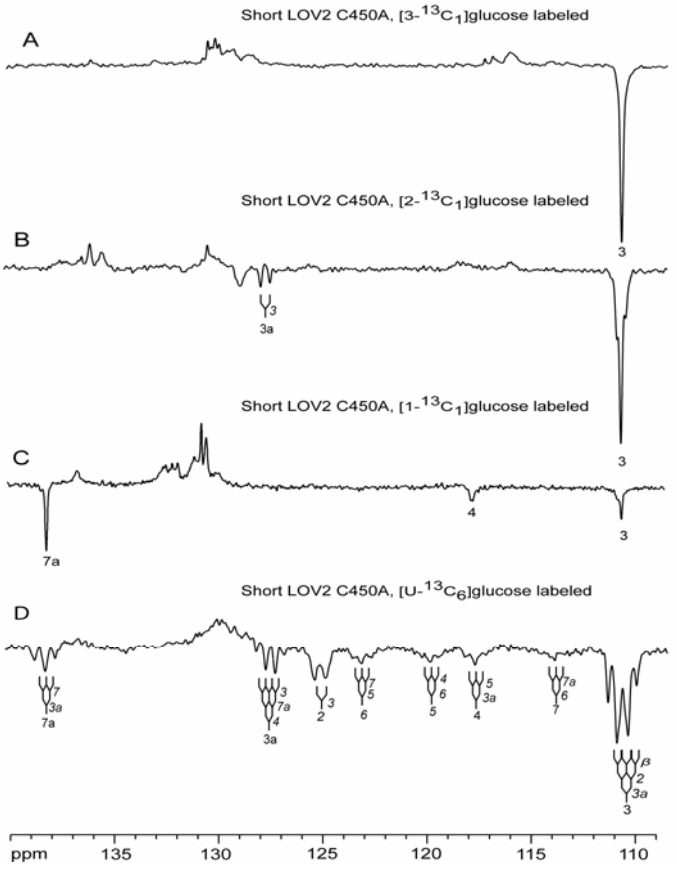

Figure 3.19 ^{13}C-NMR signals of short LOV2 C450A domain. Light spectrum of ^{13}C-labeled sample from A) [3-$^{13}C_1$]glucose. B) [2-$^{13}C_1$]glucose. C) [1-$^{13}C_1$]glucose. D) [U-$^{13}C_6$]glucose.

Whereas *in vivo* labeling with [U-$^{13}C_6$]glucose affords biosynthetic [U-$^{13}C_{11}$]tryptophan, labeling with single-labeled glucoses affords complex isotopologue mixtures of tryptophan that serve as precursors for protein synthesis. In order to unequivocally assess the labeling pattern of tryptophan in those samples, *E. coli* biomass grown with single-labeled glucose isotopologues was hydrolyzed under the same conditions as those used for protein labeling and isolated biosynthetic tryptophan by preparative HPLC. Each isolated tryptophan sample was then analyzed by ^{13}C NMR spectroscopy. Signal integrals for individual carbon atoms were referenced to integrals in the spectrum of tryptophan with natural ^{13}C abundance, thus affording ^{13}C abundances for each tryptophan carbon (Table 3.8 and Fig. 3.20).

Table 3.8 ^{13}C abundance of tryptophan isolated from short LOV2 C450A domain grown with [1-$^{13}C_1$]glucose, [2-$^{13}C_1$]glucose, [3-$^{13}C_1$]glucose. The expected ^{13}C labeling from shikimate pathway of tryptophan biosynthesis is shown in bold (cf. Fig. 3.20).

Carbon position	Coupling constant (Hz)	^{13}C abundance (%)					
		[1-$^{13}C_1$]glucose		[2-$^{13}C_1$]glucose		[3-$^{13}C_1$]glucose	
		Total	Isotopologues	Total	Isotopologues	Total	Isotopologues
Carboxyl	54[a,c]	3.1	0.7 [carboxyl, α-$^{13}C_2$]	7.3	nd	**32.8**	4.3 [carboxyl, α-$^{13}C_2$]
7a	59[a]	**29.0**	1.9 [7a, 3a-$^{13}C_2$]	6.8	nd	0.2	nd
3a	58[a],54[b,c]	6.2	3.4 [3a, 7a-$^{13}C_2$]	**36.5**	10.0 [3a, 3-$^{13}C_2$]	3.0	1.5 [3a, 3-$^{13}C_2$]
2	70[a],69[c]	**18.1**	nd	**57.5**	nd	6.5	nd
6	55[a],59[b,c]	2.8	0.8 [6, 7-$^{13}C_2$]	5.8	1.5 [6, 7-$^{13}C_2$]	**13.7**	9.2 [6, 7-$^{13}C_2$]
5	58[a],48[b],55[c]	4.8	1.9 [5, 4-$^{13}C_2$]	**20.7**	nd	2.3	nd
4	60[a,b]	**17.5**	2.5 [4, 5-$^{13}C_2$]	4.7	nd	0.6	nd
7	64[a],60[b],59[c]	3.3	1.6 [7, 6-$^{13}C_2$]	14.2	2.4 [7, 6-$^{13}C_2$]	**54.5**	12.7 [7, 6-$^{13}C_2$]
3	49[a],55[b],57[c]	1.2	0.6 [3, β-$^{13}C_2$]	16.8	6.7 [3, 3a-$^{13}C_2$]	**41.7**	7.2 [3, 3a-$^{13}C_2$]
α	34[a,b],54[a,b],55[c]	5.0	1.7 [α , β -$^{13}C_2$], 0.5 [α, carboxyl-$^{13}C_2$]	**35.0**	1.7 [α , β-$^{13}C_2$]	6.0	3.1 [α, carboxyl-$^{13}C_2$]
β	34[a],33[b],49[a,b,c]	**33.6**	2.0 [β, α -$^{13}C_2$], 1.5 [β, 3-$^{13}C_2$]	8.6	1.5 [β, α -$^{13}C_2$]	1.3	nd

[a] - coupling constant from [1-$^{13}C_1$]glucose; [b] - coupling constant from [2-$^{13}C_1$]glucose; [c] – coupling constant from [3-$^{13}C_1$]glucose; nd – not determined

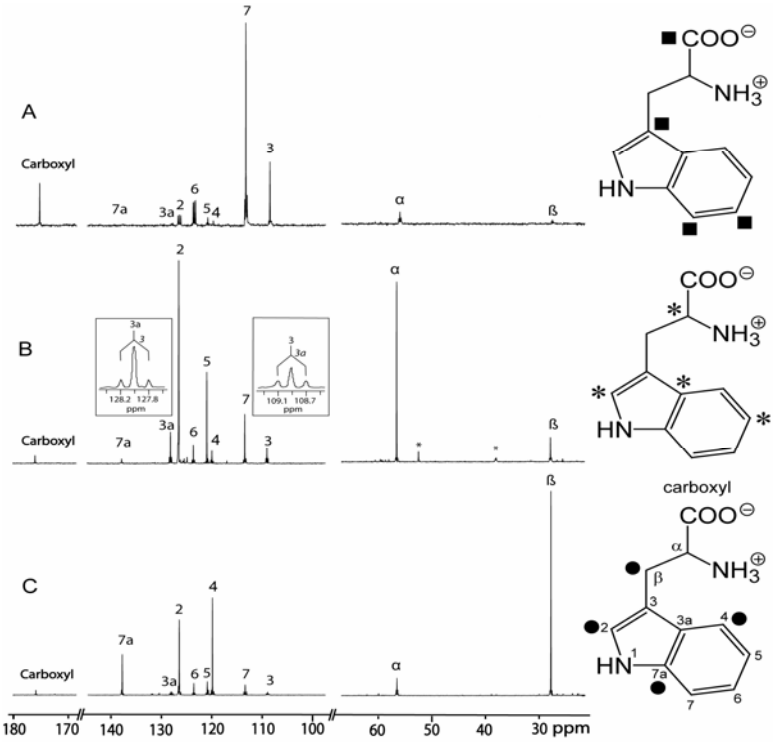

Figure 3.20 ^{13}C-NMR signals of ^{13}C abundance of tryptophan isolated from short LOV2 C450A domain grown in A) [3-$^{13}C_1$]glucose. B) [2-$^{13}C_1$]glucose. C) [1-$^{13}C_1$]glucose.

Notably, these labeling patterns are well in line with expectations based on central intermediary metabolism and the shikimate pathway in bacteria (Fig. 3.21).

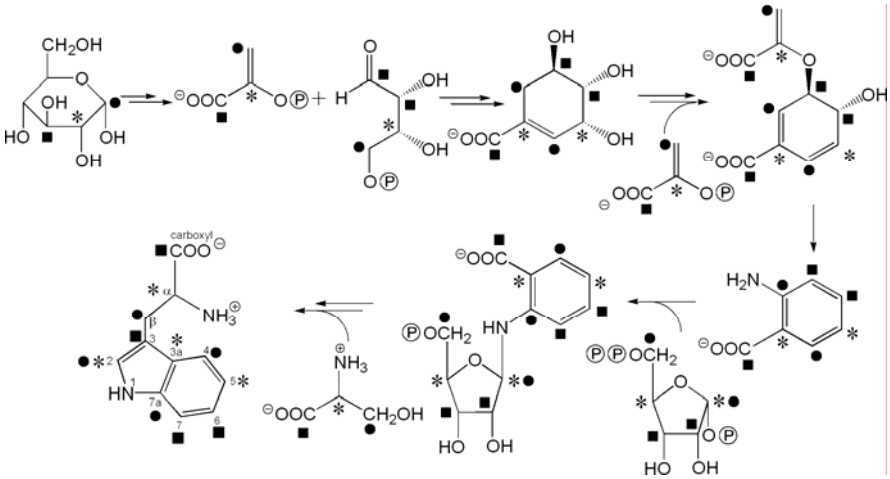

Figure 3.21 Transfer of ^{13}C label from [1-$^{13}C_1$]glucose, [2-$^{13}C_1$]glucose, [3-$^{13}C_1$]glucose into tryptophan by shikimate pathway.

It should also be noted that the ^{13}C signals of the isolated tryptophan samples appear predominantly as singlets (i.e. $^{13}C^{13}C$ coupling satellites have low relative intensities). Hence, ^{13}C atoms were typically not flanked by ^{13}C in directly adjacent positions. This aspect is relevant for the analysis of polarization transfer processes mediated by interaction of electron and nuclear spin.

From the study of LOV2 domains (long and short version) with universal labeling of tryptophan carbons or universal labeling of the entire protein, it is obvious that most if not all indole carbon atoms of tryptophan 491 can give rise to emissive ^{13}C NMR multiplets under continuous blue light irradiation, albeit with different intensity that varies by a factor of about 10. In stark contrast, only the indole carbon atoms 3, 7a, 4 and possibly 3a give rise to detectable emissive signals in protein samples, where the indole rings carry single ^{13}C labeling as opposed to universal labeling. This finding cannot be explained by low levels of labeling since all indole carbon atoms acquire a minimum of 14 % ^{13}C abundance in at least one of the labeled specimens. For example, C(4) is ^{13}C-enriched to about 18 % in the sample obtained from [1-$^{13}C_1$]glucose, C(2) and C(5) are enriched to about 57 and 21 %, respectively, in the sample from [2-$^{13}C_1$]glucose, and C(7) and C(6) are enriched to about 54 and 14 %, respectively, in the sample from [3-$^{13}C_1$]glucose. However, none of these carbons show up in the respective spectra. Relative intensities for negative emission, referenced to the level of ^{13}C abundance, are summarized in tables 3.9 and 3.10 indicating that emissive intensities of carbon atoms 2, 3a, 6, and 7 are significantly lower in the single-labeled specimens as

compared to their appearance in the multiply ^{13}C-labeled samples. For this comparison, it is relevant that the signal amplitude in multiply ^{13}C-labeled samples is diminished by signal splitting due to $^{13}C^{13}C$ coupling. These findings provide a window for the experimental study of spin polarization transfer via sets of contiguous ^{13}C atoms.

Table 3.9 Emissive signals of short LOV2 C450A domain from [U-$^{13}C_6$]glucose, [1-$^{13}C_1$]glucose, [2-$^{13}C_1$]glucose.

Carbon Position	Emissive Signals of LOV2 C450A from [U-$^{13}C_6$]glucose			Emissive Signals of LOV2 C450A from [1-$^{13}C_1$]glucose		Emissive Signals of LOV2 C450A from[2-$^{13}C_1$]glucose	
	Chemical shift [ppm]	Coupling Constant [hz]	Relative Intensity	Relative Intensity	Normalized Intensity [a]	Relative Intensity	Normalized Intensity [a]
Carboxyl							
7a	138.2	61 (t)	0.19	1.3	37.7		
3a	128.1	58 (q)	0.16			0.06	2.2
2	125.5	69 (d)	0.38				
6	123.5	55 (t)	0.22				
5	120.1	60 (t)	0.20				
4	118.3	58 (t)	0.23	0.5	8.7		
7	114.1		0.10				
3	110.6	70, 53(q)	1.0	1.0	1.2	1.0	16.8

[a] – relative intensity x ^{13}C abundance (cf.. Table 3.8)

Table 3.10 Emissive signals of long LOV2 C450A domain from [U-$^{13}C_6$]glucose, [1-$^{13}C_1$]glucose and, [2-$^{13}C_1$]glucose.

Carbon Position	Emissive Signals of LOV2 C450A from [U-$^{13}C_6$]glucose			Emissive Signals of LOV2 C450A from [1-$^{13}C_1$]glucose		Emissive Signals of LOV2 C450A from [2-$^{13}C_1$]glucose	
	Chemical shift [ppm]	Coupling Constant [hz]	Relative Intensity	Relative Intensity	Normalized Intensity [a]	Relative Intensity	Normalized Intensity [a]
Carboxyl							
7a	138.6	59 (t)	0.20	0.6	17.7		
3a	128.4	63, 54 (q)	0.11			0.04	1.5
2	123.8		0.50				
6	123.8		0.50				
5	118.9		0.53				
4	118.9		0.53	0.7	12.2		
7	113.5		-				
3	113.5	67, 53 (q)	1.0	1.0	1.2	1.0	16.8

[a] – relative intensity x ^{13}C abundance (cf. Table 3.8)

Whereas the CIDNP study has been focused on experiments with the “long” version of the LOV2 domain comprising the C-terminal helix, it is relevant to note that the chemical shift values of tryptophan 491 are substantially affected by that additional helix. Tentatively, it appears that the chemical shifts of tryptophan 557 in the long version and of tryptophan 491

in the short version are closer to those of tryptophan in aqueous solution as compared to those of tryptophan 491 in the long version. This may imply that the latter residue has a lower degree of solvation. Based on that hypothesis, the data suggest that solvation is not significantly affecting polarization transfer.

3.1.2.1 Discussion

Compared to NMR spectra obtained from LOV2 C450A in the dark, strongly polarized signals in enhanced absorption and emission were observed when NMR spectra were recorded in the presence of blue light. Polarized NMR transitions are a signature of CIDNP. The origin of CIDNP lies in the radical-pair mechanism which postulates that if the outcome of a photochemical reaction depends on the extent of singlet-triplet mixing in the radical pair intermediates and if this mixing is partly driven by the electron-nuclear hyperfine interaction, then the reaction products could have strongly polarized NMR lines (Kaptein, 1975).

In the following figure 3.22 a reaction mechanism is shown that is consistent with the above-mentioned experimental observations. The ground-state FMN in the fully oxidized (diamagnetic and hence NMR-observable) redox state is promoted into its excited singlet state, ^{1}FMN, by absorption of blue light. This is followed by intersystem crossing to the triplet state, ^{3}FMN, which is generated with high quantum yield. ^{3}FMN is a potent oxidant for redox-active amino-acid residues within the LOV2 domain, and may thus abstract an electron from a nearby redox-active amino-acid residue (species A = tryptophan residue) to form a geminate radical pair, $^{3}[FMN^{\bullet-}\cdots A^{\bullet+}]$, in a spin-correlated triplet electron-spin configuration. This radical pair may either evolve to an electronic singlet state, $^{1}[FMN^{\bullet-}\cdots A^{\bullet+}]$, which subsequently may undergo spin-allowed back electron transfer to regenerate the ground-state reactants (FMN and A), or may loose its spin correlation by a subsequent second electron-transfer step to form uncorrelated radicals. Due to the different rates with which the ground-state reactants are formed *via* the singlet and the triplet radical-pair channels, the nuclear enhancements of opposite signs will no longer cancel out, and an effective nuclear spin polarization will prevail in the ground states (FMN and A).

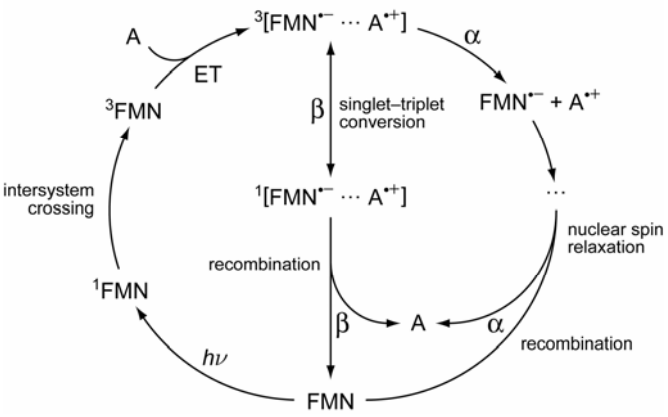

Figure 3.22 Proposed reaction mechanism for the photoinduced reaction of LOV2 C450A. α and β denote the nuclear-spin state of ^{13}C nuclei.

As mentioned above, a recombinant short LOV2 domain has shown to afford an emissive ^{13}C NMR signal at 110.6 ppm under blue light irradiation, which cannot be attributed to the FMN cofactor. Universal labeling of that protein by growth of a recombinant *E. coli* hyperexpression strain with [U-$^{13}C_6$]glucose afforded a multiplet in emissive mode at 110.6 ppm under blue light irradiation. Several additional emissive signals ^{13}C NMR signals were observed in the range of 110 – 140 ppm. These signals showed fine structure arising by $^{13}C^{13}C$ coupling and were tentatively interpreted as the CIDNP signature of a photochemically induced tryptophan radical. For a more detailed CIDNP study and for an unambiguous identification of the amino acid interacting with FMN in a photoinitiated radical-pair mechanism, C-terminal helix region was included in the construct extending amino acid residue 559 of phototropin (long LOV2 domain). Whereas the short LOV2 domain contains one tryptophan residue (W491), the long LOV2 domain contains two tryptophan residues (W491 and W557). In the long LOV2 domain, W491 and W557, are both well separated [(>1.3 nm in a calculated structure of *A. sativa* LOV2 C450A based on *Adiantum* LOV2 as a model (Crosson et al., 2001)] from the FMN chromophore thus fulfilling the requirements for the generation of nuclear-spin polarization governed by nuclear hyperfine interactions.

The replacement of tryptophan 557 by alanine did not change the NMR pattern but the replacement of tryptophan 491 by alanine quenched the emissive signal. These observations suggest that tryptophan 491 and the FMN chromophore jointly form a radical pair upon blue light irradiation. The emissive tryptophan signals are believed to arise by polarization transfer during the photochemical generation of biradical states where one electron is located on the flavin cofactor and the other is located on a tryptophan residue.

3.1.3 CIDNP study on LOV2 domain C450A mutant reconstituted with 5-deaza-FMN

In contrast to natural flavocoenzymes, the deaza analog can serve as a hydride transponder but fails to form a radical in the electronic ground state, although it can form a radical after optical excitation. A radical mechanism has been implicated in the photoadduct formation by LOV domains (Kay et al., 2003). It was therefore of interest, whether the deaza FMN could replace the natural cofactor, FMN, in the photocycle of the light sensing domain.

LOV2 domain of *A. sativa* phototropin was reconstituted with 5-deaza-FMN, a flavocoenzyme analog that has been used intensely in mechanistic studies of flavoenzymes involved in redox reactions (Jorns and Hersh, 1976).

The FMN cofactor of the LOV2 domain of *A. sativa* can be released under mild conditions by treatment with urea. The apoprotein could be reconstituted with 5-deaza-FMN affording a complex with absorption maxima at 402 nm and a shoulder at 420 nm.

Blue light irradiation was conducive to the progressive disappearance of long wavelength absorbance and shifted the apparent maximum of the lowest energy optical transition to 337 nm. When the irradiated protein was kept in the dark at 4°C, the absorption spectrum remained unchanged for periods of at least several days. However, ultraviolet irradiation was conducive to the regeneration of the "as isolated" form of the protein with absorbance maxima at 402 nm. The entire photocycle could be repeated without apparent permanent changes in the spectra. Serial spectra acquired during the reversible conversion in both directions are shown in figure 3.23.

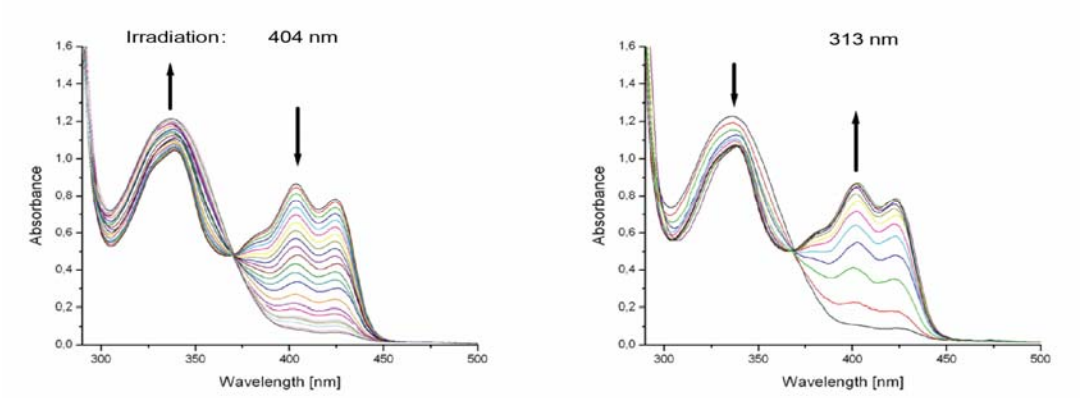

Figure 3.23 Reversible bleaching (left side) and recovering (right side) of the long wavelength absorbance of the reconstituted LOV2 domain from *A. sativa* with 5-deaza-FMN during irradiation with 404 and 313 nm, respectively.

The blue light induced transition to the state absorbing at 337 nm is accompanied by substantial modulation of the circular dichroism (CD) spectrum. Notably, the form absorbing at shorter wavelength is characterized by strong cotton effects in the short wavelength range (Fig. 3.24).

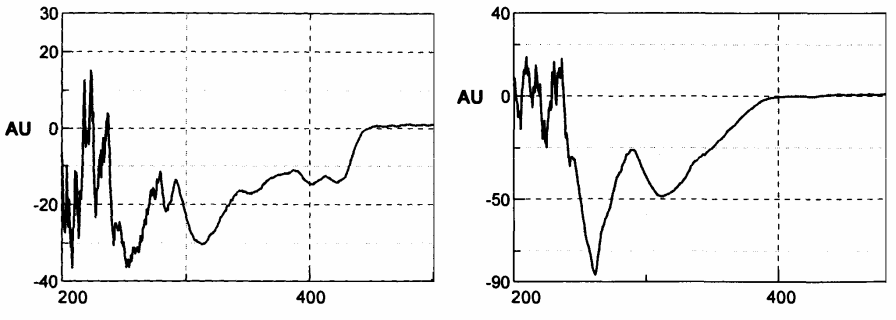

Figure 3.24 CD spectra of the 5-deaza-FMN reconstituted LOV2 domain "as isolated" (left side) and after blue light irradiation (right side).

In an analogous experiment, the C450A mutant of the LOV2 domain was reconstituted with 5-deaza-FMN. The reconstituted protein had an absorption maximum at 403 nm. The spectrum was not significantly modified by either blue light or ultraviolet irradiation.

A ^{13}C NMR spectrum of the mutant protein loaded with 5-deaza-FMN which was acquired under continuous blue light irradiation shows a negative signal at 111 ppm (Fig. 3.25) that is not observed under dark condition.

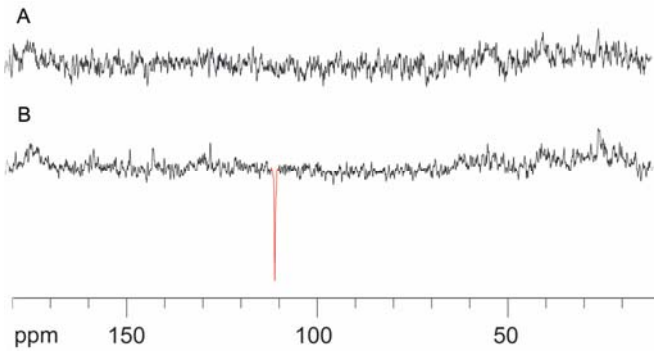

Figure 3.25 ^{13}C NMR spectrum of the LOV2 C450A domain (*A. sativa*) loaded with 5-deaza-FMN. (A) Under dark condition. (B) Under continuous blue light irradiation.

In order to assign the emissive signal to a specific amino acid residue, ^{13}C-labeled LOV2 C450A protein reconstituted with 5-deaza- FMN sample was prepared. More specifically, the *E. coli* hyperexpression strain was grown in medium containing [U-$^{13}C_6$]glucose as carbon source affording totally ^{13}C-labeled protein.

Short and long LOV2 C450A domain labeled *in vivo* with [U-$^{13}C_6$]glucose showed similar patterns of emissive signals under blue light irradiation in the range of 110-140 ppm. A strong emissive line was recorded at 111 ppm in both long and short LOV2 C450A domain, which was split into a pseudo-quadruplet due to simultaneous ^{13}C-coupling with three adjacent ^{13}C-atoms. Next to this signal, additional emissive multiplets at lower intensities were observed. The chemical shifts, as well as the ^{13}C-multiplicities, tentatively suggest a [U-$^{13}C_{11}$]tryptophan residue as the source of the emissive signals. Specifically, the signal at 111 ppm correlates with the C(3) atom of tryptophan. The pseudo-quadruplet pattern can be explained by simultaneous ^{13}C-coupling with C(2), C(β) and C(3a) of tryptophan. The other emissive signals with their specific multiplet structures were also in good agreement, with C(2), C(7a), C(7), C(5), C(4), C(6) and C(3a) of a tryptophan residue, and were most prominent in short LOV2 domain. So this preliminary assignment was further confirmed by the emissive signals observed from long LOV2 domain, with the specifically ^{13}C-labeled protein sample from [1-$^{13}C_1$]glucose and [2-$^{13}C_1$]glucose as shown in figure 3.26.

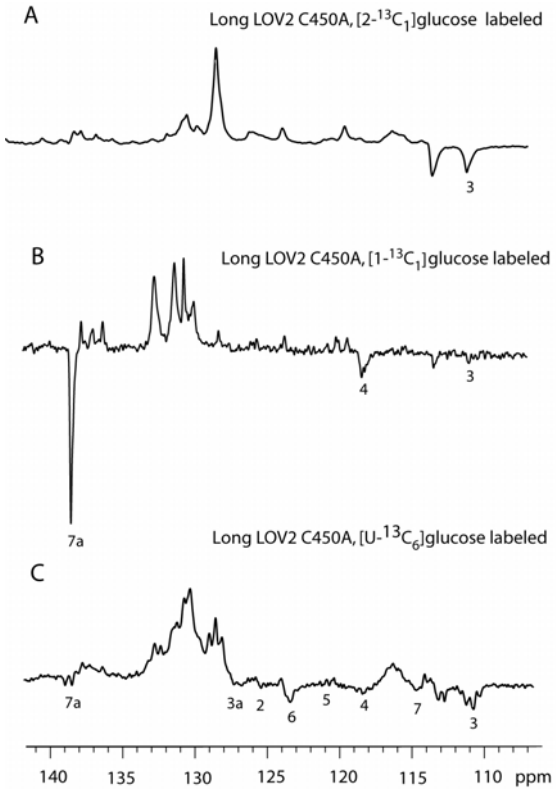

Figure 3.26 ^{13}C-NMR spectra of long LOV2 C450A domain reconstituted with deaza FMN. Light spectrum of ^{13}C-labeled sample from A) [2-$^{13}C_1$]glucose. B) [1-$^{13}C_1$]glucose. C) [U-$^{13}C_6$]glucose.

As shown above, emissive CIDNP signals from tryptophan radicals can be observed in LOV domains even without labeling. Figure 3.27 shows NMR spectra of the recombinant LOV2 C450A domain and of a double mutant that were both reconstituted with deaza FMN but were not ^{13}C-labeled.

The long and short LOV2 domain shows an emissive signal at 111.0 ppm (Fig. 3.27A and 3.27B) despite of nonsignificant signal from long LOV2 domain. The replacement of tryptophan 557 by alanine in the long protein version did not change the NMR pattern (Fig. 3.27C); but the replacement of tryptophan 491 by alanine quenched the emissive signal (Fig. 3.27D). These observations suggest that tryptophan 491 and the FMN chromophore jointly form a radical pair upon blue light irradiation.

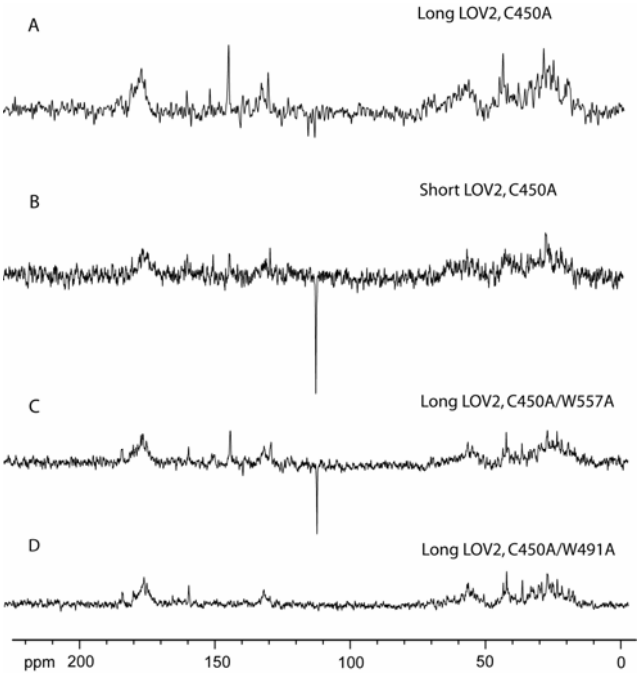

Figure 3.27 Overlay of ^{13}C NMR spectra of LOV2 samples reconstituted with deaza FMN under blue light irradiation. (A) Long LOV2 domain C450A mutant; (B) Short LOV2 domain C450A mutant; (C) Long LOV2 domain C450A/W557A mutant; (D) Long LOV2 domain C450A/W491A mutant.

The double mutant strain was also grown in medium containing [U-$^{13}C_6$]glucose as a carbon source affording totally ^{13}C-labeled protein and reconstituted with deaza FMN. ^{13}C NMR spectra of the two respective mutant proteins labeled with [U-$^{13}C_6$]glucose obtained under blue light illumination are shown in figure 3.28. In agreement with previous experiments, the replacement of tryptophan 491 by alanine (W491A) was accompanied by the loss of the emissive signal (Fig. 3.28D).

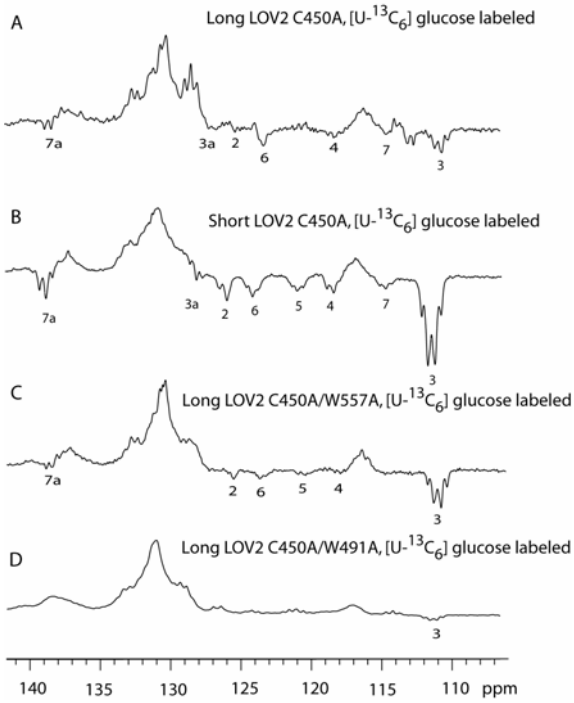

Figure 3.28 ^{13}C NMR spectra of LOV2, C450A mutant and double mutants labeled with [U-$^{13}C_6$]glucose and reconstituted with deaza-FMN, under blue light irradiation. (A) Long LOV2 C450A; (B) Short LOV2 C450A; (C) Long LOV2 C450A/W557A; (D) Long LOV2 C450A/W491A.

In order to further establish the tentative assignment of the signal, the mutant genes were expressed in a tryptophan auxotroph of *E. coli* that was grown with a supplement of [U-$^{13}C_{11}$]tryptophan. The ^{13}C NMR spectra of both mutants obtained without illumination showed characterstic sets of multiplets that could be easily assigned as tryptophan signals on the basis of chemical shifts of tryptophan, signal intensity and $^{13}C^{13}C$ coupling patterns. ^{13}C NMR spectra of the mutant proteins obtained under dark condition and under continuous blue light irradiation are shown in figure 3.29.

In the W557A mutant protein under blue light irradiation, all signals assigned to the indole ring of trp 491 appear in the emissive mode (Fig. 3.29II). Notably, the signal of the β side chain carbon atom also appears in the emissive mode, whereas the carboxylic group and α carbon atom appear in absorptive mode. No changes of the chemical shift or coupling pattern were detected compared to the chemical shift in dark condition. Hence, there can be no doubt that the emissive signals can be assigned to the neutral state of the tryptophan side chain (as opposed to a trp radical state).

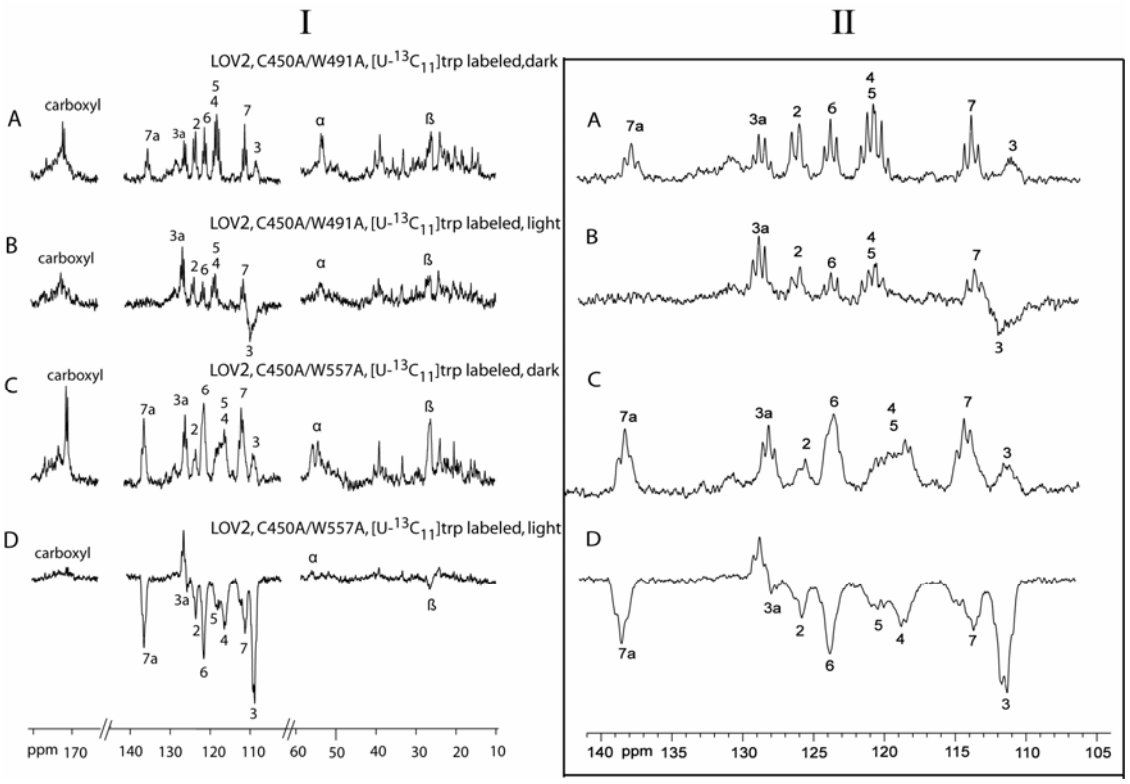

Figure 3.29 (I) ^{13}C NMR spectra of double mutant protein labeled with [$U^{13}C_{11}$]tryptophan and reconstituted with deaza-FMN. (A) LOV2, C450A/W491A under dark condition and (B) LOV2, C450A/W491A under blue light irradiation; (C) LOV2, C450A/W557A under dark condition and (D) LOV2, C450A/W557A under blue light irradiation. (II) The enlarged portion of indole region in the range of 110-140 ppm.

In the ^{13}C NMR spectrum of the C450A/W491A mutant, only the signal of C(3) appears in the emissive mode under blue light observation. That signal shows a quartet signature, which shows unequivocally that it belongs to trp557 and not to some other amino acid. The coupling patterns and the chemical shifts of the tryptophan signals are the same as those observed in the absence of light. Again, it follows that the signals observed under blue light irradiation can be assigned to the tryptophan side chain. The chemical shift data of both mutant proteins are summarized in figure 3.30 and table 3.11.

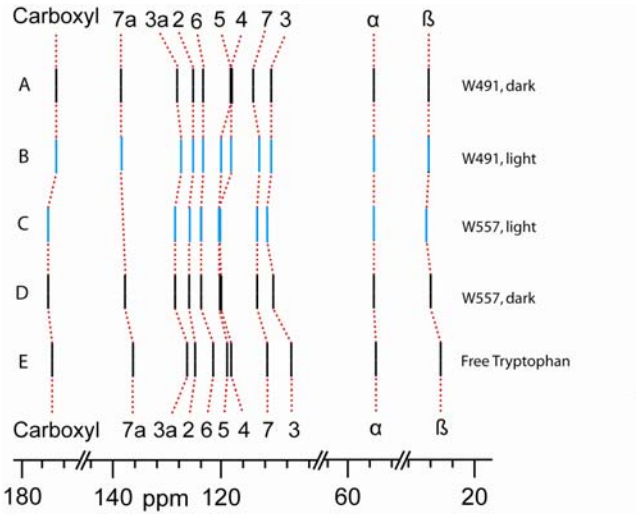

Figure 3.30 ^{13}C chemical shifts of long LOV2 double mutant domain as detected in [U-$^{13}C_{11}$]tryptophan labeled protein, reconstituted with deaza-FMN:
A) W491, dark –W557A, [U-$^{13}C_{11}$]tryptophan labeled, long LOV2 domain in dark condition.
B) W491, light–W557A, [U-$^{13}C_{11}$]tryptophan labeled, long LOV2 domain in light condition.
C) W557, dark –W491A, [U-$^{13}C_{11}$]tryptophan labeled, long LOV2 domain in dark condition.
D) W557, light –W491A, [U-$^{13}C_{11}$]tryptophan labeled, long LOV2 domain in light condition.

Table 3.11 ^{13}C NMR chemical shifts of LOV2C450A/W491A, LOV2C450A/W557A double mutant labeled with [U$^{13}C_{11}$] tryptophan.

Carbon Position	Free tryptophan	LOV2 C450A/W491A		LOV2 C450A/W557A	
		Dark	Light	Dark	Light
Carboxyl	176.4	175.0	175.2	173.5	173.5
7a	138.2	137.9	-	138.5	138.5[e]
3a	128.3	128.5	128.7	128.2	127.7[e]
2	126.9	126.1	126.1	125.5	125.5[e]
6	123.8	123.7	123.7	123.5	123.5[e]
5	121.2	120.5	120.7	118.5	120.1[e]
4	120.2	120.5	120.7	118.5	118.2[e]
7	113.7	113.6	113.5	114.1	113.1[e]
3	109.2	110.7	111.7[e]	111.0	111.0[e]
α	56.9	55.5	55.5	55.4	55.4
β	28.2	28.2	28.7	28.4	28.4[e]

[e] - emmisive signal

3.1.3.1 Discussion

The UV/vis data suggest that the thiol group of cystein 450 can form an adduct with the artificial deazaflavin cofactor which fails to undergo spontaneous fragmentation but can be cleaved by ultraviolet irradiation. It is assumed that the wild type protein undergoes a light-

driven addition of the C450 thiol group to carbon 5 of the deaza-FMN chromophore instead of the 4a adduct formation that is characteristic of the natural FMN chromophore. That adduct is characterized by a high degree of stability at room temperature in the dark, but fragmentation can be induced by ultraviolet irradiation.

The strong negatively polarized NMR signal in the ^{13}C NMR spectrum of the C450 A mutant under blue light illumination suggests that the reaction steps after the excitation of the 5-deaza-FMN cofactor also follow a radical pair mechanism.

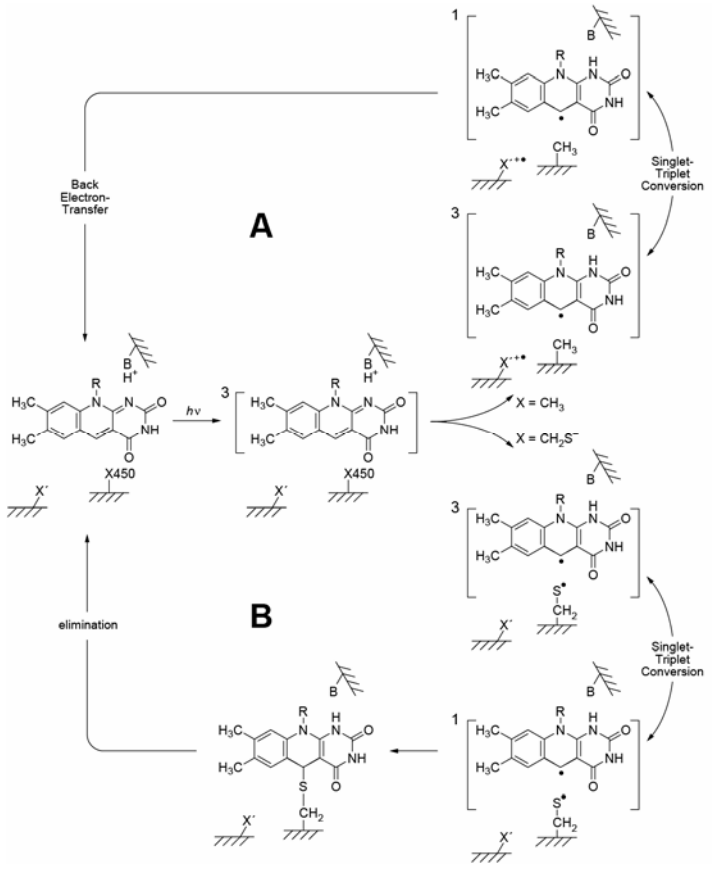

Figure 3.31 Hypothetical radical-pair mechanism for the formation of the 5-deaza-FMNH• radical in the LOV2 C450A mutant reconstituted with 5-deaza-FMN (A) or the 5-deaza-FMN-C(5)-cysteinyl adduct in the wild-type LOV2 domain (B) after absorption of blue light by 5-deaza-FMN cofactor.

The ^{13}C NMR spectrum of C450A mutant obtained under blue light illumination of universally ^{13}C-glucose and universally ^{13}C-tryptophan labeled LOV domain reconstituted with 5-deaza-FMN showed several multiplets in emissive mode that could be assigned to a tryptophan 491 residue. The emissive lines are believed to arise by polarization transfer during the recombination of a photochemically generated biradical state.

3.1.4 ENDOR spectroscopy of LOV2 domain C450A mutant

ENDOR (Electron-Nuclear Double Resonance) spectroscopy is a technique that is useful for learning about the structure of paramagnetic molecules, as well as to get information about the distances and orientations of atoms surrounding paramagnetic centres. ENDOR makes use of the electron-nuclear hyperfine couplings between the unpaired electrons and neighbouring nuclei and measures them with much higher precision than may be possible by EPR spectroscopy alone causing the fragmentation of one EPR line into several lines. Because it examines nuclei in the vicinity of unpaired electrons, ENDOR can provide information that conventional NMR misses, due to the short relaxation times of these nuclei. The technique uses two frequencies: a fixed microwave frequency to partially saturate electronic Zeeman transitions and monitor the intensity of the EPR signal, and a strong radiofrequency which is varied in order to excite nuclear (NMR) Zeeman transitions.

ENDOR spectroscopy usually is performed on paramagnetic species in liquids and solids. In liquids, ENDOR spectra typically give information on the isotropic hyperfine couplings, while in solids (single crystals, powders, frozen solutions) both isotropic and anisotropic hyperfine interactions are observed. From the isotropic hyperfine coupling constant, information about the electron density at the nucleus can be gained, whereas from the anisotropic hyperfine coupling constant, information about geometry of the molecule can be gleaned.

Coenzyme analogs labeled with ^{13}C, ^{15}N have been used as probes enabling the spectroscopic analysis like ENDOR with a specific emphasis on flavoproteins. In principle, stable isotope labeling in ENDOR visualize/enhance the complete assignment of coupling constant of flavocoenzyme.

ENDOR spectroscopy done in co-operation with PD Dr. Stefan Weber enabled for the first time the complete assignment of the hyperfine coupling constant for flavocoenzyme in complex with LOV2 domain C450A mutant.

Figure 3.32 depicts the W-band EPR spectrum of the $FMNH^{\bullet}$ cofactor of LOV2 C450A recorded at 80 K. The signal shape is asymmetric due to the anisotropy of the Zeeman interaction, which under solid-state conditions is dominant at magnetic-field strengths corresponding to EPR transitions at W-band frequencies. By spectral simulation, the principal values of the g-matrix have been extracted: $g_X = 2.0042$, $g_Y = 2.0035$ and $g_Z = 2.0020$ (X, Y, and Z denote the directions of the principal axes of g) (Kay et al., 2003). By recording ENDOR spectra at different magnetic-field strengths within the range of EPR resonances,

hyperfine spectra are obtained that contain only signals arising from the subset of those molecules that are on resonance at the respective position in the EPR signal. In general, two ENDOR lines are expected under solid-state conditions per group of magnetically equivalent nuclei. These are separated by the orientation-dependent hyperfine coupling constant *A* that characterizes the coupling of the nuclear magnetic moment to the electron magnetic moment.

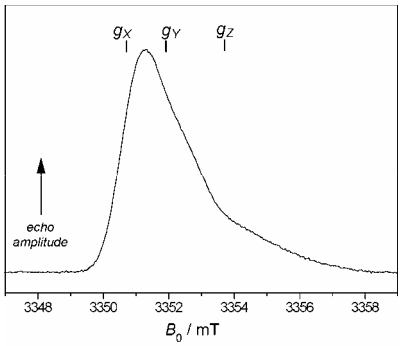

Figure 3.32 W-band EPR spectrum of $FMNH^{\bullet}$ in *A. sativa* LOV2 domain (C450A mutant). The position g_X, g_Y and g_Z denote the maxima of the simulated principal axes of g.

As the ENDOR resonances from all ^{13}C nuclei overlap in the ^{13}C W-band ENDOR spectra of the C450A mutant of *A. sativa* LOV2 reconstituted with [U-$^{13}C_{17}$,U-^{15}N4]FMN, it is very difficult to extract the signal contributions of single ^{13}C nuclei. Therefore, an assignment of the hyperfine couplings is difficult. To overcome this problem, ENDOR studies were done on a series of proteins that have been reconstituted with selectively ^{13}C-labeled FMN isotopologues. The spectra from these protein samples with ^{13}C hyperfine couplings of carbons in the xylene ring of $FMNH^{\bullet}$ and in the ribityl side chain of $FMNH^{\bullet}$ are shown in figure 3.33.

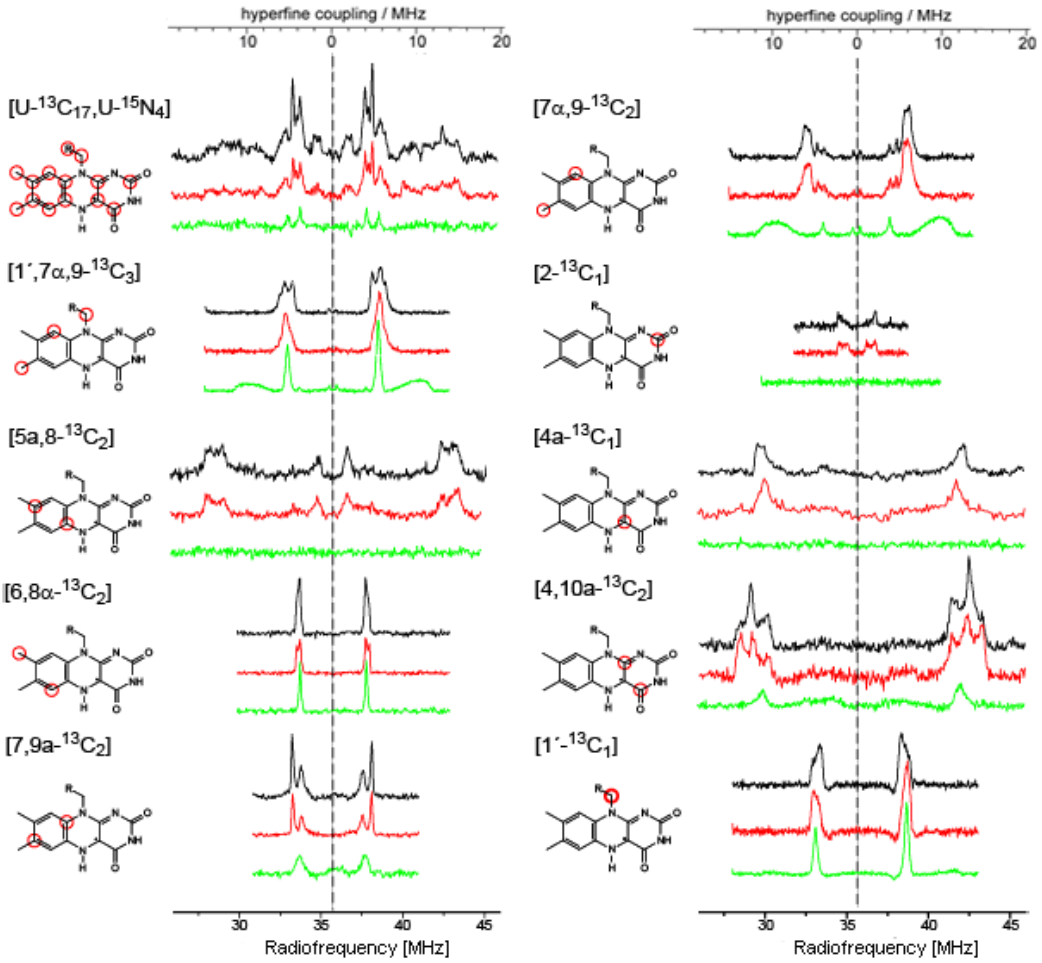

Figure 3.33 W-band frozen-solution pulsed (Davies) ENDOR spectra of universally and selectively labeled FMN in C450A mutant of *A. sativa* LOV2 domain recorded at three different magnetic-field position. Black spectrum: ENDOR spectrum recorded at g_X, red spectrum: ENDOR spectrum recorded at g_Y, green spectrum: ENDOR spectrum recorded at g_Z.

To disentangle the signals of ^{13}C resonances from those of other magnetic nuclei (^{1}H, ^{14}N) resonating at about the same frequency range at standard X-band (9.5 GHz/350 mT) ENDOR, experiments were performed under high-magnetic-field conditions at 94 GHz/3.5 T (W-band). At such high microwave frequencies and corresponding magnetic fields, the Larmor precessional frequencies of ^{1}H, ^{14}N, and ^{13}C nuclei are well separated allowing for a precise measurement of the ^{13}C hyperfine couplings without spectral overlap.

The analysis of ENDOR spectra requires a computer simulation in order to determine the precise values of the hyperfine interactions. This information, which may take the form of a matrix for each nucleus, can, in turn, be analyzed to determine the distances and orientations of nuclei in the vicinity of the paramagnetic electrons. With the help of quantum-

mechanically simulated hyperfine couplings, complete assignment of the ^{13}C-ENDOR-signals of a protein-bound flavin radical became possible.

Table 3.12 Comparison of experimental and calculated (Weber et al., 2001) carbon hyperfine couplings. All hyperfine couplings are accurate to within ±0.2 MHz.

Atom number		calculated values / MHz		experimental values / MHz	
		FMN	LOV		LOV
C2	A_1	–2.7	–1.6	A_X	(–)2.3
	A_2	–4.4	–1.9	A_Y	(–)1.2
	A_3=A_Z	–5.4	–3.3	A_Z	---
C4	A_1	–16.1	–14.5	A_X	–11.3
	A_2	–13.7	–12.3	A_Y	–14.9
	A_3=A_Z	–9.8	–7.4	A_Z	(≈ –4–5)
C4a	A_1	–13.0	–12.4	A_X	(–)12.8
	A_2	–12.1	–12.4	A_Y	(–)11.8
	A_3=A_Z	+ 69.4	+ 59.7	A_Z	---
C5a	A_1	–11.1	–11.2	A_X	(–)13.5
	A_2	–13.5	–13.3	A_Y	(–)15.4
	A_3=A_Z	–18.5	–15.0	A_Z	---
C6	A_1	+0.2	–0.5	A_X	---
	A_2	+ 0.8	+ 0.2	A_Y	---
	A_3=A_Z	+ 13.8	+ 10.3	A_Z	---
C7	A_1	– 5.6	–4.2	A_X	(–)4.9
	A_2	–4.6	–4.1	A_Y	(–)4.9
	A_3=A_Z	–4.4	–1.9	A_Z	–4.1
C7α	A_1	0	–0.1	A_X	0.4
	A_2	0	–0.5	A_Y	0.4
	A_3=A_Z	+0.4	–0.5	A_Z	0.5
C8	A_1	+0.7	+0.4	A_X	1.8
	A_2	+1.4	+1.0	A_Y	1.8
	A_3=A_Z	+22.7	+23.0	A_Z	---
C8α	A_1	–3.2	–3.2	A_X	(–)4.1
	A_2	–3.8	–3.8	A_Y	(–)4.5
	A_3=A_Z	–3.4	–3.3	A_Z	(–)4.1
C9	A_1	–5.1	–5.3	A_X	(–)6.4
	A_2	–4.1	–4.3	A_Y	(–)5.9
	A_3=A_Z	–10.9	–11.7	A_Z	(–)11.7
C9a	A_1	–3.6	–4.3	A_X	(–)3.8
	A_2	–3.1	–4.0	A_Y	(–)3.8
	A_3=A_Z	+13.9	14.9	A_Z	---
C10a	A_1	–18.2	–16.2	A_X	–13.5
	A_2	–15.1	–14.0	A_Y	–13.5
	A_3=A_Z	–17.3	–15.8	A_Z	(–)12.1
C1’	A_1	–4.4	–4.8	A_X	(–)5.0
	A_2	–5.7	–6.2	A_Y	(–)5.7
	A_3=A_Z	–5.2	–5.6	A_Z	(–)5.6

3.2 *Escherichia coli* DNA photolyase E109A mutant

3.2.1 Isolation of *Escherichia coli* DNA photolyase E109A mutant

The recombinant *Bacillus subtilis* strain, harbouring plasmids [pBl1] and [p602E109A], was cultured in LB medium supplemented with uniformly or selectively isotope labeled riboflavin in a final concentration of 3 mg/l. E109A mutant of DNA photolyase from *E. coli* was isolated by a sequence of three chromatographic steps on a column of Blue Sepharose, HiPrep desalting column and Heparin Sepharose column respectively. The entire purification was routinely carried out in a single day. In the *E. coli* photolyase, the redox-active FAD cofactor is reversibly transformed into its neutral radical form, $FADH^{\bullet}$, upon isolation and purification of the protein in an aerobic environment.

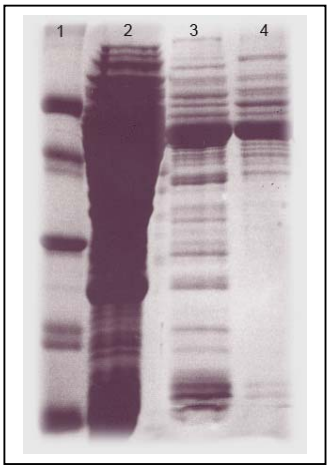

Figure 3.34 15% SDS PAGE of the purified E109A mutant of DNA Photolyase from *E. coli*: 1. Protein marker (66 kDa, 45 kDa, 30 kDa, 20 kDa and 13 kDa); 2. Crude extract from *B. subtilis*; 3. Combined fractions after Blue Sepharose purification; 4. Combined fractions after Heparin Sepharose purification.

3.2.2 Optical spectroscopy

The absorption spectrum of E109A mutant of DNA photolyase from *E. coli* by UV/vis spectroscopy shows peaks at 480 and 580 nm and the shoulder at 625 nm that originate from the $FADH^{\bullet}$ blue-neutral radical, which is shown in figure 3.35.

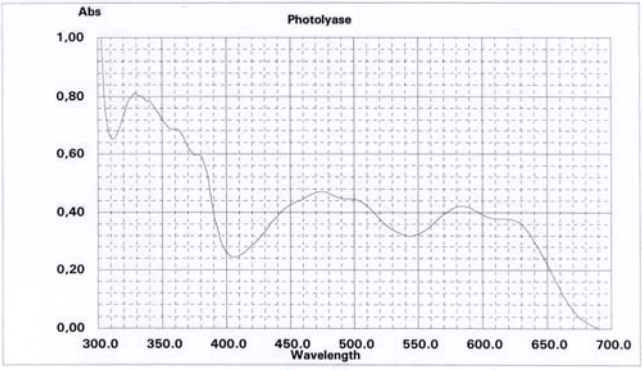

Figure 3.35 Detection of flavin neutral radical in E109A mutant of DNA photolyase from *E. coli* by UV/vis spectroscopy.

3.2.3 ENDOR spectroscopy of *Escherichia coli* DNA photolyase E109A mutant

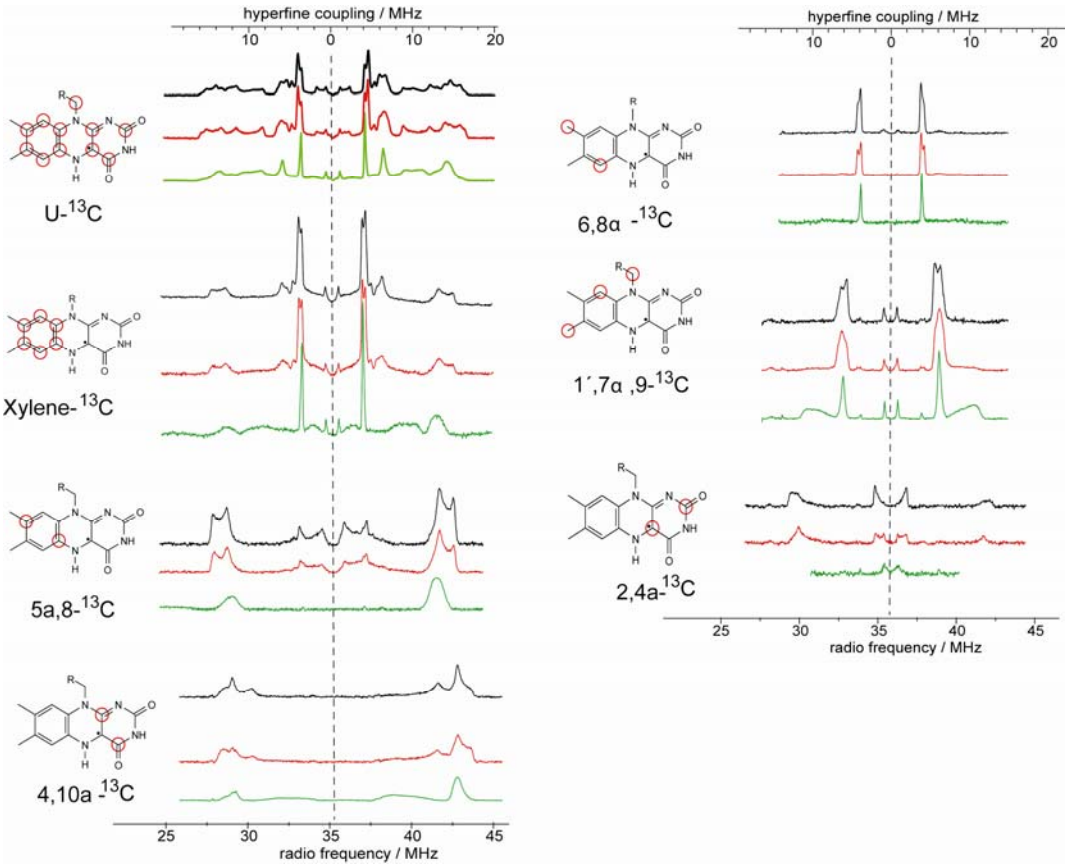

Figure 3.36 W-band ENDOR spectra of universally and selectively labeled riboflavin in E109A mutant of DNA photolyase from *E. coli* recorded at three different magnetic-field positions. Black spectrum: ENDOR spectrum recorded at g_X, red spectrum: ENDOR spectrum recorded at g_Y, green spectrum: ENDOR spectrum recorded at g_Z.

Flavocoenzymes labeled with stable isotopes are important reagents for the study of flavoproteins using isotope – sensitive spectroscopic methods like ENDOR spectroscopy.

The $FADH^{\bullet}$ blue neutral radical, isolated after purification of E109A mutant DNA photolyase can be viewed as a naturally occurring spin probe for ENDOR spectroscopy. To achieve an assignment of the ^{13}C ENDOR signals to individual carbons in the 7,8-dimethyl isoalloxazine ring of the flavin, *E. coli* DNA photolyase was reconstituted with universally and selectively ^{13}C labeled riboflavin isotopologues. The W-band ENDOR spectrum of the $FADH^{\bullet}$ radical from E109A mutant of *E. coli* DNA photolyase, exhibits a detailed hyperfine structure of the flavin semiquinone, as shown in figure 3.36.

3.3 *Escherichia coli* flavodoxin

3.3.1 Isolation of *Escherichia coli* flavodoxin

The recombinant, histidine tagged flavodoxin from *E. coli* could be purified by affinity chromatography on nickel chelating resin. Flavodoxin (fldA) protein after reconstitution with ^{13}C and ^{15}N isotope-labeled FMN appeared on the column as dark orange coloured band and appeared homogenous after elution as judged by SDS polyacrylamide gel electrophoresis (Fig. 3.37). The histagged flavodoxin has a molecular weight of 21.1 kDa.

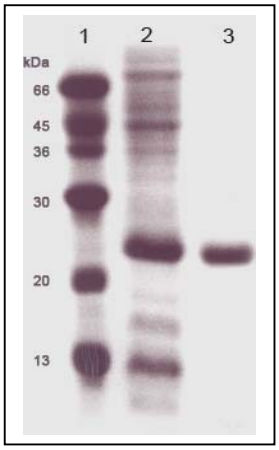

Figure 3.37 SDS PAGE of flavodoxin from *E. coli*: 1. protein marker; 2. cell extract of recombinant *E. coli* strain expressing the flavodoxin gene; 3. purified recombinant flavodoxin protein after affinity chromatography on nickel chelating sepharose fast flow.

3.3.2 Optical spectroscopy

The UV/vis spectrum of flavodoxin from *E. coli* showed absorption maxima at 369 and 464 nm in the oxidised state and absorption maxima at 580 nm in the reduced state (Fig. 3.38).

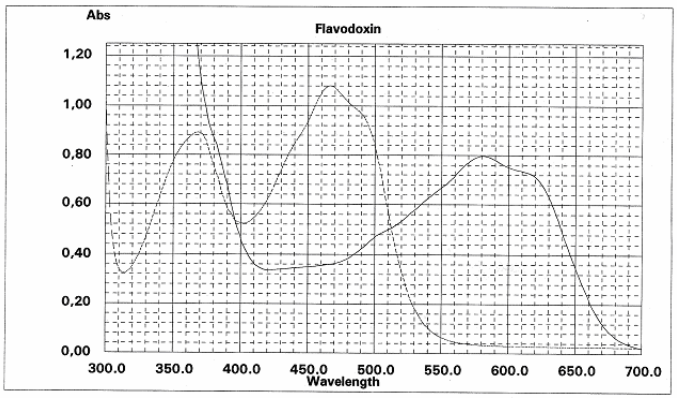

Figure 3.38 Absorption spectrum of flavodoxin from *E. coli*. Dashed and solid line indicates the absorbance peak from oxidised and reduced state respectively.

3.3.3 NMR spectroscopy

The recombinant flavodoxin from *E. coli* was reconstituted with various isotope-labeled FMN samples and analysed, in their oxidised and reduced states, by ^{13}C and ^{15}N NMR spectroscopy. The absorption spectrum of the reconstituted protein was virtually identical to that of the native recombinant protein before reconstitution. Signal assignments were based on comparison of proteins reconstituted with universally labeled, ordered and random isotopologue libraries of FMN and $^{13}C^{13}C$ coupling patterns of the universally ^{13}C-labeled ligand in complex with the protein.

^{13}C NMR spectra of the recombinant flavodoxin from *E. coli* reconstituted with [U-$^{13}C_{17}$]FMN, [xylene-$^{13}C_8$]FMN and with two isotopologue mixtures of FMN obtained by biotransformation of [1-$^{13}C_1$]- and [2-$^{13}C_1$]glucose in the oxidised state is shown in figure 3.39. Due to the specific ^{13}C-enrichments in the ribityl moiety of the FMN samples, the signals for 1', 2' and 4' are observed in the isotopologue mixture from [2-$^{13}C_1$]glucose, whereas only the signals for 1' and 5' are detected in the spectrum of the isotopologue mixture from [1-$^{13}C_1$]glucose. Using the same isotopologue editing approach, unequivocal signal assignments can be obtained for the carbon atoms of the isoalloxazine ring. Thus, [2-$^{13}C_1$]glucose transfers the label to the ring carbon atoms 4a, 5a, 6, and 8. The carbon atoms 2, 4, 6, 7α, 8α and 9 acquire ^{13}C-label from [1-$^{13}C_1$]glucose. Additional validation is provided by [xylene-$^{13}C_8$]FMN which detects the signals in the aromatic region. In summary, the observed signal intensities in the spectra with universally ^{13}C-labeled FMN and two isotopologue libraries of FMN (i.e. FMN obtained from biotransformation of [2-$^{13}C_1$]- and [3-$^{13}C_1$]glucose), together with [xylene-$^{13}C_8$]FMN allowed the assignments of all 17 carbon atoms of FMN (Table 3.13).

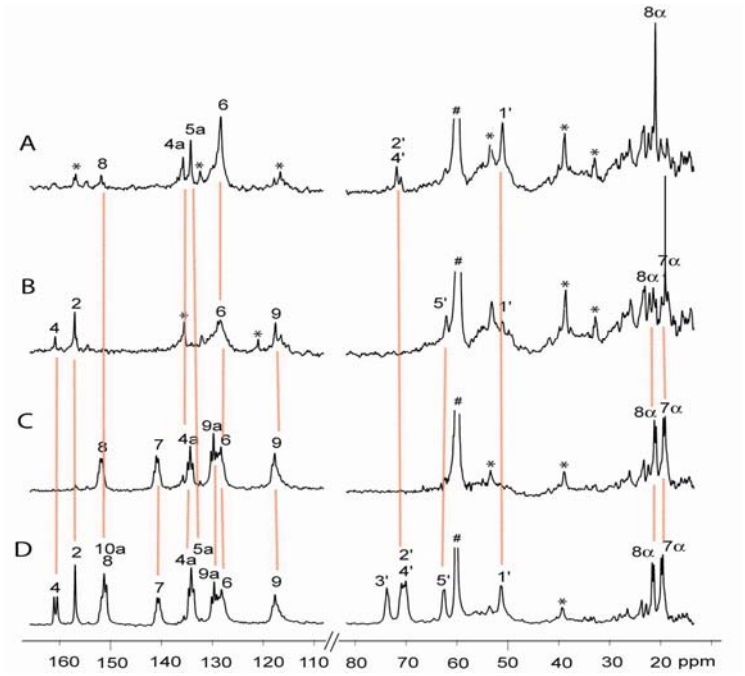

Figure 3.39 ^{13}C-NMR spectra of *E. coli* flavodoxin reconstituted with (A) FMN obtained from [2-$^{13}C_1$]glucose; (B) FMN obtained from [1-$^{13}C_1$]glucose; (C) [xylene-$^{13}C_8$]FMN; (D) [U-$^{13}C_{17}$]FMN in the oxidised state. Asterisks marks impurities and # marks the signal from 100 mM tris buffer.

Table 3.13 ^{13}C and ^{15}N-NMR chemical shifts (in ppm) of flavin in solutions and FMN bound to flavodoxin protein in the oxidised state.

Atom	Free FMN	Free TARF	FMN bound to *E. coli* flavodoxin
C(2)	159.8	154.4	156.9
C(4)	163.7	159.2	160.9
C(4a)	136.2	135.1	134.8
C(5a)	136.4	134.5	134.2
C(6)	131.8	132.5	128.9
C(7)	140.4	137.2	140.8
C(7α)	19.9	19.5	19.6
C(8)	151.7	148.7	151.4
C(8α)	22.2	21.6	21.5
C(9)	118.3	115.8	117.7
C(9a)	133.5	131.4	129.6
C(l0a)	152.1	150.8	151.2
C(1')	48.8	45.0	51.3
C(2')	70.7	70.2	70.0
C(3')	73.1	70.0	73.7
C(4')	74.0	69.5	70.4
C(5')	66.4	62.1	62.4
N(1)	190.8[a]	200.1[a]	186.2
N(3)	160.5[a]	159.6[a]	159.5
N(5)	334.7[a]	346.0[a]	332.7
N(10)	163.5[a]	151.9[a]	160.8

[a] Taken from Vervoort et al., 1986a

The ^{13}C chemical shift due to the C(2) atom and C(4) atom of FMN bound to flavodoxin are upfield shifted by 2.9 ppm and 2.8 ppm, respectively in comparison with that of FMN in aqueous solution. With respect to TARF, C(2) atom shows a downfield shift of 2.5 ppm and 1.7 ppm for C(4) atom (figure 3.40).

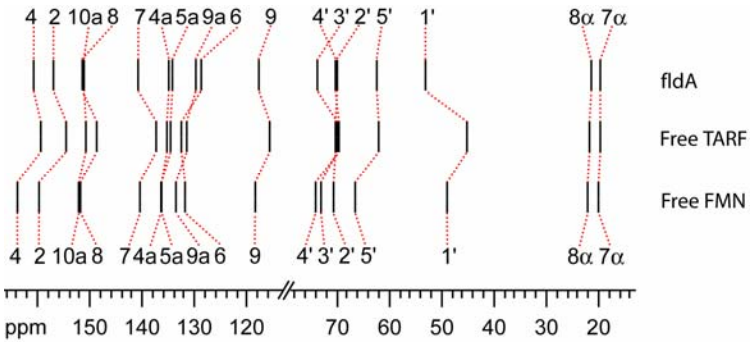

Figure 3.40 Correlation diagram of ^{13}C-NMR chemical shifts of flavins in solution and FMN bound to flavodoxin from *E. coli* in the oxidised state.

The ^{13}C chemical shifts due to C(2) of FMN in flavodoxin from different organisms, namely: *Megasphaera elsdenii, Desulfovibrio vulgaris, Clostridium MP, Azotobacter vinelandii* are very similar and resemble that of FMN in aqueous solution, (Vervoort et al., 1986b). In sharp contrast, C(2) of FMN in flavodoxin from *E. coli* is upfield shifted by more than 2 ppm with respect to the reported C(2) values of the FMN bound to flavodoxin from different organisms.

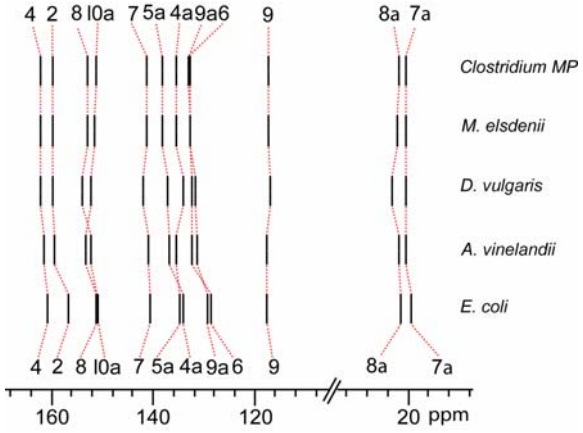

Figure 3.41 Correlation diagram of ^{13}C-NMR chemical shifts of FMN bound to flavodoxin from different organisms in the oxidised state. ^{13}C-NMR chemical shifts of FMN bound to flavodoxin from *M. elsdenii, D. vulgaris, Clostridium MP* and *A. vinelandii*, in the oxidised state, are taken from Vervoort et al, 1986b.

As shown by model studies, polarization of the isoalloxazine ring of flavin through hydrogen bonding at the C(2)O and the C(4)O groups (FMN in water) influences the π-

electron density on C(8), C(8α), C(9a), N(5) and C(10a) through conjugative effects leading to a downfield shift of the corresponding ^{13}C chemical shifts, and to an upfield shift of C(6) (Kainosho and Kyogoku, 1972), as compared with TARF. These effects are observed, except for C(9a) which is upfield shifted by 1.8 ppm. The chemical shifts of these atoms follow a similar trend in the other flavodoxins from four different organisms (Vervoort et al., 1986b), except that the chemical shift due to C(9a) and C(10a) are upfield shifted from that of TARF. The ^{13}C chemical shifts of C(5a), C(7α), C(7) and C(9) are downfield shifted in comparison to those of TARF. This is observed with other flavodoxins as well (Vervoort et al., 1986b). The ^{13}C chemical shift of C(4a) of *E. coli* fldA resonates 1.4 ppm upfield from that of FMN and 0.3 ppm upfield shift from that of TARF.

With respect to FMN, the ^{13}C chemical shift of C(1') is downfield shifted, C(3') C(4') and C(5') are upfield shifted and the resonances due to C(2') is practically unaffected (Fig. 3.39 and 3.40).

^{13}C NMR spectra of recombinant flavodoxin from *E. coli* reconstituted with [U-$^{13}C_{17}$]FMN, [xylene-$^{13}C_8$]FMN and with two isotopologue mixtures of FMN obtained by biotransformation of [1-$^{13}C_1$]- and [2-$^{13}C_1$]glucose in the reduced state respectively, is shown figure 3.42 and summarized in table 3.14.

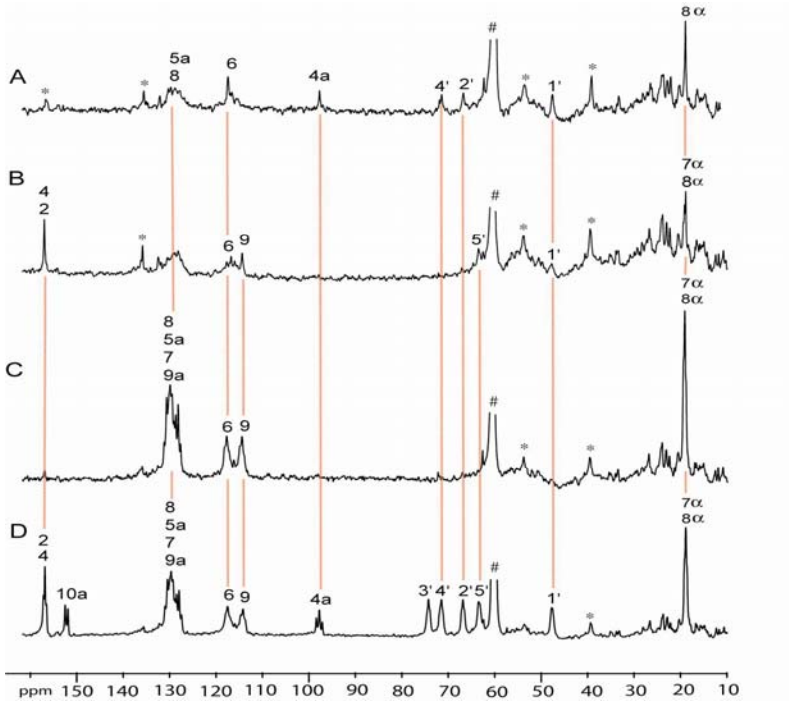

Figure 3.42 ^{13}C-NMR spectra of *E. coli* flavodoxin reconstituted with (A) FMN obtained from [2-$^{13}C_1$]glucose; (B) FMN obtained from [1-$^{13}C_1$]glucose; (C) [xylene-$^{13}C_8$]FMN; (D) [U-$^{13}C_{17}$]FMN in the reduced state. Asterisks marks impurities and # marks the signal from 100 mM tris buffer.

Table 3.14 ^{13}C and ^{15}N-NMR chemical shifts (in ppm) of reduced flavins in solutions and FMN bound to flavodoxin protein in the reduced state.

Atom	$FMNH^-$ [a]	$FMNH_2$ [a]	$TARFH_2$ [a]	FMN bound to *E. coli* fldA
C(2)	158.2	151.1	150.6	156.8
C(4)	157.7	157.2	157.0	156.8
C(4a)	101.4	103.1	105.2	97.7
C(5a)	134.2	134.4	136.0	129.6
C(6)	117.3	117.1	116.1	117.5
C(7)	133.0	134.3	133.6	129.6
C(7α)	19.0	19.1	19.1	18.8
C(8)	130.3	130.4	129.0	129.6
C(8α)	19.4	19.4	19.3	18.8
C(9)	116.8	11 7.4	118.0	114.1
C(9a)	130.9	130.4	128.2	129.6
C(l0a)	155.5	144.3	137.1	152.1
C(1')	46.0[b]	51.1 [b]	47.4[c]	47.6
C(2')	71.2 [b]	71.4 [b]	69.7[c]	66.7
C(3')	73.0 [b]	72.6 [b]	70.0[c]	74.2
C(4')	73.9 [b]	73.3 [b]	70.1[c]	71.4
C(5')	66.5 [b]	67.7 [b]	62.0[c]	63.2
N(1)	181.3	128.0	119.9	180.4
N(3)	150.0	149.7	149.0	148.1
N(5)	58.4	58.0	59.4	51.9
N(10)	96.5	87.2	76.8	94.0

[a] Taken from Vervoort et al., 1986a. [b] Taken from Müller et al., 1988.
[c]Taken from van Schagen and Müller, 1980.

The ^{13}C-NMR resonance due to C(2) is downfield shifted by 6.2 ppm and 5.7 ppm in comparison with $TARFH_2$ and $FMNH_2$, respectively, and resonates at upfield shift of 1.4 ppm in $FMNH^-$ (Table 3.14, Fig. 3.43). The ^{13}C chemical shift due to C(4) is upfield shifted with respect to all the reduced forms.

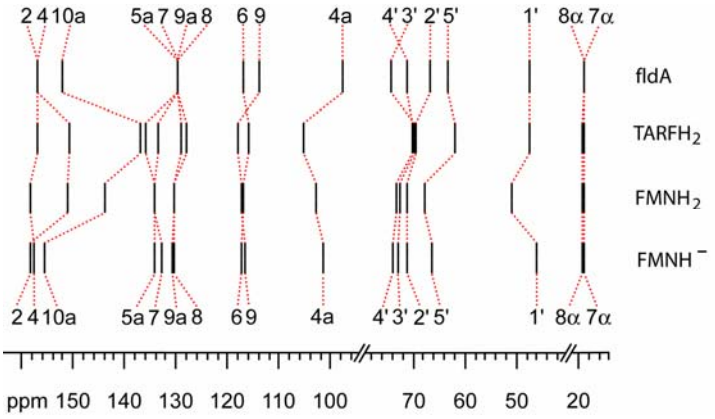

Figure 3.43 Correlation diagram of ^{13}C-NMR chemical shifts of flavins in solution and FMN bound to *E. coli* flavodoxin in reduced state. The values for $FMNH^-$, $FMNH_2$ and $TARFH_2$ are taken from the literature as cited in table 3.14 above.

Of the remaining carbon atoms constituting the isoalloxazine ring of protein, with respect to the ^{13}C chemical shifts of $FMNH_2$, C(10a), C(7α) and C(8α) are considerably downfield shifted (π-electron density decrease), whereas C(4a), C(5a), C(9a), C(7) and C(9) are upfield shifted (π-electron density increase). The resonances due to C(8), C(6) are similar to those of $FMNH_2$. The signal of C(4a) is upfield shifted in all cases 7.5 ppm from the value in $TARFH_2$, 5.1 ppm from the value in $FMNH_2$ and 3.7 ppm from the value in $FMNH^-$.

With respect to $FMNH^-$, C(4a), C(5a), and C(8) atoms of *E. coli* fldA are upfield shifted, C(7) shows a similar shift as that of $FMNH^-$, and all other atoms of the isoalloxazine ring are downfield shifted. In other flavodoxins, an upfield shifts are observed for the resonances of all sp^2 carbon atoms in flavodoxins, except for those of C(4a), C(5a), and C(9a) (these are downfield shifted) with respect to $FMNH^-$.

In comparison with the oxidised state, C(1') and C(2') undergo the largest upfield shift. The chemical shifts due to the C(2') and the C(1') atoms are upfield shifted by 5.3 ppm and 3.2 ppm respectively. C(3'), C(4'), C(5') are downfield shifted (Table 3.14).

For the ^{15}N chemical shifts, the following points were considered. The flavin molecule contains four nitrogen atoms. In the oxidized state, the N(1) and N(5) atoms of flavin are so-called pyridine- or β-type nitrogen atoms. The chemical shifts of such atoms are rather sensitive to hydrogen bonding and undergo a relatively large upfield shift upon hydrogen bond formation (Moonen et al., 1984). The N(10) and N(3) atoms are so-called pyrrole- or α-type nitrogen atoms and are much less sensitive to hydrogen bonding leading to a small downfield shift. In reduced flavin all four nitrogen atoms belong to the later class of nitrogen atoms. When observable, $^{15}N–^{1}H$ coupling constants were also taken into consideration for the assignment of nitrogen atoms and to determine the degree of hybridization of the corresponding nitrogen atom.

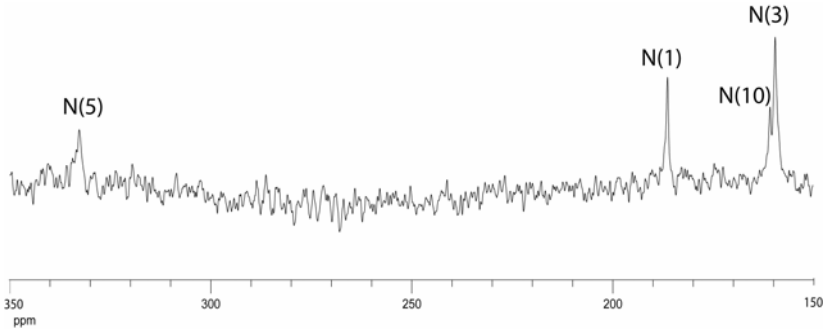

Figure 3.44 ^{15}N-NMR spectrum of *E. coli* flavodoxin reconstituted with [U-$^{15}N_4$]FMN in the oxidised state.

Figure 3.44 shows ^{15}N NMR spectum of the recombinant flavodoxin from *E. coli* reconstituted with [U-$^{15}N_4$]labeled FMN in the oxidised state. The chemical shifts are summarized in table 3.13.

The N(1) and N(5) atoms of protein-bound FMN in *E. coli* flavodoxin resonate at higher field than those of FMN in water and TARF in chloroform (Table 3.13, Fig. 3.44 and 3.45). With respect to FMN, the chemical shifts of the N(5) and N(1) atoms are upfield shifted by 4.6 ppm and 2 ppm, respectively.

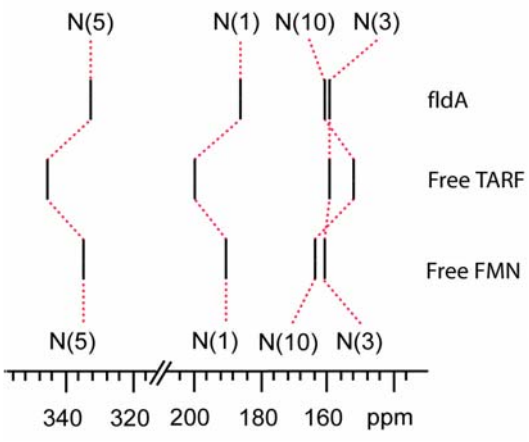

Figure 3.45 Correlation diagram of ^{15}N-NMR chemical shifts of flavins in solution and FMN bound to *E. coli* flavodoxin in oxidised state. The ^{15}N-NMR chemical shifts of free FMN and free TARF are taken from Vervoort et al., 1986a (Table 3.13).

The N(3) atom of protein-bound FMN resonates at 159.5 ppm, which is upfield from that of free FMN and TARF by 5.0 ppm and by 0.1 ppm respectively.

Model studies have shown that the N(10) atom in free flavin exhibits an unexpected large downfield shift on going from apolar to polar solvents (Moonen et al., 1984). This pyrrole-like nitrogen atom cannot form a hydrogen bond. Therefore, this observation was explained by an increase of sp^2 hybridization of the N(10) atom. The resulting mesomeric structures are preferentially stabilized by hydrogen bonds to the carbonyl functions at position 2 and 4, as supported by ^{13}C-NMR data (Moonen et al., 1984). The ^{15}N chemical shift of the N(10) atom bound to *E. coli* fldA appears at 160.8 ppm, 3.8 ppm upfield from that of free FMN (Table 3.13) implicating an increase of π-electron density at the N(10) atom.

N5 of apoflavodoxin bound FMN show differences in chemical shift between the flavodoxins from different organisms with the most upfield shift in *E. coli* fldA (Fig. 3.46).

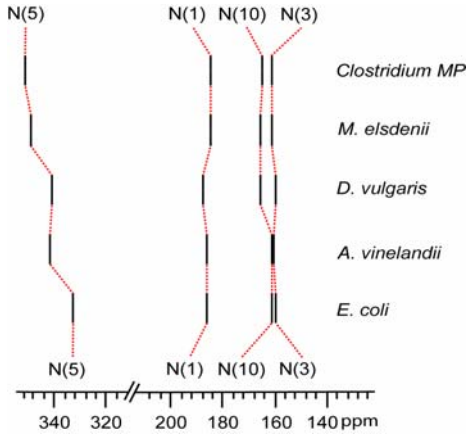

Figure 3.46 Correlation diagram of ^{15}N-NMR chemical shifts of FMN bound to flavodoxin from different organisms in the oxidised state. ^{15}N-NMR chemical shifts of FMN bound to flavodoxin from *M. elsdenii, D. vulgaris, Clostridium MP* and *A. vinelandii*, in the oxidised state, are taken from Vervoort et al., 1986b.

The ^{15}N NMR spectrum of *E. coli* flavodoxin in the reduced state is given in figure 3.47.

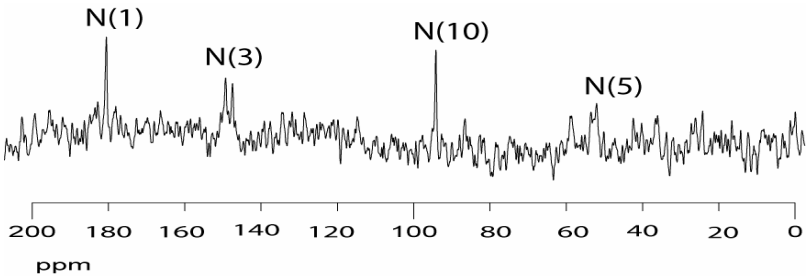

Figure 3.47 ^{15}N-NMR spectrum of *E. coli* flavodoxin reconstituted with [U-$^{15}N_4$]FMN in the reduced state.

The N(1) atom resonates at 180.4 ppm, 60.5 ppm downfield from that of $TARFH_2$ in chloroform (119.9 ppm). The ^{15}N chemical shift of the N(5) atom is upfield shifted by 6.1 ppm and 7.5 ppm in comparison to those of $TARFH_2$ and $FMNH_2$, respectively (Fig. 3.48). The apparent coupling constant of the N(5)H group is 73 Hz. The chemical shift of the N(10) atom shows the downfield shift of 6.8 ppm and 17.2 ppm in comparison to $FMNH_2$ and $TARFH_2$, respectively. With respect to $TARFH_2$ and $FMNH_2$ the ^{15}N chemical shift of the N(3) atom is upfield shifted by 0.9 ppm and 1.6 ppm. A coupling constant of 92 Hz is determined for the N(3)H atom.

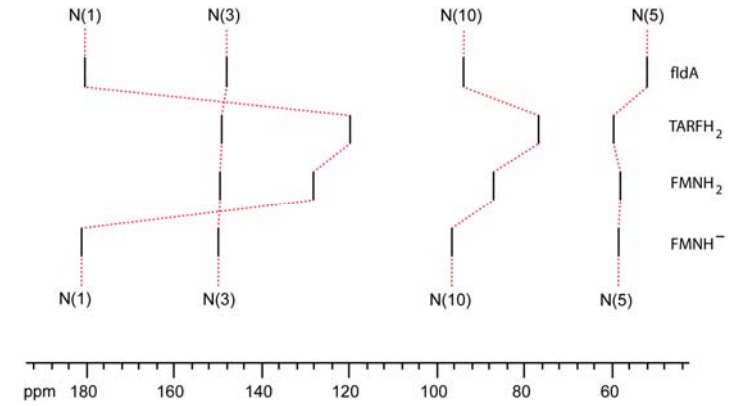

Figure 3.48 Correlation diagram of ^{15}N-NMR chemical shifts of flavins in solution and FMN bound to *E. coli* flavodoxin in the reduced state. The values for $FMNH^-$, $FMNH^2$, $TARFH^2$ are taken from the literature as cited in table 3.14 above.

The chemical shift of N1, N3 and N10 of FMN bound to *E. coli* in reduced state appears at similar field as in other flavodoxins (Fig. 3.49).

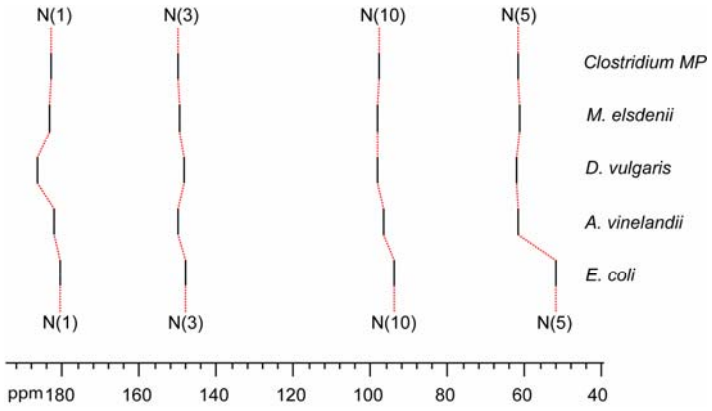

Figure 3.49 Correlation diagram of ^{15}N-NMR chemical shifts of FMN bound to flavodoxin from different organisms in the reduced state.^{15}N-NMR chemical shifts of FMN bound to flavodoxin from *M. elsdenii, D. vulgaris, Clostridium MP* and *A. vinelandii*, in the reduced state, are taken from Vervoort et al, 1986b.

3.3.4 Discussion

The resonances of the C(2'), C(3'), C(4') and C(5') atoms in *E. coli* flavodoxin are upfield shifted as compared to FMN and downfield shifted compared to TARF indicating strong hydrogen bond interactions with the respective hydroxyl groups. The downfield shift of the C(1') methylene group reflects the specific configuration of this atom in protein-bound FMN.

The ^{13}C chemical shifts of C(2) in *E. coli* flavodoxin is upfield-shifted as compared with that in FMN but downfield from that of TARF in $CHCl_3$ indicating weak hydrogen bonding

with C(2). The ^{13}C chemical shifts due to C(2) of FMN in all four flavodoxins from different organisms namely: *M. elsdenii, D. vulgaris, Clostridium MP, A. vinelandii* are very similar and resemble that of FMN in aqueous solution but differ and downfield shifted from that of TARF in $CHCl_3$ (Vervoort et al., 1986a). This indicates that a rather strong hydrogen bond exists between C(2) and the apoflavodoxins. These hydrogen bondings seem to be of similar strength in all four flavodoxin as deduced from the ^{13}C chemical shifts. The ^{13}C chemical shifts of C(4) in all flavodoxins studied before (Vervoort et al., 1986b) and sutdied here are upfield shifted as compared with that in FMN but are downfield from that of TARF in $CHCl_3$. This indicates that the π electron density at C(4) in the flavodoxins is increased with respect to that of FMN and decreased with regard to that of TARF, indicating weak hydrogen bonding with C(4). Thus, our result agrees perfectly with the previous experiment of Vervoort et al., (Vervoort et al., 1986b). The resonance due to the C(4a) atom appears at higher fields than those of FMN or TARF. According to the study of Moonen et al., (Moonen et al., 1984), the upfield shift of the C(4a) resonance indicates π-electron density increase at this position as compared to FMN in water and TARF in chloroform. This extra π-electron density must come from N(10) atom that resonates at lower field than that of TARF.

According to Vervoort et al., polarization of the carbonyl group C(2) by hydrogen bonding leads to a downfield shift of the resonances due to C(8), C(9a) and C(10a) and an upfield shift of that due to C(6) (Vervoort et al., 1986b). This is indeed observed for C(8), C(l0a) and C(6), but not for the C(9a) which shows a shift in the opposite direction i.e., is upfield shifted by 1.8 ppm. The unexpected upfield shift of C(9a) can be ascribed to a slight conformational change with respect to molecular plane of this atom (Grande et al., 1977). The resonances due to C(8), C(9a) and C(10a) are also downfield shifted as compared to those of TARF. These data suggest that these atoms lost some π-electron density via mesomeric structure due to the hydrogen bond at C(2) (Moonen et al., 1984).

The chemical shift changes of the C(4a), C(5a), C(7) and C(9) atoms with respect to TARF can be explained by the high degree of sp^2 hybridization of the N(10) atom. An increase in sp^2 hybridization of N(10) in free flavin leads to a downfield shift of the resonances due to C(9), C(7), C(7a), and C(5a) as a result of delocalization of the partial positive charge on N(10) (Moonen et al., 1984). This is observed with the flavodoxins studied before and the downfield shifts indeed parallel that of N(10), except for C(9). In this study, the upfield shift of C(5a) and C(9) was observed. Similar values of the relative upfield shifts

of C(5a) in *D. vulgaris* and in *A. vinelandii* compared to *M. elsdenii* and *Clostridium MP* and *E. coli* flavodoxins probably reflect the weak hydrogen bond to N(5) in the former two.

The ^{15}N chemical shifts reported here agree very well with those reported earlier for flavodoxin from different organisms by Vervoort et al. (Vervoort et al., 1986b).

The ^{15}N chemical shifts of the N(1) and the N(5) atoms (β-type nitrogen) in *E. coli* flavodoxin in oxidized state are upfield shifted with respect to TARF. The upfield shifts exceed those observed in FMN. This indicates the presence of strong hydrogen bonding interactions between these atoms of protein-bound FMN and the apoprotein. The shifts for the N(5) atom of FMN in *D. vulgaris* (Vervoort et al., 1986b) and *A. vinelandii* flavodoxin appear at an intermediate level between that of TARF and FMN, indicating the formation of a weak hydrogen bond between the apoflavodoxins and the N(5) atom of protein-bound FMN. From the results it can be concluded that *M. elsdenii* and *Clostridium MP* apoflavodoxins do not form a hydrogen bond with the N(5) atom of FMN. This conclusion follows from the fact that the ^{15}N chemical shifts due to the N(5) atom of FMN in these two flavodoxins appear even at lower field than that of TARF in an apolar solvent ($CHCl_3$). The fact that the ^{15}N chemical shifts of N(5) in the former flavodoxins are downfield from that of free FMN also suggests that the π- electron density at the N(5) atom of protein-bound FMN is lower than that in free oxidized flavin.

The ^{15}N chemical shift of N(l) of protein-bound FMN appears at higher field than that of free FMN in all four flavodoxin as reported by Vervoort et al. (Vervoort et al., 1986b) and also in *E.coli* flavodoxin. From this, it is concluded that all five apoflavodoxins including *E.coli* form strong hydrogen bonds with the N(l) atom of FMN. These hydrogen bonds are stronger in *Clostridium MP* and *M. elsdenii* flavodoxin than in *A. vinelandii*, *D. vulgaris* and *E.coli* flavodoxins.

The ^{15}N chemical shift of the N(3) atom bound to FMN from *E.coli* is almost identical with that observed in TARF, but is at higher field that that in FMN. It can be conlcuded that the N(3)H group of FMN forms a weak hydrogen bond. According to Vervoort et al. (Vervoort et al 1986b); the ^{15}N chemical shifts indicate that the N(3)H group of FMN forms a strong hydrogen bond with the *Clostridium MP* and *M. elsdenii* apoflavodoxins. This hydrogen bond interaction is weaker in *A. vinelandii* and *D. vulgaris* flavodoxins.

As previously described (Moonen et al., 1984), the N(10) atom in free oxidized flavin shows an unexpected large downfield shift on going from apolar to polar solvents. Since this pyrrole-like nitrogen atom cannot form a hydrogen bond, the downfield shift of its resonance

had to be explained as an increase in sp^2 hybridization. This increase in hybridization only occurs when the polarization of the isoalloxazine ring is stabilized by hydrogen bond formation with C(2) and C(4). In *E. coli* flavodoxin the chemical shift of N(10) appears at even lower field than in FMN indicating an increased degree of sp^2 hybridization. Whereas *M. elsdenii* and *D. vulgaris* flavodoxins show an increased degree of sp^2 hybridization as compared with that of free FMN *A.vinelandii* flavodoxin is considerably decreased wtih respect to that of free FMN.

As compared with $FMNH_2$, the ^{13}C chemical shifts due to C(6) is not affected by reduction. The C(4) atom is least affected by reduction, and those of C(8), C(4a), C(9a), C(9), C(5a), and C(7) are upfield shifted by a π-electron density increase coming from N(5) and N(10), respectively. In contrast, the chemical shifts of C(2) and C(10a) experience a large downfield shift upon reduction. The downfield shift of the C(2) atom cannot be ascribed solely to hydrogen bonding, but is related to the drastic π-electron density decrease at C(10a) which is partially compensated by π-electron density withdrawal from C(2).

The fact that C(4) is also strongly upfield shifted even in comparison with that in $TARFH_2$, strongly suggests that some π- electron density from N(5) is delocalized onto this atom. Similar to *D. vulgaris* flavodoxin, in *E. coli* flavodoxin the further upfield shift of the resonance of C(4), which is accompanied by a downfield shift of the resonances due to C(6) and C(8), and an upfield shift of those of C(4a), C(5a) and C(9a), suggests that π- electron density is redistributed from C(8) and C(6) onto C(4) and C(9a) [from N(5)] and from N(10) onto C(5a) and C(4a) due to a further increase of the sp^2 hybridization of N(10).

All nitrogen atoms in the reduced state of flavin are of the pyrrole type. The chemical shifts of N(l) of FMN bound to *E. coli* apoflavodoxin and similar to this result, all of the apoflavodoxins studied by Vervoort et al. (Vervoort et al., 1986b) are very similar to that of $FMNH^-$. This indicates that the prosthetic group in reduced flavodoxins is ionized. The ionization of $FMNH^-$, in the flavodoxins is also supported by the fact that no N(1)-H coupling is observed. The ionization of N(1) is also reflected by the large downfield shift of the resonance due to the neighbouring carbon atoms C(2) and C(l0a).

The N(3) chemical shifts of apoflavodoxin-bound $FMNH^-$ appear either downfield (*Clostridium MP, M. elsdenii,* and *A. vinelandii)* or upfield *(D. vulgaris)* as compared with that of $FMNH^-$. This suggests that a hydrogen bond is present in the first group of flavodoxins and also in *D. vulgaris* flavodoxin (Vervoort et al., 1986b), although in this case the bond is weak (Vervoort et al., 1986b). Similar to the result of *D. vulgaris*, the N(3) resonance in *E.*

coli flavodoxin appears upfield compared to $FMNH^-$ indicating a weak hydrogen bonding to this atom.

The signal of N(5) of $FMNH^-$ in *E. coli* flavodoxin was weak compared to other signals of nitrogen atoms but tentatively on the basis of apparent coupling constant of 73 Hz and similar values in other flavodoxin, the signal at 51.9 ppm was assigned to be the signal arising from N(5) atom. The N(5) chemical shifts of apoflavodoxin-bound $FMNH^-$ *E. coli* appeared upfield as compared with that of $FMNH^-$ indicating a weak hydrogen bonding to this atom. The resonance of N(5) of $FMNH^-$ in other flavodoxin studied, is downfield with respect to that of free $FMNH^-$ (Vervoort et al, 1986b).

The N(10) chemical shifts in the *E. coli* flavodoxin were detected at higher field than in $FMNH^-$. The same pattern was found in *A. vinelandii* flavodoxin, whereas a downfield shift was observed in *M. elsdenii, Clostridium MP,* and *D. vulgaris* flavodoxins. This indicates that the sp^2 character of the N(10) atom is somewhat decreased in *E. coli* and *A. vinelandii* flavodoxins and increased in *M. elsdenii, Clostridium MP,* and *D. vulgaris* flavodoxins.

3.3.5 ENDOR spectroscopy of *Escherichia coli* flavodoxin

To learn more on the specific reactivity of protein-bound flavins mediated by their surroundings, knowledge on the delocalization of the unpaired electron spin and the electron-density distribution of flavin in the radical state are required. Using ^{13}C ENDOR spectroscopy at high microwave frequencies and corresponding magnetic fields nearly all of the hyperfine couplings of the carbons in the isoalloxazine that hosts the majority of the unpaired electron spin density could be detected and assigned by isotopologue editing.

The unpaired electron-spin densities at the positions of carbons in the isoalloxazine ring of FMN have been obtained by ENDOR studies on *E. coli* flavodoxin samples reconstituted with ^{13}C FMN isotopologues (Fig. 3.50).

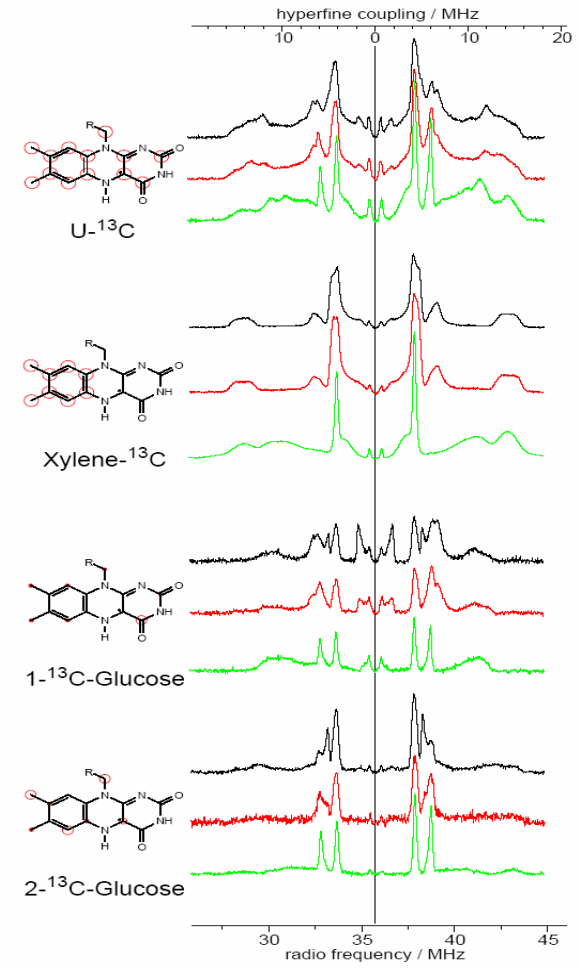

Figure 3.50 W-band ENDOR spectra of flavodoxin from *E. coli* reconstituted with [U-$^{13}C_{17}$]FMN, [Xylene-$^{13}C_8$]FMN and FMN isotopologues obtained from [1-$^{13}C_1$] glucose and [2-$^{13}C_1$] glucose recorded at three different magnetic-field positions. Black spectrum: ENDOR spectrum recorded at g_X; red spectrum: ENDOR spectrum recorded at g_Y, green spectrum: ENDOR spectrum recorded at g_Z. Labeling patterns are shown in the left panel.

4 Summary

The application of magnetic resonance methods in biophysics frequently depends on the labeling of the investigated probes with suitable isotopes. In this work, several flavoproteins (phototropin LOV domain, DNA photolyase and *E. coli* flavodoxin) were labeled with ^{13}C- and/or ^{15}N- isotopolouges of the flavocoenzyme and studied by NMR and ENDOR spectroscopy.

The plant blue light receptor phototropin comprises a protein kinase domain and two FMN-binding LOV domains (LOV1 and LOV2). Blue light irradiation of recombinant LOV domain is conducive to the addition of a cysteinyl thiolate group to carbon 4a of the FMN chromophore, and spontaneous fragmentation of that photoadduct completes the photocycle of the receptor. Amplitude modulation observed after reconstitution with random libraries of ^{13}C-labeled FMN isotopologues were utilized for the assignment of the ^{13}C NMR signals of FMN bound to LOV domains of different origins. The method enables the rapid and unequivocal assignment of all ^{13}C signals of the protein-bound cofactor (including the ribityl side chain signals) in the dark as well as the blue-light irradiated state. All ^{13}C signals of FMN bound to LOV1 and LOV2 domains of *Avena sativa* and to LOV2 domain of *Adiantum capillus-veneris* could be unequivocally assigned under dark and under blue light irradiation conditions. ^{13}C Chemical shifts of FMN are shown to be differently modulated by complexation with the LOV domains under study, indicating slight differences in the binding interations of FMN and the apoproteins.

If the photoreactive cysteine residue of LOV2 domain is replaced by mutagenesis, blue light irradiation is conducive to the formation of a blue flavin radical instead of a photoadduct. The recombinant C450A mutant of the LOV2 domain of *A. sativa* phototropin was reconstituted with universally ^{13}C-labeled FMN and NMR spectra were acquired with or without blue-light irradiation. Compared to NMR spectra obtained in the dark, strongly polarized signals in enhanced absorption and emission are observed when NMR spectra were recorded in the presence of blue light.

The observation of spin-polarized ^{13}C nuclei in the NMR spectra of the mutant LOV2 domain is clear evidence for radical-pair intermediates in the reaction steps following optical excitation. In order to check this assignment and the concept of photochemical biradical formation, the experiments were performed with recombinant short and long LOV2 domains comprising amino acid residues 409-525 or 404-559 of *A. sativa* phototropin, respectively. A strong emissive signal in short and long LOV2 domain respectively was tentatively assigned

to C(3) (IUPAC numbering) of a tryptophan residue on the basis of NMR analysis of totally or selectively ^{13}C-labeled apoprotein. Whereas the replacement of either of the two tryptophan residues in position 491 and 557, respectively, had only minor impact on the photochemical properties, the emissive ^{13}C NMR line was absent in the C450A/W491A mutant and was therefore assigned to the W491 residue. *In vivo* labeling of both mutants with [U-$^{13}C_{11}$]tryptophan or [U-$^{13}C_6$]glucose subsequently confirmed that all ring carbons as well as the side chain C(β) of tryptophan 491 appear in the emissive ^{13}C NMR mode under blue light irradiation. On the other hand, only C(3) of tryptophan 557 gives rise to an emissive signal under these conditions, and even the intensity of the single emissive signal is relatively weak by comparison with tryptophan 491 signals. The emissive tryptophan signals are believed to arise by polarization transfer during the photochemical generation of biradical states, where one electron is located on the flavin cofactor and the other is located on a tryptophan residue. In order to analyze the influence of cross polarization in multiply ^{13}C-labeled tryptophan residues on the emission intensities of individual indole ring carbon atoms, the samples were prepared by fermentation of LOV2 expression strains with [1-$^{13}C_1$]-, [2-$^{13}C_1$]- or [3-$^{13}C_1$]glucose. The labeling patterns of tryptophan that were biosynthesized from the differently labeled glucose precursors were determined by ^{13}C NMR analysis after hydrolysis of biomass. These data served as the basis for the calibration of the emissive tryptophan signals observed under blue light irradiation of the proteins labeled from different glucose isotoplogues. The normalized intensity data enable the analysis of emission intensity modulation by $^{13}C^{13}C$ coupling in multiply ^{13}C labeled tryptophan residue.

A recombinant LOV2 domain of *A. sativa* was also reconstituted with 5-deaza-FMN. The reconstituted protein shows absorbance maxima at 402 nm and can be converted into a species with absorbance maxima at 337 nm by blue light irradiation. The latter species was stable at 4°C for several days but could be reverted to the “as isolated" form of protein by ultraviolet irradiation. Repeated photoactivation/photoreversion cycles could be performed without apparent hysteresis. The UV/vis data suggest that the thiol group of cystein 450 can form adduct with the artificial deazaflavin cofactor which fails to undergo spontaneous fragmentation but can be cleaved by ultraviolet irradiation. ^{13}C NMR spectra of the reconstituted mutant protein showed an emissive line at 111 ppm. The ^{13}C NMR spectrum obtained under blue light illumination of universally ^{13}C-labeled LOV domain reconstituted with 5-deaza-FMN showed several multiplets in emissive mode that could be assigned to a tryptophan residue. The emissive lines are believed to arise by polarization transfer during the

recombination of a photochemically generated biradical state. The strong negatively polarized NMR signal in the ^{13}C NMR spectrum of the C450A mutant under blue light illumination suggests that the reaction steps after the excitation of the 5-deaza-FMN cofactor also follow a radical pair mechanism.

Flavodoxin (fldA) from *Escherichia coli* was reconstituted with ^{15}N- and ^{13}C-enriched FMN and analysed, in their oxidized and in the two-electron-reduced states, by ^{13}C- and ^{15}N-NMR spectroscopy. All carbon atoms of the isoalloxazine ring and ribityl carbon atoms of the protein-bound prosthetic group were assigned on the basis of isotopologue editing. The results are interpreted in terms of specific interactions between the apoprotein and the prosthetic group and the chemical structure of protein-bound FMN. In the oxidized state, weak H-bonds exist between the apoprotein and the N(3), C(2)O and C(4)O atoms of FMN. The N(1) and N(5) atoms of FMN form strong H-bonds. The isoalloxazine ring of FMN is strongly polarized and the N(10) atom shows an increased sp^2 hybridization compared to that of free FMN in aqueous solution. Of the ribityl carbon atoms C(3'), C(4') and C(5') are the most affected by binding to the apoprotein and the large downfield shift of the C(3') atom indicates strong hydrogen bonding with the apoprotein. In the reduced state, the H-bond pattern is similar to that in the oxidized state but a weak H-bond is observed between the N(5)-H group of FMN and the apoprotein.

While NMR techniques are well suited for flavoproteins with their flavin cofactor in either the fully oxidized or fully reduced redox state, their application to the one-electron reduced paramagnetic flavin is restricted because of the dominant interaction of the unpaired electron with the spins of magnetic nuclei. In this case, the method of choice is electron electron nuclear double resonance (ENDOR) spectroscopy, which can provide information on the detection of hyperfine coupling (hfc) arising from the interaction of nuclei with the unpaired electron spin.

ENDOR studies of all proteins specified above were enabled for the first time, the complete assignment of the hyperfine coupling constants for flavocoenzymes in complex with the investigated flavoproteins.

5 References

Ataka, K., Hegemann, P. and Heberle, J., (2003) Vibrational Spectroscopy of an Algal Phot-LOV1 Domain Probes the Molecular Changes Associated with Blue-Light Reception. *J. Biophy.* **84,** 466-474.

Atherton, N.M., (1993) Principles of Electron Spin Resonance, Ellis Horwood LTD., Chichester.

Aubert, C., Mathis, P., Eker, A.P.M., and Brettel, K., (1999) Intraprotein electron transfer between tyrosine and tryptophan in DNA photolyase from *Anacystis nidulans*. *Proc. Nat. Acad. Sci. USA* **96,** 5423-5427.

Aubert, C., Vos, M.H., Mathias, P., Eker, A.P.M. and Brettel, K., (2000) Intraprotein radical transfer during photoactivation DNA photolyase. *Nature* **405,** 586-590.

Bacher, A., Eberhardt, S., Fischer, M., Mortl, S., Kis, K., Kugelbrey, K., Scheuring, J., and Schott, K., (1997) Biosynthesis of riboflavin: GTP cyclohydrolase II, deaminase, and reductase. *Methods Enzymol.* **280,** 389-399.

Bacher, A., Eberhardt, S., Eisenreich, W., Fischer, M., Herz, S., Illarionov, B., Kis, K. and Richter, G., (2001) Biosynthesis of riboflavin. *Vitam. Horm.* **61,** 1-49.

Bargon, J., Fischer, H. *Z. Naturforsch*. (1967) ***22A***, 1556-1562.

Baum, G., Long, J.C., Jenkins, G.I., and Trewavas, A.T., (1999) Stimulation of the blue light phototropic receptor NPH1 causes a transient increase in cytosolic Ca^{2+}. *Proc. Nat. Acad. Sci. USA* **96,** 13554-13559.

Beach, R.L. and Plaut, G.W., (1970) Investigations of structures of substituted lumazines by deuterium exchange and nuclear magnetic resonance spectroscopy. *Biochemistry* **9,** 760–770.

Bianchi, M.W., Guivarc'h, D., Thomas, M., Woodgett, J.R. and Kreis, M., (1993) Arabidopsis homologs of the shaggy and GSK-3 protein kinases: molecular cloning and functional expression in *Escherichia coli. Mol. and General Genetic MGG* **242,** 337-345.

Blaschkowski, H. P., Neuer, G., Ludwig-Festl, M. and Knappe, J., (1982) Routes of flavodoxin and ferredoxin reduction in *Escherichia coli*. CoA-acylating pyruvate: flavodoxin and NADPH: flavodoxin oxidoreductases participating in the activation of pyruvate formate-lyase. *Eur. J. Biochem.* **123**, 563–569.

Briggs, W.R., and Huala, E., (1999) Blue-light photoreceptors in higher plants. *Annu. Rev. Cell Dev. Biol.* **15,** 33-62.

Budisa, N., Karnbrock, W., Steinbacher, S., Humm, A., Prade, L., Neuefeind, T., Moroder, L., and Huber, R., (1997) Bioincorporation of telluromethionine into proteins: a promising new approach for X-ray structure analysis of proteins**.** *J. Mol. Biol.* **270**, 616–623.

Budisa, N., Alefelder, S., Bae, J.H., Golbik, R., Minks, C., Huber, R., and Moroder, L., (2001) Proteins with ß-(thienopyrrolyl) alanines as alternative chromophores and pharmaceutically active amino acids. *Protein Science* **10,** 1281-1292.

Bullock, W. O., Fernandez, J. M., and Short, J. M., (1987) XL1-Blue: A high efficiency plasmid transforming *rec*A *Escherichia coli* with beta galactosidase selection. *Biotechniques* **5**, 376-380.

Burkhart, R., Schulte, D., Hu, D., Musahl, C., Gohring, F., and Knippers, R., (1995) Interactions of human nuclear proteins P1Mcm3 and P1Cdc46. *Eur. J. Biochem.* **228,** 431-438.

Carrington, A and McLachlan, A.D (1969) Introduction to Magnetic Resonance, Harper International Edition, New York.

Cashmore,A.R., Jarillo, J.A., Wu, Y.J. and Liu, D., (1999) Cryptochromes: Blue Light Receptors for Plants and Animals. *Science* **284,** 760-765.

Cecchini, G., Perl, M., Lipsick, J., singer, T.P., and Kearney, E.B., (1979) Transport and binding of riboflavin by Bacillus subtilis. *J. Biol.Chem*. **254**, 7295-7301

Christie, J.M. and Briggs, W.R., (2005) Blue light sensing and signalling by the phototropins. In *Handbook of Photosensory Receptors*, ed. W.R. Briggs, J.L. Spudlich, pp. 277-304. Weinheim:Wiley-VCH.

Christie, J. M., Reymond, P., Powell, G. K., Bernasconi, P., Raibekas, A. A., Liscum, E. and Briggs, W. R., (1998) *Arabidopsis* NPH1: A flavoprotein with the properties of a photoreceptor for phototropism. *Science* 282, 5394, 1698-1701.

Christie, J. M., Salomon, M., Nozue, K., Wada, M. and Briggs, W. R., (1999) LOV (light, oxygen, or voltage) domains of the blue-light photoreceptor phototropin (nph1): Binding sites for the chromophore flavin mononucleotide. *Proc. Natl. Acad. Sci. USA* **96,** 8779-8783.

Clubb, R.T., Thanabal, V. and Wagner, G., (1991) A new 3D HN(CA)HA experiment for obtaining fingerprint HN-Hα cross peaks in ^{15}N- and ^{13}C-labeled proteins. *J. Biomol. NMR* **2,** 203-210.

Corchnoy, SB., Swartz, TE., Lewis, JW., Szundi, I., Briggs, WR., Bogomolni, RA., (2003) Intramolecular proton transfers and structural changes during the photocycle of the LOV2 domain of phototropin 1. *J. Biol. Chem.* **278**,724–731.

Crosson, S., (2005) LOV-Domain Structure, Dynamics, and Diversity. In *Handbook of Photosensory Receptors*, ed. W.R. Briggs, J.L. Spudlich, pp. 323-335. Weinheim:Wiley-VCH.

Crosson, S., Rajagopal, S., and Moffat, K., (2003) The LOV domain family: photoresponsive signaling modules coupled to diverse output domains. *Biochemistry* **42,** 2-10.

Crosson, S. and Moffat, K., (2001) Structure of a flavin-binding plant photoreceptor domain: Insights into light-mediated signal transduction. *Proc. Natl. Acad. Sci. USA* **98,** 2995-3000.

Crosson, S. and Moffat, K., (2002) Photoexcited Structure of a Plant Photoreceptor Domain Reveals a Light-Driven Molecular switch. *The Plant Cell* **14,** 1067-1075.

Delbrueck, M., Katzir, A. and Presti, D., (1976) Responses of Phycomyces indicating optical excitation of the lowest triplet state of riboflavin. *Proc. Natl. Acad. Sci. USA* **73,** 1969-1973.

Dower, W.J, Miller, J.F., and Ragsdale, C.W., (1988) High efficiency transformation of *E. coli* by high voltage electroporation. *Nucl. Acids Res.* **16,** 6127–6144.

Dwyer, T. M., Mortl, S., Kemter, K., Bacher, A., Fauq, A., and Frerman, F. E., (1999) The intraflavin hydrogen bond in human electron transfer flavoprotein modulates redox potentials and may participate in electron transfer. *Biochemistry* **38**, 9735-9745.

Dym, O. and Eisenberg, D., (2001) Sequence-structure analysis of FAD-containing proteins. *Protein Science* **10**, 1712–1728.

Edmondson, D. E., and Tollin, G. (1971) *Biochemistry* **10,** 133-145.

Eggink, G., Engel, H., Vriend, G., Terpstra, P. and Witholt, B., (1990) Rubredoxin reductase of *Pseudomonas oleovorans*. Structural relationship to other flavoprotein oxidoreductases based on one NAD and two FAD fingerprints. *J. Mol. Biol.* **212**, 135–142.

Erbel, P.J.A., Card, P.B., Karakuzu, O., Bruick, R.K. and Gardner, K.H., (2003) Structural basis of PAS domain heterodimerization in the basic helix-loop-helix-PAS transcription factor hypoxia-inducible factor. *Proc. Natl. Acad. Sci. USA* **100,** 15504-15509.

Federov, R., Schlichting, I., Hartmann, E., Domratcheva, T., Fuhrmann, M. and Hegemann, P., (2003) Crystal structures and molecular mechanism of a light-induced signaling

switch: the phot1-LOV domain from *Chlamydomonas reinhartii*. *Biophys. J.* 84**,** 2474–2482.

Fleischmann, G., Lederer, F., Müller, F., Bacher, A. & Rüterjans, H., (2000) Flavin–protein interactions in flavocytochrome b2 as studied by NMR after reconstitution of the enzyme with ^{13}C- and ^{15}N-labelled flavin. *Eur. J. Biochem.* **267**, 5156–5167.

Folta K. M. and Spalding, E. P., (2001) Unexpected roles for cryptochrome 2 and phototropin revealed by high- resolution analysis of blue light-mediated hypocotyl growth inhibition. *Plant J.* **26,** 471–478.

Fraaije, M.W. and Mattevi, A., (2000) Flavoenzymes: diverse catalysts with recurrent features. *Trends Biochem. Sci.* **25**, 126–132.

Freidberg, E.C., (1995) DNA Repair and Mutagenesis. ASM Press, Washington, D.C.

Fujii, K., Galivan, J.H, and Huennekens, R.M., (1977) Activation of methionine synthetase: a further characterization of the flavoprotein system. *Arch. Biochem. Biophys.* **178,** 662-670.

Ghisla, S. and Massey, V., (1986) New flavins for old: artificial flavins as active site probes of flavoproteins. *Biochem. J.* **239**, 1–12.

Ghisla, S., Massey, V., Lhoste, J.M., and Mayhew, S.G., (1974) *Biochemistry* **13,** 589-597.

Gindt, Y. M., Vollenbroek, E., Westphal, K., Sackett, H., Sancar, A. and G. T. Babcock. G.T., (1999) Origin of the transient electron paramagnetic resonance signals in DNA photolyase. *Biochemistry* **38,** 3857-3866.

Grande, H.J., Gast, R., van Schagen, C.G., van Berkel, W.J.H., and Müller, F. (1977) ^{13}C-NMR study onisoalloxazine and alloxazine derivatives. *Helv. Chim. Acta* **60,** 367-379.

Hamm-Alvarez, S., Sancar, A., and Rajagopalan, K.V. (1989) The role of the enzyme-bound 5,10-methenyltetrahydropteroylpolyglutamate in catalysis by *Escherichia coli* DNA photolyase. *J. Biol. Chem.* **264,** 9649-9656.

Hamm –Alvarez, S.W., Sancar, A. and Rajagopalan, K.V. (1990) The folate cofactor of *Eischerichia coli* DNA photolyase acts catalytically. *J. Biol. Chem.* **265,** 18656-18662.

Harm, H. and Rupert, C.S. (1968) Analysis of Photoenzymatic Repair of UV Lesions in DNA by Single Light Flashes. I. in vitro Studies with Haemophilus Influenzae Transforming DNA and Yeast Photoreactivating enzyme. *Mutat. Res.* **6,** 355-70.

Harm W., Harm H, Rupert C.S. (1968) Analysis of photoenzymatic repair of UV lesions in DNA by single light flashes II. *In vivo* studies with *Escherichia coli* cells and bacteriophage. *Mutat. Res.* **6,** 371–385.

Harm, H. and Rupert, C.S. (1970) Analysis of photoenzymatic repair of UV lesions in DNA by single light flashes: VII. Photolysis of enzyme-substrate complexes in vitro. *Mutat. Res.* **10**, 307–318.

Harm, H. and Rupert, C.S. (1976) Analysis of photoenzymatic repair of UV lesions in DNA by single light flashes. XI. Light-induced activation of the yeast photoreactivating enzyme. *Mutat. Res.* **34,** 75–92.

Harper, S.M., Neil, L.C., and Gardner, K.H. (2003) Structural Basis of a Phototropin Light switch. *Science* **301,** 1541-1544.

Harper, S.M., Christie, J.M., and Gardner, K.H. (2004) Disruption of the LOV – Jα Helix Interaction Activates Phototropin Kinase Activity. *Biochemistry* **43,** 16184-16192.

Harper, S.M., Neil, L.C., Day, I.J., Hore, P.J. and Gardner, K.H. (2004) Conformational Changes in Photosensory LOV Domain Monitored by Time-Resolved NMR Spectroscopy. *J. Am. Chem. Soc.* **126,** 3390-3391.

Havel, T.F. (1993) Predicting the structure of the flavodoxin from *Escherichia coli* by homology modeling, distance geometry and molecular dynamics, *Mol. Sim.* **10,** 175-210.

Hecht, S., Richter, G., Bacher, A., Joshi, M., Römisch, W., Greiner, G., Frank, R.,Weber, S., Eisenreich, W., and Fischer, M., (2005) Photocycle of a blue light receptor LOV2 domain reconstituted with 5-deaza-FMN in "Flavins and Flavoproteins 2005", T. Nishino, R. Miura, M. Tanokura, K. Fukui (Editors),ARchiTect Inc., Tokyo, pp. 569–574.

Heelis, P.F., Parsons, B.J., and Phillips, G.O. (1979) The pH dependence of the reactions of flavin triplet states with amino acids. *Biochem. Biophys. Acta* **587,** 455-462.

Heelis, P.F., Kim, S.T., Okamura, T., and Sancar, A. (1993) The photo repair of pyrimidine dimers by DNA photolyase and model systems. *J. Photochem. Photobiol*. 17, 219-228.

Henner, D.J. (1990) Expression of heterologous genes in Bacillus subtilis. *Methods Enzymol.* **185,** 199-201.

Hoff, A.O., Cote, G.J., Fritsche, Jr. H.A., Qiu, H., Schultz, P.N., and Gagel, R.F. (1999) Calcium-induced activation of a mutant G-protein-coupled receptor causes in vitro transformation of NIH/3T3 cells. *Neoplasia* 1, 485-491.

Hoover, D. M., and Ludwig M. L., (1997) A flavodoxin that is required for enzyme activation: The structure of oxidized flavodoxin from *Escherichia coli* at 1.8 A resolution. *Protein Science*, **6**, 2525-2537.

Holtzhauer, M., (1996) Methoden der Proteinanalytik, Springer-verlag, Berlin.

Huala, E., Oeller, P.W., Liscum, E., Han, I. S., Larsen, E., and Briggs, W.R. (1997) *Arabidopsis* NPH1: A protein kinase with a putative redox sensing domain. *Science* **278**, 2121-2123.

Illarionov, B., Fischer, M., Lee, C.Y., Bacher, A., and Eisenreich, W. (2004) Rapid Preparation of Isotopolog Libraries by in Vivo Transformation of ^{13}C-Glucose. Studies on 6,7-Dimethyl-8-ribityllumazine, a Biosynthetic Precursor of Vitamin B_2. *J. Org. Chem.* **69,** 5588-5594.

Imaizumi, T., Tran, H.G., Swartz, T.E., Briggs, W.R., and and Kay, S.A. (2003) FKF1 is essential for photoperiodic-specific light signalling in *Arabidopsis. Nature* **426,** 302-306.

Iwata, T., Tokutomi, S., and Kandori, H. (2005) *J. Am. Chem. Soc.* **124**, 11840–11841

Iwata, T., Nozaki D, Tokutomi, S., Kagawa, T.,Wada, M., and Kandori H. (2003). Light-induced tructural changes in the LOV2 domain of Adiantum phytochrome3 studied by low temperature FTIR and UV-visible spectroscopy. *Biochemistry* 42, 8183–8191.

Iwata, T., Nozaki, D., Tokutomi, S., and Kandori H. (2005). Comparative investigation of the LOV1 and LOV2 domains in Adiantum phytochrome3. *Biochemistry* 44, 7427–7434.

Jarillo, J.A., Gabrys, H., Capel, J., Alonso, J.M., Ecker, J.R., and Cashmore, A.R. (2001) *Nature* **410**, 952–954.

Jenkins, C.M and Waterman, M.R. (1994) Flavodoxin and NADPH-flavodoxin reductase from Escherichia coli support bovine cytochrome *P*450c17 hydroxylase activities. *J. Biol. Chem*. **269,** 27401-27408.

Jorns, M.S., Baldwin, E.T., Sancar, G.B., and sancar, A. (1987) Action mecanism of *Escherichia coli* DNA photolyase. 2. Role of the chromophores in catalysis. *J. Biol. Chem.* **262,** 486-491.

Jorns, M.S., Wang, B.Y., Jordan, S.P., and Chanderkar, L.P. (1990) Chromophore function and interaction in *Escherichia coli* DNA photolyase: reconstitution of the apoenzyme with pterin and/or flavin derivatives. *Biochemistry* 29; 552–561.

Jorns, M.S. and Hersh, L.B., (1976) Nucleophilic addition reactions of free and enzyme-bound Deazaflavin. *J. Biol. Chem.* **251,** 4872-4881.

Kabsch, W., and Sander, C. (1983) Dictionary of protein secondary structure: pattern recognition of hydrogen-bonded and geometrical features. *Biopolymers* **22**, 2577-2637.

Kagawa, T., Sakai, T., Suetsugu, N., Oikawa, K., Ishiguro, S., Kato, T., Tabata, S., Okada, K., and Wada, M. (2001) *Arabidopsis* NPL1: A phototropin homologue controlling the chloroplast high-light avoidance response. *Science* **291**, 2138-2141.

Kagawa, T., Kasahara, M., Abe, T., Yoshida, S., and Wada, M. (2004) Function analysis of phototropin 2 using fern mutants deficient in blue light-induced chloroplast avoidance movement. *Plant Cell Physiol.* **45**, 416–426.

Kainosho, M. and Kyogoku, Y. (1972) High resolution proton and phosphorus nuclear magnetic resonance spectra of flavin-adenine dinucleotide and its conformation in aqueous solution. *Biochemistry* **11,** 741-752.

Kaptein, R. (1975) Chemically induced dynamic nuclear polarization: theory and applications in mechanistic chemistry. *Adv. Free Rad. Chem.* **5**, 319-380.

Karthikeyan, S., Zhou, Q., Mseeh, F., Grishin, N.V., Osterman, A.L., and Zhang, H. (2003) Crystal structure of human riboflavin kinase reveals a β barrel fold and a novel active site arch. *Structure* **11**, 265–273.

Kasahara, M., Swartz, T. E., Olney, M. A., Onodera, A., Mochizuki, N., Fukuzawa, H., Asamizu, E., Tabata, S., Kanegae, H., Takano, Christie, J. M., Nagatani, A. and Briggs, W. R. (2002) Photochemical Properties of the Flavin Mononucleotide-Binding Domains of the Phototropins from Arabidopsis, Rice, and *Chlamydomonas reinhardtii*. *Plant Physiol*. **129**, 762-773.

Kay, C.W.M., Feicht, R., Schulz, K., Sadewater, P., Sancar, A., Bacher, A., Möbius, K., Richter, G., and Weber, S. (1999) EPR, ENDOR, and TRIPLE resonance spectroscopy on the neutral flavin radical in *Eischerichia coli* DNA photolyase. *Biochemistry* **38,** 16740-16748.

Kay, C.W.M., Schleicher, E., Kuppig, A., Hofner, H., Rdiger, M.S., Fischer, M., Bacher, A., Weber, S., and Richter, G. (2003) Blue Light Perception in Plants. Detection and characterization of alight-induced neutral flavin radical in a C450 mutant of phototropin. *J. Bio. Chem.* **278,** 10973-10982.

Kennis, J.T.M., Crosson, S., Gauden, M., van Stokkum, I.H.M., Moffat, K., and van Grondelle, R. (2003) Primary Reactions of the LOV2 Domain of Phototropin, a Plant Blue-Light Photoreceptor. *Biochemistry* **42,** 3385-3392.

Kennis, J.T.M., van Stokum, N.H.M., Crosson, S., Gauden, M., Moffat, K., and van Grondelle, R. (2004) The LOV2 Domain of Phototropin: A Reversible Phototromic Switch. *J. Am. Chem. Soc.* **126,** 4512-4513.

Kim, S.T. and Sancar, A. (1991) Effect of base, pentose, and phosphodiester backbone structures on binding and repair of pyrimidine dimers by *Eischerichia coli* DNA photolyase. *Biochemistry* **30,** 8623-8630.

Kim, S. T., Li, Y. F., and Sancar, A. (1992) The third chromophore of DNA photolyase: Trp-277 of Escherichia coli DNA photolyase repairs thymine dimers by direct electron transfer. *Proc. Natl. Acad. Sci. USA* **89**, 900-904.

Kim, S.T. and Sancar, A. (1993) Photochemistry, photophysics, and mechanism of pyrimidine dimer repair by DANN photolyase. *Photochem. Photobiol.* **57,** 895-904.

Kim, S.T., Sancar, A., Essenbacher, C., and Babcock, G. T. (1993) Time-resolved EPR studies with DNA photolyase: excited-state FADH0 abstracts an electron from Trp-306 to generate FADH-, the catalytically active form of the cofactor. *Proc. Natl. Acad. Sci. USA* **90,** 8023–8027.

Kis, K. and Bacher., A. (1995) Substrate channeling in the lumazine synthase/riboflavin synthase complex of *Bacillus subtilis*. *J. Biol. Chem.* **270,** 16788-16795.

Kis, K., Volk, R., and Bacher, A. (1995) Biosynthesis of riboflavin. Studies on the reaction mechanism of 6,7-dimethyl-8-ribityllumazine synthase. *Biochemistry* **34,** 2883-2892.

Komori, H., Masui, R., Kuramitsu, S., Yokoyama, S., Shibata, T., Inoue, Y. und Miki, K.(2001) Crystal structure of thermostable DNA photolyase: Pyrimidine-dimer recognition mechanism. *Proc. Natl. Acad. Sci. U S A* **98**, 13560-13565.

Kottke, T., Heberle, J., Hehn, D., Dick, B., and Hegemann, P. (2003) Phot-LOV1: Photocycle of a Blue-Light Receptor Domain from the Green Alga *Chlamydomonas reinhardtii. Biophys. J.* 84**,** 1192-1201.

Kraulis, P. J. (1991) Molscript -- a program to produce both detailed and schematic plots of protein structures. *J. Appl. Cryst.* **24**, 946-950.

Laemmli, U. K. (1970) Cleavage of structural proteins during the assembly of the head of bacteriophage T4. *Nature* **227**, 680-685.

Laudenbach, D. E., Straus, N. A., Pattridge, K. A., and Ludwig, M. L. (1987) In Flavins and Flavoproteins, edited by D. E. Edmondson & D. B. McCormick, pp. 249-260. Berlin/New York: W. de Gruyter & Co.

Lee, Y.H., Nadaraia, S., Gu, D., Becker, D.F., and Tanner, J.J. (2003) Structure of the proline dehydrogenase domain of the multifunctional PutA flavoprotein. *Nat. Struct. Biol.* **10**, 109–114.

Le Grice, S.F. (1990) Regulated promoter for high-level expression of heterologous genes in Bacillus subtilis. *Methods Enzymol.* **185,** 201-14.

Li, Y.F., Heelis, P.F., and Sancar, A. (1991) Active-site of DNA photolyase – tryptophan-306 is the intrinsic hydrogen-atom donor essential for flavin radical photoreduction and DNA-repair in vitro. *Biochemistry* **30,** 6322-6329.

Liscum, E., and Briggs, W.R. (1995) Mutations in the NPH1 locus of *Arabidopsis* disrupt the perception of phototropic stimuli. *Plant Cell* **7**, 473-485.

Losi, A., Polverini, E., Quest, B., and Gärtner, W. (2002) First evidence for phototropin-related blue-light receptors in prokaryotes. *Biophys. J.* 82, 2627–2634.

Lostao, A., El Harrous, M., Daoudi, F., Romero, A., Parody-Morreale, A., and Sancho, J. (2000) Dissecting the energetics of the apoflavodoxin-FMN complex. *J. Biol. Chem.* **275**, 9518–9526.

Malhotra, K., Kim, S.T., Batschauer, A., Dawut, L., and Sankar, A. (1995) Putative blue-light photoreceptors from *Arabidopsis thaliana* and *Sinapis alba* with a high-degree of sequence homology to DNA photolyase contain the 2 photolyase cofactors but lack DNA-repair activity. *Biochemistry* **34,** 6892-6899.

Manstein, D.J. and Pai, E.F. (1986) Purification and characterization of FAD synthetase from *Brevibacterium ammoniagenes*. *J. Biol. Chem.* **261**, 16169–16173.

Massey, V. (2000) The chemical and biological versatility of riboflavin. *Biochem. Soc. Trans.* **28**, 283–296.

Mateo, P.L. and Sturtevant, J.M. (1977) Thermodynamics of the binding of flavin adenine dinucleotide to d-amino acid oxidase. *Biosystems* **8**, 247–253.

Mathews, F.S. (1991) New flavoenzymes. *Curr. Opin. Struct. Biol.* **1**, 954–967.

Mayhew, S.G. and Ludwig, M.L. (1975) Flavodoxins and electron-transferring flavoproteins. In *The enzymes* (ed. P.D. Boyer), Vol. 12, pp. 57–118. Academic Press, New York.

Mayhew, S.G. and Tollin, G. 1992. General properties of flavodoxins. In *Chemistry and biochemistry of flavoenzymes*, Vol. 3 (ed. F. Müller), pp. 389–426. CRC Press, Boca Raton, FL.

Mewies, M., McIntire, W.S., and Scrutton, N.S. (1998) Covalent attachment of flavin adenine dinucleotide (FAD) and flavin mononucleotide (FMN) to enzymes: The current state of affairs. *Protein Science* **7**, 7–20.

Miller, S.M., Massey, V., Ballou, D., Williams, C.H. Jr., Distefano, M.D., Moore, M.J., and Walsh, C.T. (1990) Use of a site – directed mutant to trap intermediates: demonstration

that the flavin C(4a)-thiol adduct and reduced flavin are kinetically competent intermediates in mercuric ion reductase. *Biochemistry* **29,** 2831-2841.

Minks, C., Huber, R., Moroder, L., and Budisa, N. (1999) Atomic mutations at the single tryptophan residue of human recombinant annexin V: Effects on structure, stability and activity. *Biochemistry* **38,** 10649–10659.

Miyamoto, Y. and Sancar, A. (1998) Vitamin B2-based blue-light photoreceptors in the retinohypothalamic tract as the photoactiv pigments for setting the circadian clock in mammals. *Proc. Natl. Acad. Sci. USA* **95,** 6097-6102.

Moonen, C.T., Vervoort, J., and Müller, F. (1984) Reinvestigation of the structure of oxidized and reduced flavin: carbon-13 and nitrogen-15 nuclear magnetic resonance study. *Biochemistry* **23**, 4859–4867.

Müller, F. (1971) Synthesis of 2-substituted riboflavin analogs. *Methods Enzymol.* **18B**, 453-458.

Müller, F. (1992) Nuclear magnetic resonance studies of flavoproteins. In *Chemistry and Biochemistry of Flavoenzymes* (Müller, F., ed.), pp. 557–595. CRC Press Inc, Boca Raton, FL.

Nakajima, S., Sugiyama, M., Iwai, S., Hitomi, K., Otoshi, E., Kim, S.T., Jiang, C.Z., Todo, T., Britt, A.B., and Yamamoto, K. (1998) Cloning and characterization of a gene (UVR3) required for photorepair of 6-4 photoproducts in *Arabidopsis thaliana*. *Nucleic Acids Research* **26,** 638-644.

Nakasako, M., Iwata, T., Matsuoka, D., and Tokutomi, S. (2004) *Biochemistry* 43, 14881–14890.

Nozaki, D., Iwata, T., Ishikawa, T., Todo, T., Tokutomi, S., and Kandori, H. (2004) Role of Gln 1029 in the photoactivation processes of the LOV2 domain in Adiantum phytochrome3. *Biochemistry* 43, 8373–8379.

Nozue, K., Kanegae, T., Imaizumi, T., Fukuda, S., Okamoto, H., Yeh, K.C. Lagarias, C., and Wada, M. (1998) A phytochrome from the fern *Adiantum* with features of the putative photoreceptor NPH1. *Proc. Natl. Acad. Sci.* **95,** 15826-15830.

Osborne, C., Chen, L.M., and Matthews, R.G. (1991) Isolation, cloning, mapping, and nucleotide sequencing of the gene encoding flavodoxin in *Escheriachia coli*. *J.Bactriol.* 173, 1729-1737.

Otoshi, E., Yagi, T., Mori, T., Matsunaga, T., Nikaido; O., Kim, S.T., Hitomi, K., Ikenaga, M., and Todo, T. (2000) Respective roles of cyclobutane pyrimidine dimers, (6-4)

photoproducts, and minor photoproducts in ultravoilet mutagenesis of repair-deficient *Xeroderma pigentosum* A cells. *Cancer Res.* **60,** 1729-1735.

Park, H. W., Kim, S. T., Sancar, A., and Deisenhofer, J. (1995) Crystal structure of DNA photolyase from *Escherichia coli*. *Science* **268**, 1858-1869.

Payne, G., Heelis, P.F., Rohrs, B.R., and Sancar, A. (1987) The active Form of *Eischerichia coli* DNA photolyase contains a fully reduced flavin and not a flavin radical, both *in vivo* and *in vitro*. *Biochemistry* **26,** 7121-7127.

Payne, G., Wills, M., Walsh, c. and Sancar, A. (1990) Reconstitution of *Escherichia coli* photolyase with flavins and flavin analogues. *Biochemistry* **29,** 5707-5711.

Payne, G. and Sancar, A. (1990) Absolute action spectra of E-FADH2 und E-FADH2-MTHF forms of *Escherichia coli* DNA photolyase. *Biochemistry* **29**, 7715-7727.

Plaut, G. W. E. (1963) Studies on the nature of the enzymatic conversion of 6,7-dimethyl- 8-ribityllumazine to riboflavin. *J. Biol. Chem.* **238**, 2225-2243.

Ponsting1, H. and Otting, G. (1997) NMR assignments, secondary structure and hydration of oxidized *Escherichia coli* flavodoxin. *Eur. J. Biochem.* **244,** 384-399.

Quail, P.H. (2002) Phytochrome photosensory signalling networks. *Nat. Rev. Mol. Cell Biol.* **3:** 85-93.

Rao, S.T., Fathieh, S., Yu, C., Satyshur, K.A., Stockman, B.J., Markley, J.L., and Sundaralinghan, M. (1992) Structure of the oxidised long chain flavodoxin from *Anabena 7120*. *Protein Sci.* **1,** 1413-1427.

Read, S.M. and Northcote, D.H. (1981) Minimization of variation in the response to different proteins of the Coomassie Blue G dye-binding assay for protein. *Annual. Biochem.* **116**, 53–64.

Richter, G., Bacher, A.,Weber, S., Römisch, W., Joshi, M., Fischer, M., and Eisenreich, W., (2005) Studies of the photocycle of the blue-light receptor phototropin. Observation of nuclear-spin polarization by solution 13C-NMR in "Flavins and Flavoproteins 2005", T. Nishino, R. Miura, M. Tanokura, K. Fukui(Editors), ARchiTect Inc., Tokyo, pp. 587–591.

Richter, G., Weber, S., Römisch, W., Bacher, A., Fischer, M., and Eisenreich, W. (2005) photochemically Induced Dynamic Nuclear Polorization in a C450 Mutant of the LOV2 Domain of the *Avena sativa* Blue-Light Receptor Phototropin. *J. Am. Chem. Soc.* **127,** 17245-17252.

Reider, C. (1999) Retrobiosynthetic Studies of Carbon Flux by NMR detected Stable Isotope Incorporation. Biosynthesis of Molybdopterin and of *Verrucosan diterpenes*, Dissertation, Technische Universität München.

Rohdich, F. , Zepeck, F., Adam, P., Hecht, S., Kaiser, J., Laupitz, R., Gräwert, T., Amslinger, S., Eisenreich, W., Bacher, A., and Arigoni, D. (2003) The deoxyxylulose phosphate pathway of isoprenoid biosynthesis: Studies on the mechanisms of the reactions catalyzed by IspG and IspH protein. *Proc. Natl. Acad. Sci. USA* **100,** 1586-1591.

Römisch, W., Eisenreich, W., Richter, G., and Bacher, A. (2002) Rapid One-Pot Synthesis of Riboflavin Isotopomers. *J. Org. Chem.* **67,** 8890-8894.

Römisch, W. (2005) Coenzym-Isotopologe als spektroskopische Sonden, Dissertation, Technische Universität München.

Rupert, C.S. (1960) Photoreactivation of transforming DNA by an enzyme from bakers' yeast. *J. Gen. Physiol.* **43,** 573-595.

Rupert, C.S. (1962a) Photoenzymatic repair of ultraviolet damage in DNA. I. Kinetics of the reaction. *J. Gen. Physiol.* 45, 703-724.

Rupert, C.S. (1962b) Photoenzymatic repair of ultraviolet damage in DNA. II. Formation of an enzyme-substrate complex. *J. Gen. Physiol.* 45, 725-741.

Sakai, T., Kagawa, T., Kasahara, M., Swartz, T.E., Christie, J.M., Briggs, W.R., Wada, M., and Okada, K. (2001) Nph1 and npl1: Blue-light receptors that mediate both phototropism and chloroplast relocation in Arabidopsis. *Proc. Natl. Acad. Sci.* **98,** 6969-6974.

Salomon, M., Christie, J.M., Knib, E., Lempert, U., and Briggs, W.R. (2000) Photochemical and mutational analysis of the FMN-binding domains of the plant blue light receptor, phototropin. *Biochemistry* **39**, 9401-9410.

Salomon, M., Eisenreich, W., Dürr, H., Schleicher, E., Knieb, E., Massey, V., Rüdiger, W., Müller, F., Bacher, A., and Richter, G. (2001) An optomechanical transducer in the blue light receptor phototropin from *Avena sativa*. *Proc. Natl. Acad. Sci.* **98,** 12357-12361.

Salomon, M., Lempert, U., and Rüdiger W. (2004) Dimerization of the plant photoreceptor phototropin is probably mediated by the LOV1 domain. *FEBS* **572**, 8-10.

Sancar, G. B., Smith F. W., and Sancar A. (1985) Binding of Escherichia coli DNA photolyase to UV-irradiated DNA. *Biochemistry* **24,** 1849–1855.

Sancar, G. B., Smith, P. F., and Heelis, P. F. (1987) Purification of the yeast PHR1 photolyase from an *Escherichia coli* overproducing strain and characterization of the intrinsic

chromophores of the enzyme. *J. Biol. Chem.* **262**, 15457-15465.

Sancar, G. B. (1990) DNA photolyases: physical properties, action mechanism, and roles in dark repair. *Mutat Res*. **236**, 147-160.

Sancar, A. (1994) Structure and function of DNA photolyase. *Biochemistry* **33**, 2–9.

Sancar, A., (2000) Cryptochrome: the second photoactive pigment in the eye and its role in circadian photoreception. *Annu. Rev. Biochem*. **69**, 31-67.

Sancar, A. (2003) Structure and Function of DNA Photolyase and Cryptochrome Blue-Light Photoreceptors. *Chem. Rev.* **103,** 2203-2237.

Schleicher, E., Benedikt, H., Illiarinova, V., Bacher, A., Weber, S., Richter, G., and Gerwert, K. (2005) Light-induced reactions of *Escherichia coli* DNA photolyase monitoterd by Fourier transform infrared spectroscopy. *FEBS* **272,** 1855-1866.

Schleicher, E., Kowalczyk, R.M., Kay, C.W.M., Hegemann, P., Bacher, A., Fischer, M., Bittl, R., Richter, G., and Weber, S: (2004) On the Reaction Mechanism of adduct Formation in LOV Domains of the Plant Blue-Light receptor Phototropin. *J. Am. Chem. Soc.* **126,** 11067-11076.

Schleicher, E. (2002) Über den Reaktionsmechanismus der DNA-Photolyase, Dissertation, Technische Universität München.

Schuttrigkeit, T., Kompa, C. et al., (2003). *Chem. Phys.* **294,** 501-508et al., 2003

Schwerdtfeger, C. and Linden, H. (2003) VIVID is a flavoprotein and serves as a fungal blue light photoreceptor for photoadaptation. *EMBO. J.* **22,** 4846-4855.

Sedlmaier H., Muller F., Keller P.J., and Bacher, A. (1987) Enzymatic synthesis of riboflavin and FMN specifically labeled with ^{13}C in the xylene ring. *Z. Naturforsch. [C]* **42**, 425-429.

Short, T.W., Porst, M., Palmer, J.M., Fernbach, E., and Briggs, W.R. (1994) Blue light induces phosphorylation at multiple sites on a pea plasma membranep rotein. *Plant. Physiol.* In press

Smith, W.W., Burnett, R.M., Darling, G.D., and Ludwig, M.L. (1977) Structure of the semiquinone form of flavodoxin from *Clostridum MP.* Extension of 1.8 Å resolution and some comparisons with the oxidized state. *J. Mol. Bio.* **117,** 195-225.

Smith, W.W., Pattridge, K.A., and Ludwig, M.L. (1983) Structure of oxidized flavodoxin from *Anacystis nidulans. J. Mol. Biol.* **165,** 737-755.

Spencer, R., Fisher, J., and Walsh, C. (1976) Preparation, characterization, and chemical properties of the flavin coenzyme analogues 5-deazariboflavin, 5-deazariboflavin 5'-

phosphate, and 5-deazariboflavin 5'-diphosphate, 5' leads to 5'-adenosine ester. *Biochemistry* **15**, 1043–1053.

Stüber, D., Matile, H. and Garotta, G. (1990) System for high-level production in *Escherichia coli* and rapid purification of recombinant proteins: application to epitope mapping, preparation of antibodies, and structure-function analysis. In Immunological methods IV (Lefkovits, I. und Pernis, P. eds.) pp. 121-152, Academic Press, Orlando, Florida.

Stockman, B.J., Westler, W.M., Mooberry, E.S., and Markley, J.L (1988a) Flavodoxin from Anabena 7120: Uniform nitrogen-15 enrichment and hydrogen 1, nitrogen-15, and phosphrous-31 NMR investigations of the flavinmononucleotide binding site in the reduced and oxidised states. *Biochemistry* **27,** 136-142.

Stockman, B.J., Westler, W.M., Darba, P., and Markley, J.L (1988b) Detailed analysis of carbon -13 NMR spin systems in a uniformly carbon-13 enriched protein: Flavodoxin from *Anabena 7120. J. Am. Chem. Soc*. **110,** 4095-4096.

Stockman, B.J., Krezel, A.M., and Markley, J.L. (1990) Hydrogen- 1, Carbon- 13, and Nitrogen- 15 NMR Spectroscopy Flavodoxin: Assignment of β-Sheet and Flavin Binding Site.

Resonances and Analysis of Protein-Flavin Interactions. *Biochemistry* **29,** 9600-9609.

Sturtevant, J.M. and Mateo, P.L. (1978) Proposed temperature-dependent conformational transition in d-amino acid oxidase: a differential scanning microcalorimetric study. *Proc. Natl. Acad. Sci. USA* **75,** 2584–2587.

Swartz, T.E. and Bogomolni, R.A., (2005) LOV-domain Photochemistry. In *Handbook of Photosensory Receptors*, ed. W.R. Briggs, J.L. Spudlich, pp. 305-321. Weinheim:Wiley-VCH.

Swartz, T.E., Corchnoy, S.B., Christie, J.M., Lewis, J.W., Szundi, I., Briggs, W.R., and Bogomolni, R. (2001) The photocycle of a flavin-binding domain of the blue-light photoreceptor phototropin. *J. Biol. Chem.* **276:** 36493-36500.

Swartz, T.E., Wenzel, P.J., Corchnoy, S.B., Briggs, W.R., and Bogomolni, R.A. (2002) Vibration Spectroscopy Reveals Light-Induced Chromophore and Protein Structural Changes in the LOV2 Domain of the Plant Blue-Light Receptor Phototropin 1. *Biochemistry* **41,** 7183 -7189.

Taylor, B. L., and Zhulin I. B. (1999) PAS Domains: Internal Sensors of Oxygen, Redox Potential, and Light. *Microbio. Mol. Biol. Rev.* **63,** 479-506.

Todo, T. (1999) Functional diversity of the DNA photolyase blue light receptor family. *Mutation Res-DNA Repair* **434,** 89-97.

Todo, T., Takemori, H., Ryo, H., Ihara, M., Matsunaga, T., Nikaido, O., Sato, K., and Nomura, T (1993) A new photoreactivating enzyme that specifically rapairs ultravoilet light-induced (6-4) photoproducts. *Nature* **361,** 371-374.

Vallon, O. (2000) New sequence motifs in flavoproteins: evidence for common ancestry and tools to predict structure. *Proteins* **38**, 95–114.

van Berkel, W.J.H., van den Berg., W.A.M., and Mueller, F. (1988) *Eur. J. Biochem.* **178,** 197-207.

van Schagen, C.G., and Müller, F. (1981) A 13C nuclear-magnetic-resonance study on free flavins and Megasphaera elsdenii and Azotobacter vinelandii flavodoxin. 13C-enriched flavins as probes for the study of flavoprotein active sites. *Eur J Biochem* **120,** 33-39.

Vervoort, J., Müller, F., O'Kane, D. J., Lee, J. und Bacher, A. (1986a) Bacterial luciferase: a carbon-13, nitrogen-15, and phosphorus-31 nuclear magnetic resonance investigation. *Biochemistry* **25**, 8067-8075.

Vervoort, J., Müller, F., Mayhew, S.G., van den Berg, W.A., Moonen, C.T. & Bacher, A. (1986b) A comparative carbon-13, nitrogen-15, and phosphorus-31 nuclear magnetic resonance study on the flavodoxins from *Clostridium MP*, *Megasphaera elsdenii*, and *Azotobacter vinelandii*. *Biochemistry* **25**, 6789–6799.

Vetter, H. J. and Knappe, J. (1971) Flavodoxin and ferredoxin of *Escherichia coli*. *Hoppe-Seyler's J physiol. Chem.* **352**, 433–466.

Volk, R. and Bacher, A. (1990) Studies on the four carbon precursor in the biosynthesis of riboflavin. Purification and properties of L-3,4-dihydroxy-2-butanone 4-phosphate synthase. *J. Biol. Chem*. **265,** 19479-19485.

Wacker, H., Harvey, R. A., Winestock, C. H., and Plaut, G. W. E. (1964) 4-(1'-D-ibitylamino)5-amino-2,6,-dihydroxypyrimidine, the second product of the riboflavin synthase reaction. *J. Biol. Chem.* **239**, 3493-3497.

Ward, H. R.; Lawler, R. G. *J. Am. Chem. Soc.* (1967) **89,** 5518-5519.

Weber, S., Richter, G., Schleicher, E., Bacher, A., Möbius, K., and Kay, C. W. M. (2001a) Substrate binding to DNA photolyase studied by electron paramagnetic resonance spectroscopy. *Biophys. J.* **81**, 1195-1204.

Weber, S., Möbius, K., Richter, G., and Kay, C. W. M. (2001b) The Electronic Structure of the Flavin Cofactor in DNA Photolyase. *J. Am. Chem. Soc.* **123**, 3790-3798.

Weber, S. (2005) Light-driven enzymatic catalysis of DNA repair: a review of recent biophysical studies on photolyase. *Biochim. Biophys. Acta* **1707,** 1-23.

Williams, D. M., Duvall, E. J., and Lovett, P. S. (1981) Cloning restriction fragments that promote expression of a gene in *Bacillus subtilis*. *J. Bacteriol.* **146,** 1162–1165.

Yalloway, G.N., Lohr, F., Wienk, H.L., Mayhew, S.G., Hrovat, A., Knauf, M.A., and Ruterjans, H. (2003) ^{1}H, ^{13}C and ^{15}N assignment of the hydroquinone form of flavodoxin from *Desulfovibrio vulgaris* (Hildenborough) and comparison of the chemical shift differences with respect to the oxidized state. *J. Biomol. NMR* **25**, 257–258.

Zacherl, M., Huala, E., Rüdiger, W., Briggs, W.R., and Solomon, M. (1998) Isolation and characterization of cDNAs from oat encoding a serine/threonine kinase: An early component in signal transduction for phototropism (Accession Nos. AF 033096 and AF033097) (PGR98–028). *Plant Physio.* **116,** 869- .

Zhao, S.Y. and Sancar, A. (1997) Human blue-light photoreceptor hCRY2 specifically interacts with protein serine/threonine phosphatase 5 and modulates its activity. *Photochem. Photobiol.* **66,** 727-731.

Zhulin, I. B., Taylor, B.L., and Dixon, R. (1997) PAS domains S-boxes in archea, bacteria and sensors for oxygen and redox. *Trends Biochem. Sci.* **22**, 331-333.